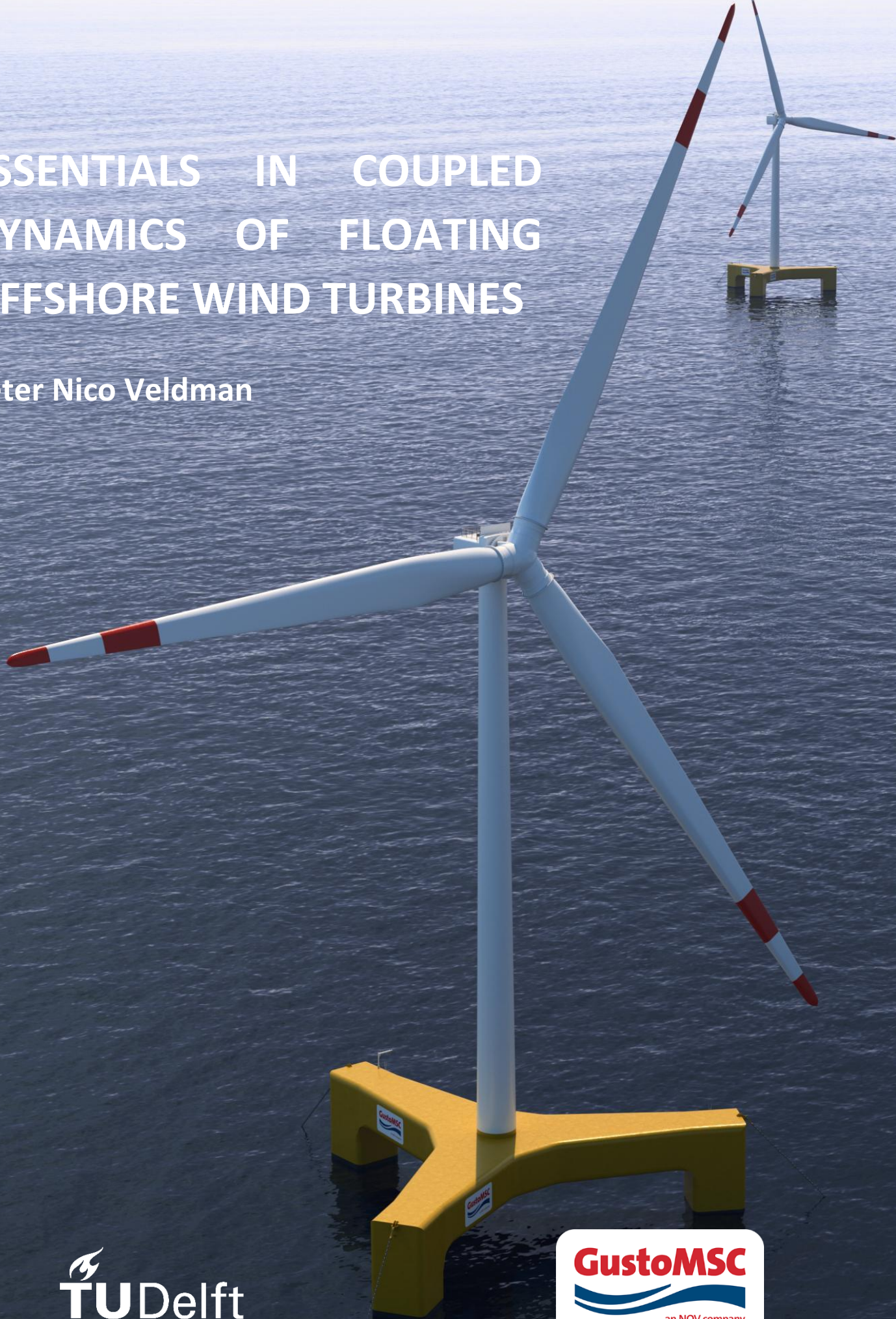


ESSENTIALS IN COUPLED DYNAMICS OF FLOATING OFFSHORE WIND TURBINES

Peter Nico Veldman



Essentials in Coupled Dynamics of Floating Offshore Wind Turbines

'A RESEARCH ON SIMPLIFIED MODELLING OF A FLOATING OFFSHORE
WIND TURBINE'

by

P.N. (Peter Nico) Veldman

to obtain the degree of Master of Science,
at the Delft University of Technology,
to be defended publicly on Friday October 30, 2020 at 03:00 PM.

Student number:	4164261	
Project duration:	November 18, 2019 - October 30, 2020	
Thesis committee:	Dr. ir. I. Akkerman,	TU Delft, chairman & supervisor
	Dr. ing. S. Schreier,	TU Delft
	Dr. ir. H. Polinder,	TU Delft
	Ir. F.A. Huijs,	GustoMSC

An electronic version of this thesis is available at <http://repository.tudelft.nl/>.



Abstract

At the moment, offshore wind is an indispensable source of energy. Compared to onshore wind, wind speeds offshore are considerably higher and more constant. Furthermore, offshore wind turbines reduce noise and visual impacts. In contrast to fixed bottom foundations, floating wind can be economically feasible in global offshore waters that exceed a depth of 60 meters. However, floating wind has its challenges.

Research has shown that the interaction between floater motions and wind turbine controller can be significant, especially above rated wind speed. The interaction between the hydrodynamics and aerodynamics above rated wind speed is the main reason why fully coupled aero-hydro-servo-elastic simulations are needed to determine the motions and mooring loads of the system. The downside of fully coupled simulations is, next to the need of comprehensive technical background, the high computational time which makes these simulations unsuitable for concept design studies. The purpose of the research is to develop a fast and simplified model that can be used for design iterations in concept design stages of Floating Offshore Wind Turbines (FOWTs). The simplified model must be able to predict the general motions and mooring loads with acceptable accuracy. Moreover, the simplified model should be based upon available wind turbine input data in an early design phase.

A sensitivity analysis is carried out to determine the contribution of various physical phenomena, present in fully coupled aero-hydro-servo-elastic simulations, on the motions and mooring loads of the GustoMSC Tri-Floater with a 5MW NREL wind turbine located at its center. The fully coupled simulations are performed with aNySIM-Phatas. By this analysis, the main physical contributors to the motions and mooring loads of the GustoMSC Tri-Floater are selected to include in the simplified model. It is confirmed that the interaction between the aerodynamics and hydrodynamics is significant, especially for platform pitch motions in the above rated conditions. Furthermore, the (controlled) aerodynamic thrust calculated from Blade Element Momentum (BEM) theory, as well as the wind drag loads are found to be the main driving forces on the system.

The simplified model is constructed by coupling an external Python code to the multi-body time-domain software aNySIM. Whereas aNySIM is responsible for the hydrodynamic and mooring calculations, Python is used for the simplified aerodynamic calculations. The effect of the wind turbine controller on the aerodynamic thrust is included by the use of the steady state thrust curve, aerodynamic damping ratios and filter on the incoming turbulent wind. The simplified model is compared with fully coupled aNySIM-Phatas simulations.

Compared to fully coupled simulations, obtained results suggest that in a free floating condition the differences in the mean are found to be within 5% and 10% for platform surge and platform pitch, respectively. The mean and maximum differences in the forward fairlead tension were found to be within 2% and 5%, respectively. Moreover, the results show that the simplified model is 5 times faster and much easier to construct compared to the fully coupled simulations.

The results of this research are encouraging as the simplified model can serve as a tool to predict the general motions and mooring loads with acceptable accuracy. Also, as Python is not coupled to aNySIM before to the best of the authors knowledge, this coupling opens doors to other simplified modelling strategies.

Preface

This report presents my thesis work to obtain the degree of Master of Science in Marine Technology at the Delft University of Technology. Starting at the TU Delft has helped me to developed myself, as a person, but also professionally. Finalizing this thesis would not have been possible without the help of some specific people.

First of all, I would like to thank my supervisors Fons Huijs (GustoMSC) and Ido Akkerman (TU Delft). I really would like to thank Fons for the opportunity to work on the floating wind subject. It was really a pleasure to work under your supervision. Your knowledge and enthusiasm on the subject has encouraged me to stay motivated. In my view, you are one of the key players in the floating wind industry. The four weekly progress meetings with Ido kept me pushing this project. Your bright view and sincere interest in my work has helped me a lot.

I would also like to express my gratitude to Ebert, who was always willing to answer my questions related to the subject. Furthermore, a special thanks to Fernando for proofreading my report.

A special thanks to my girlfriend, Emma, who mentally supported me throughout the whole project. You were always willing to listen and help me, even during the toughest times. Our discussions and walks around the block really helped me to stay focused.

Last but not least, I want to express sincere gratitude to my parents. Without your unconditional support, I would never have been able to start and complete this journey.

*Peter Veldman
The Hague, October 2020*

Contents

List of Figures	viii
List of Tables	xiii
List of Abbreviations	xv
1 Introduction	1
1.1 Background and motivation	1
1.2 Problem description	2
1.2.1 Research objective	2
1.2.2 Research questions	2
1.3 Thesis approach	2
1.4 Thesis outline/ reading guide	3
2 Background on floating wind	5
2.1 Why floating wind?	5
2.2 Platform configurations	6
2.3 Challenges	7
2.4 Design process	8
2.5 Modelling approaches in floating wind	9
2.5.1 Aerodynamic Models	9
2.5.2 Hydrodynamic Models	9
2.5.3 Mooring Models	10
2.5.4 Structural Models	10
2.5.5 Control Models	11
3 Literature report	13
3.1 State-of-the-art design tools	13
3.1.1 Offshore Code Comparison Collaboration (OC3)	13
3.1.2 Concluding remarks	15
3.2 Simplified models	16
3.2.1 Concluding remarks	19
3.3 Literature gap	19
4 Fully coupled model	21
4.1 Wind turbine	21
4.2 Floating platform	21
4.3 aNySIM	22
4.4 Phatas	22
4.5 Coupling aNySIM - Phatas	23

5	Sensitivity Study	25
5.1	Methodology	25
5.2	Physical phenomena	25
5.2.1	Aerodynamics (aero)	26
5.2.2	Wind turbine controllers (servo)	27
5.2.3	Structures (elastic)	28
5.2.4	Hydrodynamics (hydro)	28
5.3	Simplified aerodynamic models	28
5.4	Model outputs	29
5.5	Environmental conditions	30
5.6	Sensitivity results	30
5.6.1	Rated wind speed: 11.4 m/s	31
5.6.2	Above rated wind speed: 25 m/s	35
5.7	Conclusions and recommendations	39
5.7.1	Recommendations	39
6	Simplified model	41
6.1	Coupling aNySIM - Python	41
6.2	Steady state thrust curve	42
6.2.1	Low-frequency turbulent wind	44
6.2.2	Platform natural pitch frequency turbulent wind	44
6.2.3	High and wave frequency turbulent wind	44
6.3	Thrust sensitivity	47
6.3.1	Decay simulations	47
6.3.2	Method A: thrust sensitivity from correlation thrust and relative wind velocity	48
6.3.3	Method B: thrust sensitivity derived from aerodynamic damping	49
6.3.4	Comparison of method A and method B	56
6.3.5	Selected method	56
6.4	Turbulent wind speed filtering	56
6.4.1	Aerodynamic thrust excitation	57
6.4.2	Filter type	57
6.5	Overview of complete simplified model	59
6.6	Conclusions and recommendations	59
6.6.1	Recommendations	60
7	Verification simplified model	63
7.1	Stair case wind verification	63
7.2	Constant uniform wind verification	66
7.2.1	Platform pitch decay - constant uniform wind	66
7.2.2	Response to irregular waves - constant uniform wind	68
7.3	Low, natural pitch and high-frequency turbulent wind loading	72
7.3.1	Low-frequency turbulent wind	72
7.3.2	Natural pitch frequency turbulent wind	72
7.3.3	High-frequency turbulent wind	72
7.4	Turbulent wind verification - platform pitch only	76
7.4.1	Platform pitch decay - turbulent wind	76
7.4.2	Calm water - turbulent wind	77
7.4.3	Response to irregular waves - turbulent wind	81
7.5	Response to irregular waves in all Degree of Freedom (DoF) - turbulent wind	84
7.5.1	Floater motions	84
7.5.2	Fairlead tension	84
7.5.3	Computational time	85
7.6	Conclusions and recommendations	89
7.6.1	Recommendations	89

8	Conclusion & Recommendations	91
8.1	Conclusions	91
8.2	Recommendations	92
A	Complete set of PSD plots obtained from the sensitivity analysis	97
A.1	Aerodynamics	98
A.1.1	Platform surge	98
A.1.2	Platform pitch	99
A.1.3	Fairlead tension	100
A.1.4	Aerodynamic thrust	101
A.1.5	Resultant bending moment in towerbase	102
A.2	Controllers	103
A.2.1	Platform surge	103
A.2.2	Platform pitch	104
A.2.3	Fairlead tension	105
A.2.4	Aerodynamic thrust	106
A.2.5	Resultant bending moment in towerbase	107
A.3	Structures	108
A.3.1	Platform surge	108
A.3.2	Platform pitch	109
A.3.3	Fairlead tension	110
A.3.4	Aerodynamic thrust	111
A.3.5	Resultant bending moment in towerbase	112
B	Comparison aNySIM-Phatas with simplified model	113
B.1	Calm water - turbulent wind	113
B.2	Irregular waves in all DoF - turbulent wind	114

List of Figures

2.1	Indicative cost estimation of fixed versus floating wind turbine foundations over water depth, where the intersection of the two lines indicate the turning point.	5
2.2	Four common type of floating wind turbine concepts with different principal of stability [6].	6
2.3	Steady state aerodynamic rotor thrust as function of wind speed for the 5MW NREL reference turbine (Jonkman [18]), indicating rated wind speed (11.4 m/s).	8
2.4	General design process of a floating offshore wind turbine, from start to end delivery . .	8
3.1	Integrated modules in aero-hydro-servo-elastic simulations [17]	14
3.2	Thrust coefficient for a land-based 5MW wind turbine [20].	17
3.3	Aerodynamic damping ratios as function of wind speed for different degrees of freedom [33]	18
4.1	Artist impression of the GustoMSC Tri-Floater with the 5MW NREL reference wind turbine positioned in the center, in irregular waves.	22
4.2	Lay-out of the fully coupled aNySIM - Phatas simulation, taken from Huijs et al. [13] .	23
5.1	Hierarchical sensitivity framework of the fully coupled aero-hydro-servo-elastic simulation model of the Tri-Floater mounted with the 5MW NREL wind turbine. The physical phenomena marked in green are considered to be included in the base case simulation. .	26
5.2	Implemented aerodynamic thrust of the simulations with thrust approximation, constant thrust and constant thrust coefficient.	29
5.3	Power Spectral Density (PSD) of the aerodynamic thrust excitation (left) and platform surge excursion (right) at rated wind speed in 180 deg wave, current and wind direction in which the aerodynamic sensitivity is displayed.	32
5.4	PSDs of the aerodynamic thrust excitation (left) and platform pitch (right) at rated wind speed in 180 deg wave, current and wind direction in which the control sensitivity is displayed.	33
5.5	PSDs of the aerodynamic thrust excitation (left) and platform pitch motion (right) at rated wind speed in 180 deg wave, current and wind direction in which the structural sensitivity is displayed.	34
5.6	PSD of the aerodynamic thrust excitation (left) and platform surge excursion (right) at cut-out wind speed in 180 deg wave, current and wind direction in which the aerodynamic sensitivity is displayed.	36
5.7	PSDs of the aerodynamic thrust excitation (left) and platform pitch motion (right) at cut-out wind speed in 180 deg wave, current and wind direction in which the control sensitivity is displayed.	37
5.8	PSDs of the aerodynamic thrust excitation (left) and platform pitch motion (right) at cut-out wind speed in 180 deg wave, current and wind direction in which the structural sensitivity is displayed.	38
6.1	Coupling of hydrodynamic software aNySIM with the Python module.	41
6.2	Time dependent external force acting as a force vector at the center of rotor, as function of wind direction in the body fixed reference system.	42

6.3	Steady state aerodynamic rotor thrust (top) and steady state aerodynamic rotor power (bottom) obtained from fully coupled aNySIM-Phatas simulations, plotted with data reported by Jonkman et al. [16]. The steady state thrust from the fully coupled aNySIM-Phatas simulations are used as input for the simplified model.	43
6.4	Aerodynamic rotor thrust plotted against relative wind speed for a range of wind speeds with low-frequency turbulence (0.015 rad/s).	44
6.5	Aerodynamic rotor thrust plotted against relative wind speed for a range of wind speeds with platform natural pitch frequency turbulence (0.21 rad/s).	45
6.6	Aerodynamic rotor thrust plotted against relative wind speed for a range of wind speeds with high-frequency turbulence (0.15 rad/s).	46
6.7	Pitch decay in 8 m/s constant wind presenting the aerodynamic thrust due to pitch decay together with the filtered thrust signal.	47
6.8	Power Spectral Density (PSD) of the aerodynamic thrust of a platform pitch decay simulation in 8 m/s constant uniform wind speed illustrating blade pass frequencies. . .	48
6.9	Filtered aerodynamic thrust plotted against relative velocity in decay simulations in constant uniform wind speeds, showing trends in the thrust force.	49
6.10	Free decay pitch motion of the Tri-Floater in calm water and no wind with and without hydrodynamic (viscous and potential) damping.	50
6.11	Free decay of pitch motion in three constant wind speeds without correction with the mean value of the steady state condition.	51
6.12	Aerodynamic pitch damping ratios determined using logarithmic decrements from decay simulations for three different control approaches in constant uniform wind.	52
6.13	Free decay of pitch motion under 8 m/s turbulent wind (one seed) showing differences between decay motion with and without external moment, for which the aerodynamic damping ratio is determined.	53
6.14	Aerodynamic pitch damping ratios determined using logarithmic decrements from decay simulations for three different control approaches and different seeds in turbulent wind.	53
6.15	Difference in aerodynamic pitch damping ratios determined using the logarithmic decrements from pitch decay simulations in constant uniform wind and turbulent wind.	54
6.16	Comparison of $\partial T/\partial \dot{x}$ derived from method A and method B. Where method A tries to capture the thrust sensitivity from correlation of aerodynamic thrust and relative wind speed, method B determines the thrust sensitivity from the aerodynamic damping.	56
6.17	PSD of platform pitch and aerodynamic thrust in a turbulent wind speed of 14 m/s, showing the negative damping effect induced by Fixed Base Control compared to the fully coupled simulation with the Floating Control+.	57
6.18	Spectral density of an incoming turbulent wind field of 14 m/s, filtered around the natural pitch frequency with different filters with a stop-band of 0.18 to 0.23 rad/s.	58
6.19	Comparison of the platform pitch and aerodynamic thrust between the fully coupled model and the simplified model with and without a simple FFT filter applied on the incoming wind speed. The filter is constructed with a stop-band of 0.21 to 0.23 rad/s, lowering the aerodynamic thrust response at the natural platform frequency.	59
6.20	Flowchart showing the steps taken in the Python script to calculate the thrust.	61
7.1	Stair case wind simulation from 3 to 13 m/s in steps of 2 m/s of the simplified model compared to the fully coupled simulation model. The aerodynamic thrust force is plotted (middle) together with the platform pitch (bottom).	64
7.2	Stair case wind simulation from 15 to 25 m/s in steps of 2 m/s of the simplified model compared to the fully coupled simulation model. The aerodynamic thrust force is plotted (middle) together with the platform pitch (bottom).	65
7.3	Platform pitch decay simulations of the fully coupled simulations and simplified model, showing the influence of the nacelle orientation.	67
7.4	Comparison of time traces of a pitch decay in a 4 m/s constant uniform wind for a fully coupled and simplified simulations.	68
7.5	Absolute difference of the logarithmic decrement over the first 4 oscillations of the decay (top), and absolute differences of the mean platform pitch period over the same first 4 oscillations.	69

7.6	Comparison of platform pitch and aerodynamic thrust spectra between fully coupled and simplified simulations in irregular waves and constant (below and above rated) winds.	70
7.7	Differences in gradients of aerodynamic thrust versus relative wind for various constant wind speeds of the simplified model and fully coupled model.	71
7.8	Platform pitch wave forces compared to pitch moment cause by aerodynamic thrust for a constant uniform wind speed of 12 m/s.	71
7.9	Comparison of the platform pitch and aerodynamic thrust between the fully coupled and simplified model, showing PSDs for wind fields of 8 and 12 m/s, containing only low-frequency turbulence.	73
7.10	Comparison of the platform pitch and aerodynamic thrust time trace between the fully coupled and simplified model, showing time traces for a wind field of 12.0 m/s, containing only low-frequency turbulence.	73
7.11	Comparison of the platform pitch and aerodynamic thrust between the fully coupled and simplified model, showing PSDs for wind fields of 8 and 12 m/s, containing only turbulence in the frequency range around the natural platform pitch frequency.	74
7.12	Comparison of the platform pitch and aerodynamic thrust between the fully coupled and simplified model, showing time traces for a wind field of 10 m/s, containing only turbulence in the frequency range around the natural platform pitch frequency.	74
7.13	Comparison of the platform pitch and aerodynamic thrust between the fully coupled and simplified model, showing PSDs for wind fields of 8 and 14 m/s, containing only high-frequency turbulence.	75
7.14	Results of decay simulations in turbulent wind, showing the absolute difference of the logarithmic decrement over the first 4 oscillations (top), and absolute differences of the mean platform pitch period over the same first 4 oscillations in turbulent wind.	76
7.15	Platform pitch and aerodynamic thrust time trace for a turbulent wind speed of 10 m/s (after the results of a decay without external force is subtracted from the results of a decay with external force), showing non linearity of the aerodynamic thrust of the fully coupled model.	77
7.16	Comparison of platform pitch mean, standard deviation and maximum values between fully coupled and simplified simulations in calm water and turbulent wind.	78
7.17	Comparison of pitch and aerodynamic thrust spectrum between fully coupled and simplified simulations in calm water and turbulent wind.	79
7.18	Aerodynamic thrust plotted versus relative wind speed for 8 m/s and 24 m/s for the simplified and fully coupled model in turbulent wind without waves.	80
7.19	Comparison of pitch and aerodynamic thrust spectrum between fully coupled and simplified simulations with waves and turbulent wind.	82
7.20	Aerodynamic thrust plotted versus relative wind speed for 8 m/s and 24 m/s for the simplified and fully coupled model in turbulent wind with waves.	83
7.21	Comparison of mean, standard deviation and maximum values between fully coupled and simplified simulations in platform surge, pitch and fairlead tension when the platform is free to float in all directions with waves and under turbulent wind.	85
7.22	Platform surge, pitch and aerodynamic thrust spectra for two under rated wind speeds when the platform is free to move in all its directions.	86
7.23	Platform surge, pitch and aerodynamic thrust spectra for two above rated wind speeds when the platform is free to move in all its directions.	87
7.24	PSD of forward fairlead in case the floater is free to move in all its directions.	88
A.1	Comparison of PSD of different aerodynamic model inputs to the base case simulation in turbulent winds for platform surge.	98
A.2	Comparison of PSD of different aerodynamic model inputs to the base case simulation in turbulent winds for platform pitch.	99
A.3	Comparison of PSD of different aerodynamic model inputs to the base case simulation in turbulent winds for the forward fairlead tension.	100
A.4	Comparison of PSD of different aerodynamic model inputs to the base case simulation in turbulent winds for the aerodynamic thrust.	101

A.5	Comparison of PSD of different aerodynamic model inputs to the base case simulation in turbulent winds for the resultant bending moment in the tower base.	102
A.6	Comparison of PSD of different control model inputs to the base case simulation in turbulent winds for the platform surge.	103
A.7	Comparison of PSD of different control model inputs to the base case simulation in turbulent winds for the platform pitch.	104
A.8	Comparison of PSD of different control model inputs to the base case simulation in turbulent winds for the forward fairlead tension.	105
A.9	Comparison of PSD of different control model inputs to the base case simulation in turbulent winds for the aerodynamic thrust.	106
A.10	Comparison of PSD of different control model inputs to the base case simulation in turbulent winds for the resultant bending moment in the towerbase.	107
A.11	Comparison of PSD of different structural model inputs to the base case simulation in turbulent winds for the platform surge.	108
A.12	Comparison of PSD of different structural model inputs to the base case simulation in turbulent winds for the platform pitch.	109
A.13	Comparison of PSD of different structural model inputs to the base case simulation in turbulent winds for the forward fairlead tension.	110
A.14	Comparison of PSD of different structural model inputs to the base case simulation in turbulent winds for the aerodynamic thrust.	111
A.15	Comparison of PSD of different structural model inputs to the base case simulation in turbulent winds for the resultant bending moment the towerbase.	112

List of Tables

4.1	Main properties of the 5MW NREL reference wind turbine taken from Jonkman et al. [16]	21
4.2	Main dimensions of the GustoMSC Tri-Floater mounted with the 5MW reference wind turbine, obtained from Huijs et al. [12]	22
5.1	Aerodynamic rotor thrust and thrust coefficients for given wind speeds used in the simulations	29
5.2	Overview of the model outputs with a short description	30
5.3	Overview of frequency regions together with natural platform surge and natural platform pitch frequency	30
5.4	Environmental conditions for the simulations used in the sensitivity analysis.	31
5.5	Relative differences between the base case and the simulations in which the aerodynamic physics are alternately turned off with respect to the base case	31
5.6	Relative differences between the base case and the simulations in which different controllers are included (together with the simplified models)	32
5.7	Relative differences between the base case simulation in which the structural physics are alternately turned off with respect to the base case	33
5.8	Relative differences between the base case and the simulations in which the aerodynamic physics are alternately turned off with respect to the base case	35
5.9	Relative differences between the base case simulation and simulations in which different controllers are included (together with the simplified models)	36
5.10	Relative differences between the base case simulation and simulations in which the structural physics are alternately turned off with respect to the base case	37
7.1	Mean (taken from the last 200 seconds of a wind step) comparison of aerodynamic thrust and platform pitch between simplified and aNySIM-Phatas simulations in a stair case wind field from 3 to 25 m/s.	64
7.2	Computational time of the fully coupled model and simplified model for a range of turbulent wind speeds.	87
B.1	Mean, standard deviation and maximum value of platform pitch in turbulent winds in calm water and irregular waves of the fully coupled model (aNySIM-Phatas) and simplified model.	113
B.2	Mean, standard deviation and maximum of platform surge and pitch when all DoF are activated for the fully coupled (aNySIM-Phatas) and simplified model.	114
B.3	Mean, standard deviation and maximum values of forward fairlead tension of the fully coupled (aNySIM-Phatas) and simplified model.	114
B.4	Mean, standard deviation and maximum values of aerodynamic rotor thrust of the fully coupled (aNySIM-Phatas) and simplified model.	115

List of Abbreviations

AnyPhatas aNySIM-Phatas

BEM Blade Element Momentum

CFD Computational Fluid Dynamics

CoG Center of Gravity

CPU Central Processing Unit

DLL Dynamically Linked Library

DoF Degree of Freedom

DoFs Degrees of Freedom

ECN Energy research Centre of the Netherlands

FEM Finite Element Method

FFT Fast Fourier Transform

FOWT Floating Offshore Wind Turbine

FOWTs Floating Offshore Wind Turbines

GDW Generalized Dynamic Wake

GW Gigawatts

GWEC Global Wind Energy Council

HF High Frequency

LF Low Frequency

MARIN Maritime Research Institute Netherlands

MBD Multi Body Dynamics

MOUs Mobile Offshore Units

MW Megawatts

NREL National Renewable Energy Laboratory

PID Proportional Integral Derivative

PSD Power Spectral Density

QTF Quadratic Transfer Function

RNA Rotor-Nacelle Assembly

RPM Revolutions Per Minute

TI Turbulence Intensity

TLP Tension Leg Platform

WF Wave Frequency

Chapter 1

Introduction

1.1 Background and motivation

The use of energy is indispensable to meet basic human needs in modern society. As a result of the worldwide population and economic growth, the demand for energy is rapidly increasing. Burning fossil fuels for energy production leads to higher greenhouse gas emissions (e.g. CO_2), which contribute to global warming. With the focus on global warming, there is public and political attention for climate change and its effect on (future) generations. In the Paris Agreement [41], ratified by 187 parties and signed by 197 parties, countries have agreed to hold the increase in the global average temperature to 'well below' 2°C above pre-industrial levels and pursuing efforts to limit the temperature increase to 1.5°C above pre-industrial levels.

In order for countries to achieve the goals of the Paris Climate Agreement, there is a need for clean sources of renewable energy to reduce the greenhouse gasses. This need has driven the development of new renewable offshore energy resources. Besides bio energy, solar energy, geothermal energy, hydro power, ocean energy (wave and tidal), wind energy plays a very important role in the energy transition. The wind energy market has been growing significantly for the past decades, and especially the offshore wind energy market. The total amount of installed offshore wind power capacity reached 29 Gigawatts (GW) up to 2019 [9]. According to data published by the Global Wind Energy Council (GWEC), a total of 6.1 GW new offshore wind capacity was installed in 2019, compared to 29 GW of the total global offshore wind capacity.

The offshore wind energy is one of the promising 'green' energy sources. Offshore wind energy is attractive, because the planet is covered by more than 70% by sea, and the wind speeds offshore are considerably higher and more constant, as they suffer less from turbulence. Also, noise and visual impacts are significantly reduced compared to onshore wind, and there is no limit with respect to offshore wind turbine size. Whereas the fixed foundation technology has dominated in the past years, floating wind is a new development in the offshore wind energy market. It is expected that at the end of 2030, floating wind accounts for 6% of the total new global wind installations. Already, a total of 66 Megawatts (MW) of floating wind capacity has been installed worldwide, as of the end of 2019 [9]: 32 MW floating wind capacity is located in the UK, 19 MW in Japan, 10.4 MW in Portugal, 2.3MW in Norway and 2 MW in France.

One of the companies with the aim of lowering the carbon footprint is GustoMSC. GustoMSC is a design and engineering company in the field of Mobile Offshore Units (MOUs) and equipment. Besides the design of jack-up vessels (wind turbine installation vessels), semi-submersibles and ships for the oil & gas industry and wind energy market, GustoMSC has designed the Tri-Floater. The Tri-Floater is a semi-submersible wind turbine support structure comprising three columns connected by a deck box, in which the wind turbine is located in the center of the unit. This thesis deals with the development of a simplified, fast and computationally efficient dynamic model to capture the motions and mooring loads of a Floating Offshore Wind Turbine (FOWT) in the concept design phase.

1.2 Problem description

Wind turbine floater motions are a result of a two-way coupling of the hydrodynamic forces on the hull and the aerodynamic forces on the wind turbine. Research has shown that the interaction between the floater motions and the wind turbine controller can be significant, especially above the rated wind velocity (when the blade pitch control is active) [18, 21]. The interaction between the floater motions and aerodynamics including the wind turbine controller is the main reason why coupled aero-hydro-servo-elastic simulations of the floater and wind turbine dynamics are needed, to assess the motions and mooring loads of the floater. As the aero-hydro-servo-elastic time-domain simulations are time consuming, they are not desired in a concept design phase. Furthermore, as the market of floating offshore wind energy is increasing, the need for comprehensive numerical models to assess the floating behavior become more important. The main problem originates from the fact that the fully coupled time-domain simulations require a lot of computational time and comprehensive technical background. Therefore, there is a need for less time consuming and simplified coupled models that still captures the general motions and mooring loads of a semi-submersible wind turbine support structure, in the concept design phase.

1.2.1 Research objective

In summary, the requirements as stated above are all combined in one objective:

Develop a simplified, fast and computational efficient model that predicts the motions and mooring loads of a Floating Offshore Wind Turbine (FOWT) in the concept design phase, based on available wind turbine input data.

1.2.2 Research questions

In order to reach the objective, three different research questions are defined. The research questions are formulated as follows:

1. Which physical phenomena, present in fully coupled state-of-the-art simulations, need to be taken into account in a simplified model?
2. How can the relevant physical phenomena be integrated in a simplified model?
3. To what extent does the simplified model compare to fully coupled aero-hydro-servo-elastic time-domain simulations, with respect to the floater motions and mooring loads?

1.3 Thesis approach

In this section the approach to answer the research questions, as formulated above, is given:

- The first step in this research is to identify all physical phenomena which are taken into account by fully coupled aero-hydro-servo-elastic simulations, utilised within GustoMSC. The fully coupled model is constructed for the semi-submersible floating wind turbine support structure developed by GustoMSC (Tri-Floater), mounted with a 5MW reference turbine, developed by National Renewable Energy Laboratory (NREL). The fully coupled simulations are performed with aNySIM-Phatas.
- Then, the most (available) influential physical phenomena, which govern the motions and mooring loads of the floater, are investigated using the fully coupled simulations. This is done by performing a sensitivity analysis.
- After having identified the most influential physical phenomena, a methodology is developed which aims for simplifying the governing physical phenomena based on available wind turbine input data in the concept design phase.
- The last step is the verification and quantification of the results of the simplified model by comparing it to the fully coupled aero-hydro-servo-elastic simulations.

1.4 Thesis outline/ reading guide

Chapter 2 gives a short background on floating wind in contrast to fixed offshore wind. Also, different platform configurations are discussed and challenges faced in floating wind are given. Also, a small note on the design process of a floating wind turbine is provided. Lastly, modelling strategies of the different physics present in fully coupled simulations are discussed.

Chapter 3 presents a literature study. It starts with an overview of papers which elaborate on different aero-hydro-servo-elastic modelling tools. Then, literature is presented on simplified modelling of floating wind together with a gap analysis.

Chapter 4 gives a brief description of the aNySIM-Phatas fully coupled aero-hydro-servo-elastic model which is used throughout this thesis.

Chapter 5 addresses a sensitivity analysis. In this chapter the most influential physical phenomena are identified with the use of fully coupled simulations, which need to be taken into account in the simplified model.

Chapter 6 presents the construction of the simplified model on the basis of the results obtained from Chapter 5.

Chapter 7 describes the verification and presents the results of the simplified model compared to the fully coupled aNySIM-Phatas model.

Chapter 8 presents the conclusions and recommendations.

Chapter 2

Background on floating wind

This chapter gives background on the floating wind subject. It starts with a brief statement on the use of floating wind, followed by the advantages and disadvantages of different platform configurations. Then, challenges are described which are encountered in the design when a wind turbine is placed on a floating platform. At last, a short summary is given on aerodynamic, hydrodynamic, structural and control modelling approaches.

2.1 Why floating wind?

With the public and political attention for climate change, there is a need for clean sources of renewable energy. As wind contains much energy, wind energy can play a very important role in the transition from fossil energy to renewable energy. At the moment, countries are installing massive wind farms in coastal areas. Coastal areas are attractive since there exist less turbulence in the wind, and noise and horizon pollution are limited. As the coastal areas have relative small water depth, it allows for fixed bottom wind turbines. When moving to deeper waters (>60 meters), the costs of fixed bottom foundations become relative large, even though fixed foundations are still technically feasible. From financial perspective, floating wind becomes interesting from a depth of approximately 60 meters with respect to fixed foundations, see Fig. 2.1. As floating wind can be installed in deeper waters, other geographical opportunities arise, where fixed bottom foundations are simply not cost effective.

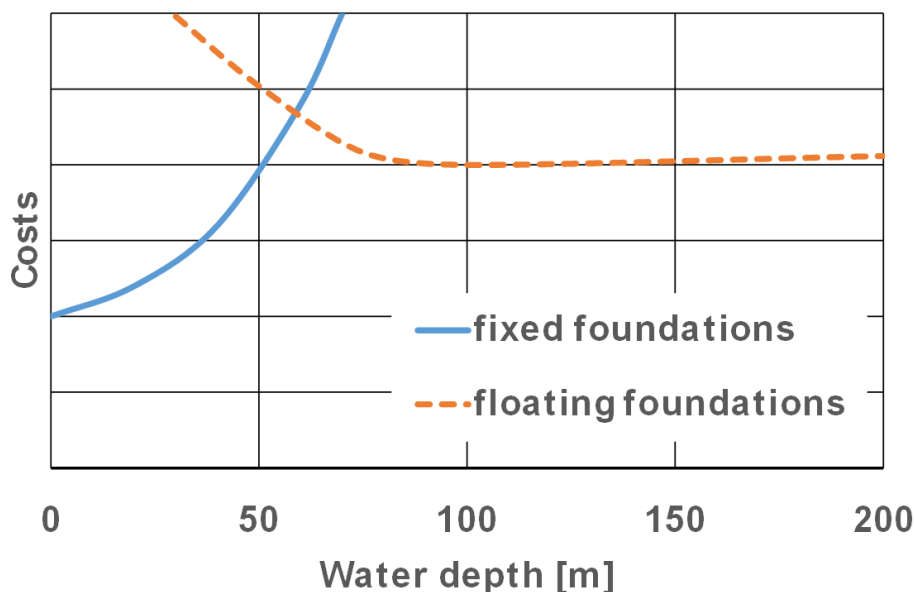


Figure 2.1: Indicative cost estimation of fixed versus floating wind turbine foundations over water depth, where the intersection of the two lines indicate the turning point.

From the figure, it is seen that the cost of fixed foundations increase strongly with water depth and intersect the cost curve of floating foundations at a water depth of 60 meters. The cost curve of floating foundations shows an optimum around a water depth of 100 meters, after which the costs increase slowly due to the longer mooring lines required and dynamic cable connection. For shallow water, the floating foundation costs increase strongly due to the challenges in the mooring system and dynamic power cable.

2.2 Platform configurations

Different configurations of the floating platforms exist in the floating offshore wind industry. In general, floating turbines can be classified into three main categories according to Butterfield et al. [2]: ballast, mooring lines and buoyancy, see Fig. 2.2. Here, only the most common platform configurations are briefly explained, together with their physical principles of stability and advantages and disadvantages with respect to construction and installation.

Spar-buoys

The spar-buoy concept achieves stability by using ballast, where the relative large mass is located below the sea-level. The main advantage of the spar-buoy is the relative simple cylindrical structure, which is very well suitable for serial production. The main disadvantage is, however, the deep draft which restricts the platform to be used in shallow waters (for example in ports). The installation needs to be done by a crane vessel instead of an onshore crane, which makes it more expensive.

Tension leg platforms (TLPs)

The Tension Leg Platform (TLP) achieves stability by the use of mooring lines. The vertical mooring lines are under tension, which keeps the TLP in upright condition. The construction of the tethers and anchors are relative expensive. A TLP needs vertical load anchors, which makes it dependent on the soil, leading to an earthquake sensitive construction. Nevertheless, the mooring system has a small footprint. The (crane vessel) installation procedure is however relative complex and expensive.

Buoyancy stabilized platforms

The buoyancy stabilized platforms, such as semi-submersibles and barges, are based on the buoyancy force which keeps the platform upright. The relative large moment of inertia of the water plane of the floater contributes to the righting moment. A semi-submersible is generally more difficult to manufacture in serial production, as it is relatively complex in shape. However, semi-submersibles do not have shallow water restrictions, which makes it possible to install the wind turbine from shore.

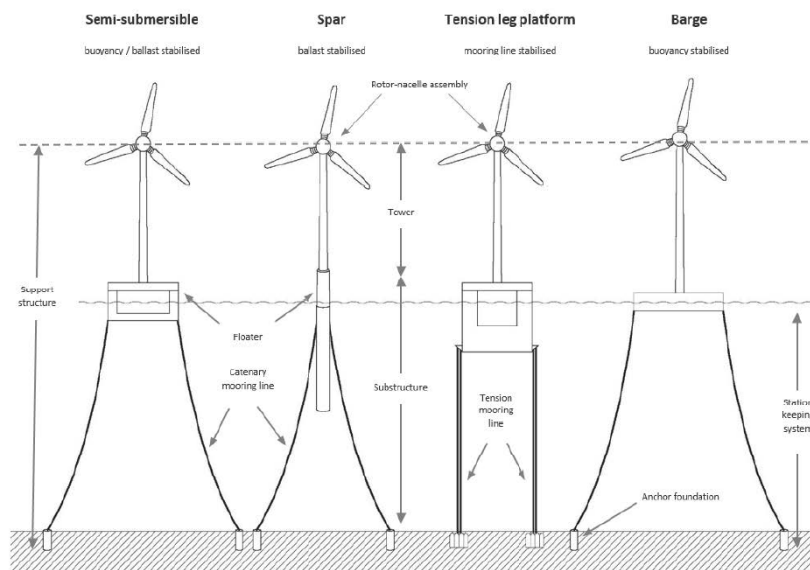


Figure 2.2: Four common type of floating wind turbine concepts with different principal of stability [6].

2.3 Challenges

The purpose of a wind turbine is to produce energy. To convert as much energy as possible from the wind into electrical energy, within safe operational limits, the wind turbine control system is an essential part. The wind turbine controller responds to changes in the environmental conditions and controls (by the use of actuators) the nacelle orientation, generator torque, and the blade pitch angle. In an upwind turbine, the rotor is always facing the wind. This is achieved by the nacelle controller, which controls the yaw angle such that the nacelle is aligned with the wind direction. Large horizontal axis wind turbines are normally of variable speed variable blade pitch configuration to maximize power output and keep structural loads within design conditions. These configurations allow the turbine to vary the rotor speed and the collective blade pitch angle. In such wind turbines, the power production is controlled by means of two control strategies: the generator torque controller and the blade pitch controller.

Cut-in, cut-out and rated wind speed

Prior to the explanation of the two control strategies, three important wind speeds are explained: cut-in, cut-out and rated wind speed. The cut-in wind speed is the lowest wind speed at which the turbine will start to generate power. To avoid the wind turbine to start and stop due to variation in the wind speed, the average wind speed needs to be higher than the cut-in wind speed, for some time. The cut-out wind speed is the highest wind speed at which the wind turbine still generates power. If the average wind speed is higher than the cut-out wind speed, the wind turbine will shut down. Rated wind speed is the wind speed between cut-in and cut-out, at which the wind turbine starts to produce maximum power (rated power).

The goal of the generator torque control is to maximise power in the below-rated conditions by keeping the generator torque proportional to the square of the filtered generator speed. The goal of the blade pitch controller is to maintain maximum constant power in above-rated conditions. The blade pitch is kept constant for wind speeds between cut-in and rated, such that the generator torque varies (variable rotor speed) and the wind turbine operates as close as possible to a constant tip speed ratio. The tip speed ratio is the ratio between the tip speed of a wind turbine blade and the undisturbed wind speed. The optimal constant tip speed ratio is the designed tip speed ratio corresponding to the maximum power coefficient obtained from a wind turbine. At the rated wind speed, the wind turbine reaches maximum (average) power and aerodynamic thrust. Above rated wind speed, the blade pitch varies in order to keep the wind turbine within its design limits.

The consequence of a variable speed variable pitch controller is a decrease in aerodynamic rotor thrust above rated wind speed, as seen in Fig. 2.3. If a wind turbine with a conventional variable speed variable pitch controller is placed on a floating platform, the whole system can become unstable. Looking at Fig. 2.3, it can be seen that up to rated wind speed the thrust gradient is positive. This positive gradient (increasing aerodynamic thrust with increasing wind speed), leads to positive damping on the platform motions. This means, if the floating wind turbine is pitching into the wind, the relative wind speed increases and so does the thrust force. The other way around, if the floating wind turbine is pitching from the wind, the aerodynamic thrust decreases. This leads to positive damping of the platform under rated condition. However, the effect in the above rated condition is vice versa. The thrust gradient is negative, leading to 'negative damping' [21]. Aerodynamic thrust decreases when the floating wind turbine pitches into the wind, and increases in case the turbine is pitching from the wind. This negative gradient above rated wind speed is caused by the pitching of the blades, to reduce the loads on the turbine.

It must be noted that for fast instantaneous changes in the above rated wind speed (e.g. tower or blade flexibility) the wind turbine controller is 'too slow' to react, leading to positive aerodynamic damping. This is however not the case if the fore-aft motion of the wind turbine is lightly damped such that the wind turbine controller has time to react on the changes of relative wind speed. In other words, if lightly damped eigenmodes are within the controller bandwidth, the platform can become unstable. The aerodynamic thrust follows the negative gradient leading to a negative damping effect. Lightly damped eigenmodes are often the fore-aft platform pitch and platform surge motions of the moored floating platform.

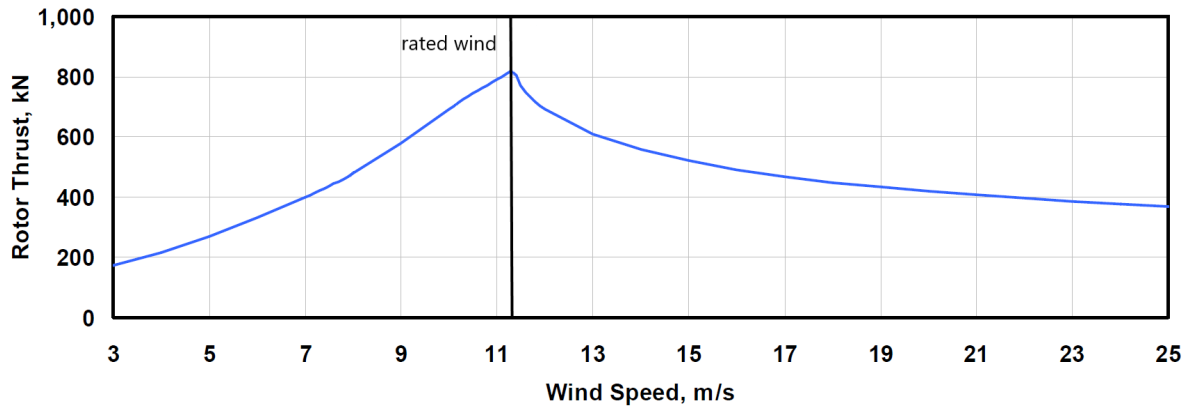


Figure 2.3: Steady state aerodynamic rotor thrust as function of wind speed for the 5MW NREL reference turbine (Jonkman [18]), indicating rated wind speed (11.4 m/s).

2.4 Design process

To model the complete behavior of a floating wind turbine, fully coupled aero-hydro-servo-elastic time-domain models are necessary. These models incorporate aerodynamic (aero), hydrodynamic (hydro), control (servo) and structural (elastic) models in a fully coupled integrated simulation environment. These fully coupled models are usually not the starting point of a floating platform design, as they require detailed description of the system. The design of, for instance, the wind turbine control system is at this stage not known, while it has a very important effect on the motions as described earlier.

A global flowchart of a design process of a floating wind turbine is given in Fig. 2.4. A first step in the design process of a floating wind farm is the site selection. After the site is selected, a met-ocean study is performed in order to estimate the environmental conditions. Based on the site selection, the most suitable floating concept is selected including concept variation (e.g. the number of mooring lines). At this stage, the basic turbine parameters such as rated power, steady-state thrust force and weights are determined. In this first phase, it is very important to reduce the complexity of the system before conducting fully coupled time-domain simulations. Therefore, simpler models are required which serve as a tool to assess the dynamic behavior the floating concept. Once the dimensions of the floater are determined, together with detailed information of the wind turbine, fully coupled simulations are performed. Also, the control system is then included.

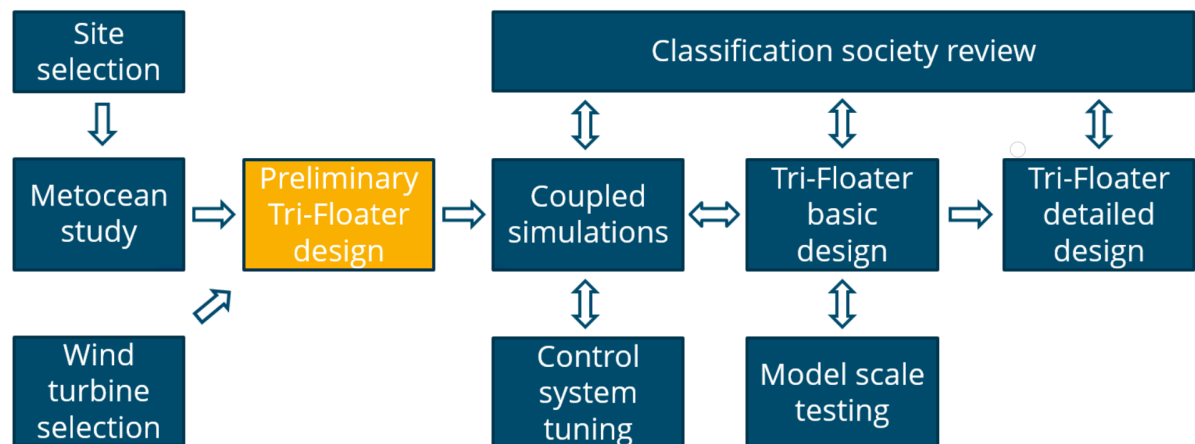


Figure 2.4: General design process of a floating offshore wind turbine, from start to end delivery

2.5 Modelling approaches in floating wind

In this section, a brief description is given of the aerodynamic, hydrodynamic, controller and structural modelling.

2.5.1 Aerodynamic Models

Aerodynamic loads on ships and offshore structures are commonly calculated using drag coefficients [19]. Wind turbines, however, require more complex models as they include rotating blades. The aerodynamic loads on wind turbines are commonly calculated by the use of Blade Element Momentum (BEM) theory [26]. Other, more accurate predictions of the aerodynamics also exists, such as Computational Fluid Dynamics (CFD) and vortex based methods. However, these computational methods require relatively long computational time which is useful if detailed information is required in a later design phase.

In the 1930s, Betz and Glauert [8] developed the classic analysis for the steady state performance of a wind turbine. In this analysis, the momentum theory and blade element theory were combined into a BEM theory in order to calculate the steady state performance characteristics of an annular section of the rotor. Blade element theory assumes that the blades of the wind turbine are divided into small sections. The lift and drag forces are calculated by the use of predefined lift and drag coefficients. By summing all elemental forces along the span of the blades, the total forces and moments on the turbine can be determined. The momentum theory assumes that there is a change in pressure as energy is extracted from the wind which leads to a decrease in linear momentum. Using the momentum theory, the induced velocities can be calculated due to the loss of momentum in the flow in the axial and tangential directions. These velocities affect the inflow on the rotor and therefore the lift and drag forces calculated by the blade element theory. The change in momentum of the air which passes the rotor is equated with the lift and drag forces calculated from the blade element theory.

The BEM theory forms the basis of many aerodynamic models for horizontal axis wind turbines, as the computational time is relatively low. However, it is shown by various experimental tests that BEM theory is not always sufficiently reliable for calculating the aerodynamic loads on the wind turbine blades. In particular, this is true for stalled and yawed rotor conditions, where the air on the low pressure side of the blade is not attached.

2.5.2 Hydrodynamic Models

Fixed bottom offshore wind turbines are generally placed on monopiles or jackets. These fixed support structures are slender in comparison with the length of the incoming wave. Therefore, the load on these fixed support structures can be determined using Morison's equation. The Morison equation is widely used in fixed offshore wind turbines with slender characteristics [4, 31]. The Morison equation can be used to compute linear wave loads and non linear viscous loads on FOWTs. The Morison equation assumes that the total wave load on the slender floating wind turbine structure is a summation of an inertial component and a drag component. Originally Morison's equation was developed for a fixed bottom cylinder, but is here extended to a floating cylinder:

$$dF_{\text{mor}}(z, t) = \frac{\rho_w \pi D^2}{4} \left(C_M \frac{\partial u}{\partial t} - (C_M - 1) \frac{\partial v}{\partial t} \right) dz + \frac{\rho_w D}{2} C_D |u - v| (u - v) dz \quad (2.5.1)$$

where ρ_w is the density of the water, D is the diameter of the cylinder, dz is the length of a differential element of the cylinder, u is the velocity of the water in transverse direction, and v is the transverse velocity of the moving cylinder. It is important to note that the water velocity considered may be due to the current and waves. C_M and C_D are the added mass coefficient and drag coefficient respectively. Both coefficients are empirically determined. The Morison equation can also be used to model the hydrodynamic forces on heave plates of a floating platform.

For large volume structures, where typically the size of the structure is not small relative to the wavelength, diffraction and radiation effects must be accounted for. Large volume structures are commonly modelled using potential flow theory. Typically, the potential flow is solved numerically by the use of a panel method. Wave-induced loads on floating platforms can be calculated by using 3D potential theory in the frequency domain. In potential theory, the flow is to be assumed homogeneous,

non-viscous, incompressible and irrotational. Using a set of boundary conditions, the velocity potential and pressures on the submerged surface of the wind turbine structure are solved. Diffraction matrices (the effects of waves diffracted due to the presence of the platform) and radiation matrices (the effects of propagating waves from the body due to oscillations of the platform) result from potential flow theory. Also, hydrostatic restoring forces are calculated.

Based on linear three-dimensional potential theory, the second order non-linear hydrodynamic loads can be calculated [34]. These second order hydrodynamic loads are proportional to the square of the wave amplitude, which implies that the loads are non linear with respect to the incoming wave height. The loads are generally smaller than the first order wave loads, but can excite eigenmodes of the floating platform when it coincides with the natural periods. Second order hydrodynamics can induce loads at the sum and difference frequencies of the incoming wave components. The low frequency part of the difference frequency can excite large resonant motions of the floating platform, such as surge and sway. The high frequency part of the sum frequency can be relevant for the natural frequencies of TLPs and structural vibration modes.

Sometimes a combination of potential theory and Morison's formulation is used. Using potential flow implies that viscous effects are not taken into account, and using Morison's equation means the wave diffraction effects are disregarded [17]. The combination result in the potential theory plus the viscous effects of the Morison formulation.

2.5.3 Mooring Models

Mooring systems are designed to maintain the position of the floating platform in current, wind and waves. Mooring systems comprises a number of mooring lines, where one end is attached to the floating platform, and the other end is anchored to the seabed. The mooring lines are constructed from steel, chain or synthetic fibres and/or a combination of these materials. Three important types of mooring systems can be distinguished [19]: catenary line mooring, taut line mooring and tension leg line mooring systems. Catenary mooring systems have catenary steel lines which primarily provide a horizontal restoring force due to the weight of the lines moving up and down when the floating structure moves. Taut lines restrict the motion of the platform and are often made from synthetic material. Tension leg mooring is a special system which restricts the platform from moving completely, used for TLPs. The tension leg mooring system is an important contributor to the stability of a TLP.

At larger excursions, the restoring forces of the mooring lines are non linear with respect to the displacement of the floating platform. In terms of modelling, two numerical analysis exist: the quasi-static and dynamic modelling. In the dynamic modelling, the mass and drag forces acting on the slender mooring lines are included. Depending on the depth, the mooring line dynamics can be neglected. For shallow water mooring systems, the mooring dynamics can be neglected because the total mass of the lines is negligible and the motion is small [27]. For deep water mooring systems, the mooring dynamics can become significant due to large platform motion and/or large drag elements [27]. According to Jonkman [17], the mooring dynamics can be neglected if the effective inertia of the mooring system is about 2% of the combined total inertia of the floating structure, which is a conservative approach. In the quasi-static approach, the mooring system is assumed to be linear between two static points for which the loads on the system are assumed constant. Furthermore, no mass and drag forces are included. Whether to use a quasi-static or dynamic approach depends on the importance of the mass and drag forces on the mooring lines.

2.5.4 Structural Models

The simplest form of structural modelling is by assuming that the wind turbine and floating structure are rigid bodies. It is however important to consider the flexibility, mass distribution, damping properties and the relevant eigenfrequencies of the structure. For structures that have low flexibility, such as the floater, rigid-body models are accepted. The tower, however, must be modelled as flexible in coupled wind turbine simulations if there is an interest in for example fatigue behavior. It is important to design the structure such that the important eigenfrequencies are away from the wave and wind excitation frequencies, to avoid high structural loading. Structural analysis becomes especially important for the

assessment of the fatigue life of flexible elements of a FOWT.

Structural modelling is inherently related to the aerodynamic loading on the turbine. Meaning that the aerodynamic loading influences the structural part and vice versa. Therefore, the structural loading on the blades is performed in so called aero-elastic models. These models combine the aerodynamic and structural calculations. The structural models used in these aero-elastic models can be categorized into two groups: 3D Finite Element Method (FEM) model and 1D beam model. The 3D FEM model is used to analyze the detailed stress distribution of a wind turbine blade. 3D FEM model is computationally expensive and therefore not desirable in aero-elastic modelling. In contrast to the computationally expensive 3D FEM model, a 1D beam model can be deployed which is much faster with respect to computational time. Therefore, almost all aero-elastic codes model the wind turbine blades as a series of 1D beam elements instead of 3D shell elements. Mostly, the Euler-Bernoulli beam model is used due to its simple implementation in aero-elastic models. In this model, in contrast to the Timoshenko beam model, the shear deformation effects are ignored.

Three discretisation methods are commonly used to discretise the turbine blade in series of 1D beam elements, i.e. modal approach, Multi Body Dynamics (MBD) models and 1D FEM. In the modal analysis approach, the deflection of the flexible body is a linear combination of mode shapes. The modal analysis approach is computational efficient but limited with respect the number of Degrees of Freedom (DoFs). In the MBD model, the turbine blade is discretised into a number of bodies connected to each other by springs or joints. The dynamics can be calculated by solving the equations of motion of the multi body system. The 1D FEM model approach provides the most accurate deformations of the turbine blades, but is slightly more computational demanding than the other two.

2.5.5 Control Models

The modelling of the generator torque and blade pitch control is typically done by using two Proportional Integral Derivative (PID) controllers. One for the generator torque control and one for the variable blade pitch control. At wind speeds below rated condition, the blade pitch controller is not active and the generator torque controller is active to maintain optimum rotor speed. With increasing wind speeds, passing the point of rated power, the variable blade pitch control is active and pitches the blades to extract less (than available) power from the wind to keep the power constant at rated power. While the generator torque control sets the desired generator torque.

Chapter 3

Literature report

This chapter presents a literature review of topics which are related to the research carried out for this thesis. At first, papers are presented of state-of-the-art aero-hydro-servo-elastic modelling tools. Thereafter, a description is given of a set of papers which cover simplified modelling. At last, from the papers about simplified models found in literature, a gap analysis is provided. The thesis is build upon the gap as presented in this literate report.

3.1 State-of-the-art design tools

In this section, literature concerning state-of-the-art models is given, together with additional literature which supports the understanding of the dynamic behavior of Floating Offshore Wind Turbines (FOWTs). It provides an overview of different floating wind modelling approaches found in literature. Only papers are presented which include the complete system dynamics of floating wind turbines. That is, the coupling between aerodynamics, hydrodynamics, controller dynamics and structural dynamics of tower and rotor blades. The first set of papers describe the integration of independent, existing hydrodynamic and aero-elastic tools for determining the complete system dynamics of a FOWT. An overview is given of several design tools, and how they include the aerodynamics, hydrodynamics, controller dynamics and structural dynamics. Thereafter, standalone codes are presented where one simulation tool is used for the full dynamic analysis.

3.1.1 Offshore Code Comparison Collaboration (OC3)

As limited data is available of floating wind turbines, there is a need to verify the accuracy of the state-of-the-art models. Therefore, to test the accuracy and correctness of new developed dynamic simulation tools, the Offshore Code Comparison Collaboration (OC3) was developed. The OC3 project focused on verification and benchmark exercises for the floating wind industry. The main activities were: discussing modelling strategies, developing benchmark models and simulations, running simulations and processing and comparing results [15].

aNySIM with Phatas (Gueydon et al. [10])

In this paper, Gueydon et al. [10] presented a coupling between an aero-elastic time-domain computer program, Phatas and a multi-body time-domain simulation program for the analysis of floating structures, aNySIM. Phatas computes the interaction between the total aerodynamic loads integrated with the structural dynamics of the tower and rotor blades, and includes a coupling with a wind turbine controller. The aerodynamic loads are solved on the basis of BEM theory with several corrections like: yawed conditions, unsteady rotor loading, dynamic stall and flow around the blade tips and root [10]. The aNySIM program accounts for the wave loading, current loading, floating body motions and mooring dynamics. The hydrodynamic loads are determined based on the potential flow theory by using a panel model. The frequency dependent potential damping and added mass are translated into the time-domain by using retardation functions. For the coupling of the two software, Phatas has been re-structured such that it could be called as a Dynamically Linked Library (DLL). As a result, the calculated positions, velocities and forces are exchanged and updated between the two programs. In this paper, they modelled a rigid floating structure with quasi-static mooring and flexible tower and

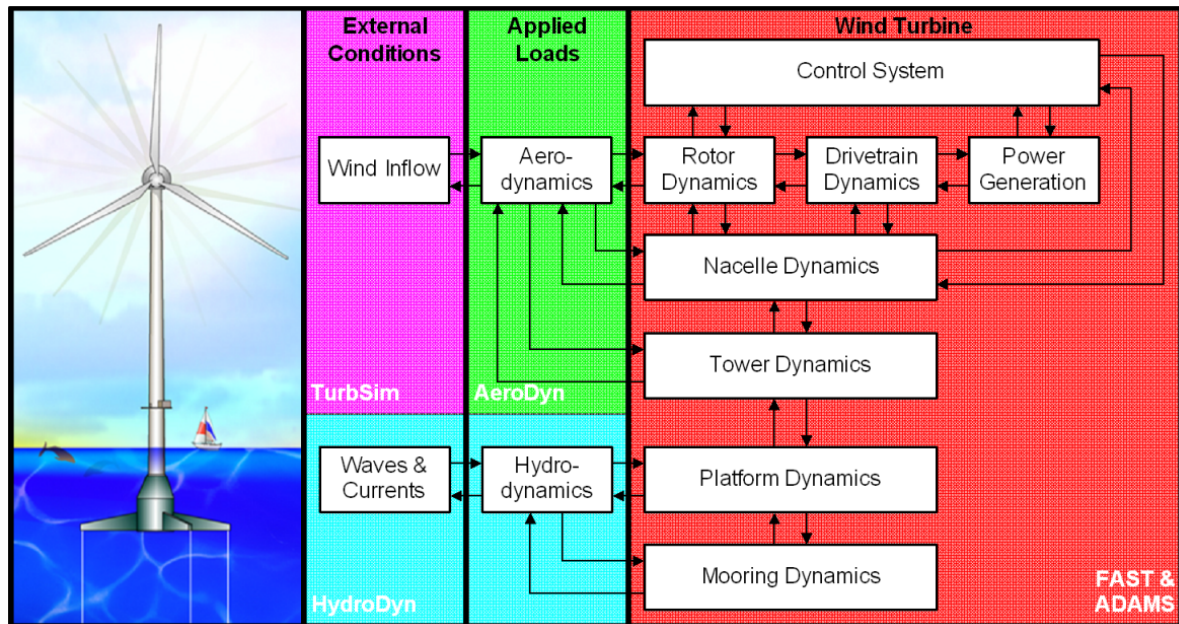


Figure 3.1: Integrated modules in aero-hydro-servo-elastic simulations [17]

turbine blades. The coupled software, aNyPhatas, has been compared with the OC3 results. They found out that the comparison in turbulent wind was not good, due to discrepancies in the turbulent wind field among the OC3 results. Limiting discrepancies in the input wind data was found to be important when codes are compared.

Ansys-AQWA with Phatas (Huijs et al. [12])

Huijs et al. [12] developed a coupled model for the comparison with model tests of the GustoMSC Tri-Floater. Here, the hydrodynamic time-domain software Ansys-AQWA is coupled with the previously described aero-elastic software Phatas including the controller. Ansys-AQWA calculates the hydrodynamic loading using a potential flow diffraction model. Using retardation functions, frequency dependent coefficients can be used in the time-domain. As in aNySIM, Ansys-AQWA allows for including an external model by using a DLL. Here, the floater and tower are assumed rigid while for operational cases the turbine blade deformation is included. They compared the time-domain coupled simulations with spectra calculated with an uncoupled frequency domain analysis. The motions and accelerations were well predicted in the wave frequency domain (0.3 - 2.0 rad/s). In the low frequency range (< 0.3 rad/s), the coupled time-domain simulations show large responses around the platform natural motion frequencies, which were unable to be captured by the uncoupled frequency domain analysis. They concluded that uncoupled frequency domain analysis can be applied to assess wave frequency response in an early design phase. However, if low frequency responses are important to assess, fully coupled time-domain simulations are absolute necessary.

FAST with HydroDyn (Jonkman [17])

In the technical report written by Jonkman [17], the development of a fully coupled aero-hydro-servo-elastic simulation tool for modelling the dynamic response of floating wind turbines is described. He interfaced the aero-servo-elastic onshore wind turbine software FAST with AeroDyn and MSC.ADAMS with AeroDyn with hydrodynamic wave-body interaction programs SWIM and WAMIT. The interfaced modules are depicted in Fig. 3.1. This overview can be considered as a general overview of the integrated system dynamics in a floating wind turbine, showing all the interactions between the system dynamic components. AeroDyn determines the rotor aerodynamics based on BEM theory, including tip and hub losses, or a Generalized Dynamic Wake (GDW) model. In the hydrodynamic model, nonlinear hydrodynamic effects like second order wave forces were not included. Also, the model does not include mooring line dynamics. The platform is considered rigid, while the tower and blades are included as

flexible members. He verified his developed tool by model-to-model comparisons. Also, he compared the results with frequency domain analysis, which were shown to be in good agreement.

FAST with Charm3D (Bae and Kim [1])

Bae and Kim [1] developed a coupling between FAST and Charm3D, where the latter is a floater-mooring coupled dynamic analysis program in the time-domain. The hydrodynamic coefficients including added mass, damping, first and second order wave forces are obtained by WAMIT. By retardation functions, these frequency dependent coefficients were able to be utilized by Charm3D. Here, they investigated the dynamic coupling effects between the rotor and floater by comparing coupled analyses to uncoupled analyses. In the coupled simulations, the tower and blades were considered flexible, while in the uncoupled simulations the tower and blades were considered rigid. They concluded that flexible turbine blades and tower cause high-frequency vibrations which are mainly important in the fatigue life assessment of a floating wind turbine.

SIMO/RIFLEX (Ormberg and Bachynski [30])

Ormberg and Bachynski [30] developed a coupled analysis tool for floating wind turbines with the use of SIMO/REFLEX, which is a time-domain software developed for the modelling and simulation of offshore structures. SIMO solves the rigid body hydrodynamics of the hull, whereas RIFLEX includes a finite element solver. The paper describes the extension of RIFLEX to include aerodynamic forces on elastic blade elements, with BEM theory. The hydrodynamics are calculated using the frequency dependent hydrodynamic coefficients, including Morison's equation. All system components are included in a nonlinear FEM model. The developed model has been compared with an external aerodynamic simulation tool AeroDyn. The comparison of the models have shown good agreement. The tool is also compared with the OC3 results in which the results have shown good agreement with existing codes.

SIMO/RIFLEX and HAWC2 (Nielsen et al. [28])

For the development of the simulation tool presented in this paper, two existing (independent) tools have been used for the coupling. HAWC2 is an aero-elastic tool for the analysis of horizontal axis turbine response in the time-domain. SIMO/RIFLEX is a simulation tool for simulating the dynamic response of floating structures. The hydrodynamic loads are calculated using Morrison's equation. For large volume structures, the software needs to be coupled to a specific wave analysis software that uses the hydrodynamic coefficients calculated using 3D diffraction software. The aerodynamic part of the model is based on BEM theory including dynamic stall, dynamic inflow, skew inflow, shear effects and effects from large displacements. Nielsen et al. [28] successfully coupled the two simulation tools for the analysis of floating wind turbines. They modelled the Hywind floating wind turbine and tested the numerical results with model test data and found very good agreement between the responses.

Other codes

Other codes which are solely developed for the dynamic analysis of floating wind turbines are also found in literature. In these codes, all system dynamics are combined in one code and can be seen as stand-alone codes. Bladed, for instance, is developed by GL Garrad Hassan [7] primarily for wind turbine industry manufacturers for the design and certification of onshore and (floating) offshore turbines. 3Dfloat is specifically developed to serve as a platform for innovation, research and education of aero-hydro-servo-elastic simulations [29]. DeepLines Wind is a software program designed in particular for the assessment of the dynamic response of floating and fixed-bottom wind turbines in offshore conditions [35]. Ashes is developed for the integrated dynamic analysis for onshore and (floating) offshore wind turbines, with the main focus to enable best user experience possible [40].

3.1.2 Concluding remarks

From the papers described above, it can be concluded that much effort has been put into the development of state-of-the-art modelling tools by either coupling existing tools or developing stand-alone tools. The reason for the development of these tools, is the challenging integration of the different interacting (aero-hydro-servo-elastic) system dynamics. Despite the computational time demanding tools, state-of-the-art tools are inevitable for a detailed design of a floating wind turbine in a later stage.

3.2 Simplified models

The fully coupled state-of-the-art design tools as described in the section above, include a full interaction between the aerodynamics, hydrodynamics, control dynamics and structural dynamics. In time-domain modelling, the equations of motion are solved for a reference period for 1 hour. As for the most time-domain models the time step of the aerodynamics is smaller than for the hydrodynamics. A lot of effort is put into the aerodynamic modelling (due to the relative complex aerodynamics). Therefore, the aerodynamic calculations are considerably more time demanding than the hydrodynamic calculations. As a result, the duration of a simulation of 1 hour reference period equals 1 hour of calculation time. Moreover, as these calculations require a detailed description of the system (which is generally not present in a concept phase, as the goal is more regarding optimizing a floater design), the simulation set-up is rather complicated. Although fully coupled time-domain simulations are essential in a later design of a floating offshore wind turbine, there is a need for simplified models which are faster and require a less detailed description of the system. For instance, simplified models can be used to assess different design concepts with their fundamental behavior and for parametric optimisation.

In this section, literature regarding simplified models is discussed. Several approaches for simplified modelling, as published in literature, are described. In general, these approaches can be categorised as simplified nonlinear time-domain models or linearised frequency domain models. Examples from literature are described below.

Simplified method for coupled analysis of FOWTs (Karimirad and Moan [20])

Karimirad and Moan [20] presented a simplified approach for dynamic response analysis of floating wind turbines. The method relies on the simplification of aerodynamic forces on floating wind turbines in the time-domain, with the use of a constant c_T . The goal of the approach presented in the paper is to investigate a simplified method for the aerodynamic forces, to speed up the computation time significantly with acceptable accuracy. It uses an external DLL, which is used for the external simplified aerodynamic input for a spar type wind turbine.

In the method they simplified the aerodynamic loads and applied the thrust forces as function of the relative wind speed. The aerodynamic forces are applied at the rotor center. The thrust force at each time step, is dependent on the instantaneous relative wind speed, v_{rel} , considering the platform motion and is calculated by Eq. (3.2.1). Where ρ_a is the air density, R the rotor radius and c_T the thrust coefficient given as a function of the relative wind speed, see Fig. 3.2. However, they did not include the gyroscopic effect in their analysis. A filter is applied on the relative wind speed to model a control system with a very simplistic approach. However, the filter is not automatically enabled or disabled depending on the operational condition. For a turbulent wind field at rated condition there may be a loss of the damping effect when the wind speed is above or below rated condition.

$$T = \frac{1}{2} \rho_a R^2 c_T v_{rel}^2 \quad (3.2.1)$$

To include the behavior of the controller in the above rated region, the relative wind speed is filtered to remove the velocities of the wind speed close to the pitch natural frequency. The filtered velocity is then used to look up the relative wind speed dependent thrust coefficient (c_T). Subsequently, the aerodynamic thrust force on the center of the rotor is calculated using Eq. (3.2.1). By doing this, the negative damping effect for the pitch motion is eliminated, above rated condition. The filter on the wind speed is not active below rated wind speeds. The simple model is validated against a comprehensive aero-hydro-servo-elastic simulation, and the results show that the wave-only case, as well as the wave and wind cases agree well. However, in the paper they did not account for yaw rotation in case the wind and waves are not co-linear. Also, they were unable to implement the tower dynamics, which might have an effect on the surge and pitch natural frequencies. It seems that they were not able to automatically apply the filter for wind speeds around the rated wind speed, which might be important in the case the filter is disabled when the turbine experiences above rated wind speeds.

Reduced nonlinear spar model OC3Hywind (Sandner et al. [36])

A way to simplify the numerical models, and thereby speeding up the calculation, is by using reduced-order models. It means that the model is reduced to only a set of relevant DoFs. In this paper,

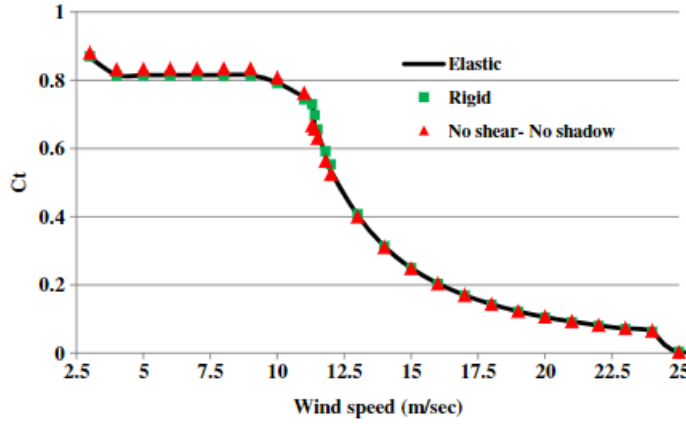


Figure 3.2: Thrust coefficient for a land-based 5MW wind turbine [20].

they presented a reduced-order model in the time-domain for a spar floating concept. For the simplified model, they focused on the unconstrained 3D platform motion, rotor speed, blade pitch angle, tower top displacement and main internal forces. Higher frequency structural modes, such as blade and generator flexibility are not covered in this research. By reducing the number of DoFs to nine, a relative simple model is build.

The aerodynamics, as well as the mooring line model, are simplified using interpolations of pre-processed look-up tables. The lift and drag forces on the rotor blades are calculated using BEM theory in a pre-processing step. This implies that BEM theory, which is an iterative procedure and computational demanding, is avoided in the numerical simulations. Using the pre-calculated c_T and c_P coefficients, which are dependent on the blade pitch and tip speed ratio, thrust and torque can be calculated by only using the relative wind speed. Using the coefficients, the thrust and torque are computed using Eqs. (3.2.2) and (3.2.3), respectively. Where ρ is the density of air, R the radius of the rotor and v_{rel} the relative wind speed, defined by the nacelle velocity $\dot{r}_{rotor,x}$ minus the wind speed v_0 , see Eq. (3.2.4).

To compare the responses of SLOW with FAST at above rated condition, a conceptual PI-controller is developed.

$$F_{aero} = \frac{1}{2} \rho \pi R^2 c_T(\lambda, \theta) v_{rel}^2 \quad (3.2.2)$$

$$M_{aero} = \frac{1}{2} \rho \pi R^3 \frac{c_P(\lambda, \theta)}{\lambda} v_{rel}^2 \quad (3.2.3)$$

$$v_{rel} = \dot{r}_{rotor,x} - v_0 \quad (3.2.4)$$

In this paper, they achieved a real-time factor of around 100. Which means that the simulation is about 100 times faster than the simulated time. This method, however, depends on the use of a BEM solver in the pre-processing step. Therefore, for each wind speed, the thrust and torque coefficients must be determined. Also, for the hydrodynamic model the Morrison Equation is used, which is valid for slender structures but not for structures with larger water plane areas, such as a semi-submersibles where radiation and diffraction play an important role.

Quick Load Analysis of Floating wind turbines(QuLAF) (Pegalajar-Jurado et al. [33])

QuLAF is a simplified model in the frequency domain, which represents the aerodynamic loads through pre-computed rotor loads and aerodynamic damping coefficients. This model is an improved model of the developed simplified frequency domain code with two DoFs, as presented in Pegalajar-Jurado et al. [32]. The model relies on the use of state-of-the-art model tools, from which pre-computed hydrodynamic and aerodynamic data are extracted. The hydrodynamic properties are pre-computed with WAMIT, while the aerodynamic loads and mooring forces are pre-computed with FAST. In this model, four DoFs are solved: floater surge, floater heave, floater pitch and elastic deformation at the wind turbine tower top.

The aerodynamic damping is extracted from decay simulations in the time-domain for all relevant DoFs, to include the effects of the controller, see Fig. 3.3. For each wind speed, a simulation in steady wind and calm water is carried out with rigid foundation and tower and with an active controller. The time series of the aerodynamic loads are stored. The decay simulations were carried out with all hydrodynamic and structural damping disabled, such that the aerodynamic damping is the only contributor to the damping. A damping ratio is determined by Eq. (3.2.5), where d_i is the logarithmic decrement, n is the number of decaying peaks and the ζ_{aero} the local damping ratio for a given degree of freedom and wind speed [33].

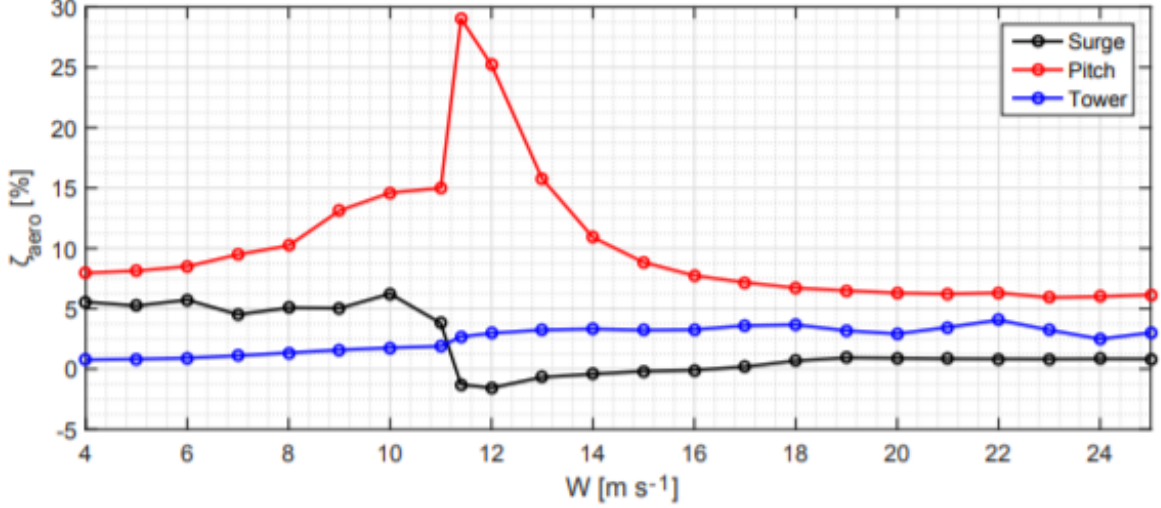


Figure 3.3: Aerodynamic damping ratios as function of wind speed for different degrees of freedom [33]

$$d_i = \log \frac{x_{\text{hub},i}}{x_{\text{hub},i+1}}, \quad \Rightarrow \quad \zeta_i = \frac{d_i}{\sqrt{4\pi^2 + d_i^2}}, \quad \Rightarrow \quad \zeta_{\text{aero}} = \frac{1}{n-1} \sum_1^{n-1} \zeta_i. \quad (3.2.5)$$

The damping ratios for the specific degree of freedom are then converted to a damping coefficient as function of wind speed by,

$$b_{\text{aero},i}(W) = 2\zeta_{\text{aero},i}(W)\sqrt{C_{ii}(M_{ii} + A_{ii}(\omega))}, \quad (3.2.6)$$

where C_{ii} , M_{ii} and A_{ii} are the stiffness matrix, mass matrix and added mass matrix, respectively for the specific DoF. Since the decay simulations are carried out in steady wind, but the damping coefficients are used in the model with turbulent wind, an averaging is applied on the turbulent wind. This is done by estimating the probability of occurrence within the wind speed time series of each discrete value of W . Then, the aerodynamic coefficient for a given turbulent wind condition is given by

$$b_{\text{aero},i} = \sum_{j=1}^{N_w} \text{PDF}(W_j) b_{\text{aero},i}(W_j), \quad (3.2.7)$$

where PDF is the probability density function.

Looking at the computational speed, this model performs with a ratio of simulated time to Central Processing Unit (CPU) time of around 1400 for a 1-hour simulated time. Therefore, this frequency model looks very suitable for early conceptual design stages. In this paper, there is a need for state-of-the-art simulation models such as FAST. Also, a controller needs to be present. However, this level of detail is generally not available in a conceptual design stage of a floating wind turbine.

Simplified Low-Order Wind turbine (SLOW) (Lemmer et al. [22])

The simplified floating offshore wind turbine model SLOW, developed at the University of Stuttgart, aims at a fast simulation of the nonlinear coupled dynamics. The main simulation outputs, as in Sandner et al. [36] are the unconstrained 3D platform motions, rotor speed, blade pitch angles, tower top displacements and main internal forces. The approach in this model is the same as described in Sandner et al. [36], however, the hydrodynamic forces in the reduced model are calculated using potential theory and Morrison Equation is not used. Results from a simulation with the state-of-the-art FAST model was used as benchmark. They concluded that SLOW was capable of predicting the fatigue performance in operating conditions. In extreme conditions, however, SLOW was in limiting agreement with the results of FAST. The differences were attributed to the difference in control, damping and mooring system models.

Frequency domain modelling of floating wind turbines (Lupton [25])

Lupton [25] presented a linear numerical tool in the frequency domain for the analysis of the OC3-Hywind spar floating wind turbine. In the numerical tool he reduced the DoFs to eight. Three platform modes, floater surge, pitch and heave, two tower modes and one blade mode per blade. Linearised models of the structural dynamics, hydrodynamics, aerodynamics, and control system dynamics were developed and integrated to find the overall linear response of the system under the action of harmonic wave and wind loading for the OC3-Hywind spar floating wind turbine. Linear hydrodynamics were included by a potential flow method. The aerodynamics were linearised using harmonic and tangent linearisation approaches. Mooring loads are included as linear stiffness matrices. The frequency domain code was benchmarked against Bladed, a state-of-the-art simulation tool. The frequency domain linear numerical tool was 37 times faster than Bladed. In the model he did not take into account second order wave forces and viscous forces. Also, he was not able to fully capture the control behavior.

Preliminary design of FOWT support structure and cost assessment (Casale et al. [3])

To fully eliminate the coupling between the platform motions and the aerodynamic rotor thrust, the rotor thrust is assumed to be constant regardless of the platform motions. By assuming constant thrust, the low-frequency loads due to the wind are eliminated. It also means that any control action is not present. This approach makes the overall behavior too simple, to be comparable with fully coupled time-domain simulations.

3.2.1 Concluding remarks

From the papers it becomes clear that there exist frequency domain simplified codes and time-domain simplified codes. Although, frequency domain models are significantly faster in terms of computation time, they do not capture the nonlinear behavior present in the dynamics of a floating wind turbine. In frequency domain models, loads are considered that depend linearly on the response and its time derivatives. They are unable to capture loads that depend nonlinear on the response, such as the controller behavior and mooring loads. In frequency domain models, these nonlinear effects are then simplified and linearised which give less accurate results compared to nonlinear models. Therefore, in this thesis, it is decided to use time-domain modelling since the focus is on the prediction of the (nonlinear) motions and mooring loads of a floating wind turbine in the concept design phase.

3.3 Literature gap

A gap analysis is made after researching literature. Concerning fully coupled state-of-the-art modelling simulations, it is concluded that these simulations are indispensable in the complete design of a floating offshore wind turbine. However, in an early design stage, the fully coupled simulations require a high level of detail of the total system (mainly from the aero-elastic side). The papers about state-of-the-art modelling tools provided a clear and rough sketch of the current situation of available literature in floating wind. It helped to get a better understanding of (1) the (challenging) dynamics involved in floating wind, and (2) the need for simpler and faster models in the concept design phase of a floater.

As can be concluded from the literature relating to the simplified models, the need for simplified models is confirmed, and attempts have been made to develop such models. Whereas QuLAF and SLOW still depend on pre-processed data of state-of-the-art aerodynamic modelling tools, the simplified model of

Karimirad and Moan [20] only depend on the thrust and power curves of a specific wind turbine. Also, frequency and time-domain simplified models can be distinguished in literature. In this thesis, a choice is made to develop a simplified model in the time-domain, since it is able to accommodate the nonlinear motions and mooring loads without compromising their accuracy.

It has been decided to develop a simplified code analogous to that of the simplified method as presented in the paper of Karimirad and Moan [20]. They captured the behavior of the control in the above rated conditions by applying a filter on the relative wind speed to include the effect of the controller on the thrust force. The calculated thrust force is based on the thrust curve as given for a wind turbine. From the paper, however, it is not really clear what filter they applied to filter the velocities close to the pitch natural frequency.

In this thesis, the incoming wind speed is filtered to attenuate the aerodynamic thrust excitation around platform pitch natural frequency. To achieve this, the integration of an external Python code within the multi-body time-domain simulation code aNySIM is investigated. Simplifying the aerodynamics, by means of a Python code, gives a simplified tool for the prediction of the motions and mooring loads of the floating wind turbine.

Also, the implementation of the damping coefficients, as determined in Pegalajar-Jurado et al. [33], in the simplified time-domain model is investigated. This is done to improve the results regarding the negative damping effect above rated condition.

Chapter 4

Fully coupled model

For the analyses throughout this thesis, the floating platform concept developed by GustoMSC is used (Tri-Floater). This chapter briefly elaborates on the coupling of the fully coupled aero-hydro-servo-elastic simulation tool, in which the Tri-Floater with a 5MW NREL reference turbine is modelled. It starts with the description of the wind turbine and floater, after which the (coupled) simulation tools are described.

4.1 Wind turbine

The horizontal axis wind turbine considered in this thesis is a representative utility-scale 5MW wind turbine developed by NREL, described in Jonkman et al. [16]. The wind turbine is a three-bladed upwind variable speed variable blade pitch turbine and developed to support concept studies intended for assessing offshore wind technology. The main properties of the NREL 5MW reference wind turbine are presented in Table 4.1.

Table 4.1: Main properties of the 5MW NREL reference wind turbine taken from Jonkman et al. [16]

Rating	5MW
Rotor Orientation, Configurations	Upwind, 3 Blades
Control	Variable Speed, Collective Pitch
Drivetrain	High Speed, Multiple-Stage Gearbox
Rotor, Hub Diameter	126 m, 3m
Hub Height	90 m
Cut-in, Rated, Cut-out Wind Speed	3 m/s, 11.4 m/s, 25 m/s
Cut-in, Rated Rotor Speed	6.9 RPM, 12.1 RPM
Rated Tip Speed	80 m/s
Overhang, Shaft Tilt, Precone	5m, 5 degrees, 2.5 degrees
Rotor Mass	110 ton
Nacelle Mass	240 ton
Tower Mass	348 ton

4.2 Floating platform

The GustoMSC Tri-Floater concept design is considered in this thesis as the floating platform. The Tri-Floater comprises three columns connected by a deck box above the waterline. Flat steel panels are used, to reduce the complexity of series production. Damper boxes are welded under each column to increase the buoyancy, added mass and hydrodynamic damping. The main dimensions of the floating platform used in this thesis are provided in Table 4.2. Due to its shape, the natural periods of heave, roll and pitch are outside the range where the wave spectrum contains most of its energy. This results in limited first order wave induced motions. An artist impression is shown in Fig. 4.1.

The Tri-Floater is moored with a conventional catenary mooring system, consisting of 3 mooring lines. The mooring system of the Tri-Floater is designed such that it contributes to the stability of the floater. One end of the mooring lines is connected at the main deck level of the floater (using fairleads), in order to minimize the wind overturning moment. The influence of the mooring system on the motions and stability of the Tri-Floater can be found in Huijs [11]. For the basis of design, the design methodology and a detailed description of the floater, the reader is referred to Huijs et al. [14].



Figure 4.1: Artist impression of the GustoMSC Tri-Floater with the 5MW NREL reference wind turbine positioned in the center, in irregular waves.

Table 4.2: Main dimensions of the GustoMSC Tri-Floater mounted with the 5MW reference wind turbine, obtained from Huijs et al. [12]

Hub height above SWL	90.0 m	Depth (keel to main deck)	31.2 m
Radius to column center	36.0 m	Design draft	13.2 m
Column dimensions	8.0 x 8.0 x 24.0 m	Air gap to deck structure	12.0 m
Damper box dimensions	19.0 x 19.0 x 1.2 m	Displacement	3627 t

4.3 aNySIM

The hydrodynamic calculations are done by using the multi-body time-domain software aNySIM (v.12.2.0), developed by Maritime Research Institute Netherlands (MARIN). Typically, the software is applied in the offshore oil and gas industry, for offloading operations, mooring simulations, multi-body lifting operations and dynamic capability studies [10]. aNySIM solves the coupled differential equations at each time step, using frequency dependent wave forces, added mass and damping calculated by a potential flow linear diffraction model. The viscous loads acting on the floater are included by quadratic damping terms. By applying retardation functions, the frequency dependent terms can be used to perform the time-domain simulations [5]. The second order wave forces are included using a full Quadratic Transfer Function (QTF) and current forces are included using current coefficients, for different directions.

4.4 Phatas

The time-domain aero-elastic calculations are performed using Phatas computer program developed by Energy research Centre of the Netherlands (ECN). Phatas accounts for unsteady rotor aerodynamics,

structural dynamics of the tower and rotor blades, drive train dynamics and the control system of the turbine. The aerodynamic loads on the blades of the wind turbine are calculated using the Blade Element Momentum (BEM). The blade flexibility of the wind turbine is included by a non linear deflection model. The Craig-Bampton method is used for the tower flexibility of the wind turbine. However, there is currently no capability to combine floating wind simulations with a flexible tower, because of numerical instability. Therefore, all simulations are performed with a rigid wind turbine tower. An optimized control system, specifically design for the 5MW NREL turbine on the GustoMSC Tri-Floater, is developed by ECN and is described in Savenije [37].

4.5 Coupling aNySIM - Phatas

A modular version of Phatas has been developed for the integration of the wind turbine analysis program with other programs, named 'WTmodule'. Figure 4.2 shows the relation between the modules in the fully coupled model. By providing a DLL, WTmodule can be called by aNySIM such that the aerodynamic forces are applied as external forces on the floater. In the call to WTmodule, the position and motion of the floating platform are communicated at the tower base at every time step. In return, Phatas provides the loads at the tower base together with an inertia matrix to aNySIM. aNySIM solves the equations of motion by using the loads and inertia matrix. By this an aNySIM-Phatas (AnyPhatas) is constructed.

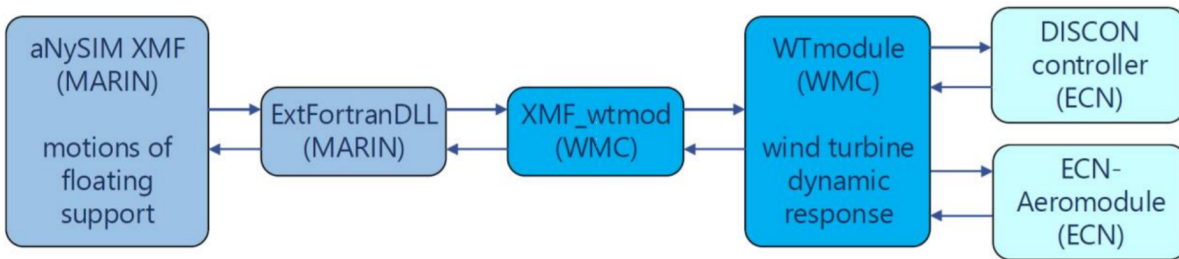


Figure 4.2: Lay-out of the fully coupled aNySIM - Phatas simulation, taken from Huijs et al. [13]

For hydrodynamic and mooring analysis, it is common to perform numerical simulations for a three-hour reference period. The three-hour reference period is needed to obtain statistically independent values for the motions and mooring response of the floater. The typical reference period for wind turbine analyses is ten minutes. The fact that both simulations are integrated, as described earlier, means that the selection of the reference period is a trade-off between calculation time and statistical accuracy. For the sensitivity analysis in this thesis, the total simulation time is set to 70 minutes. From the total simulation time, the first 10 minutes are not included in the post-processing since this is the time which is needed to reach a steady state condition (including wave build up effects). The effective simulation time is therefore reduced to 1 hour.

The wind turbine aero-elastic dynamic response is calculated for more time increments than the hydrodynamic response of the floater, to capture the turbine flexible dynamics. The time step used in the hydrodynamic analysis is 0.05 seconds, while the time step for the wind turbine analysis is 0.0125 seconds. There is no need to reduce the aNySIM simulation time step to the same time step as used for the wind turbine simulation. This approach reduces computational effort significantly. The time increment of the motion of the floating structure is four times larger than the time increment of the wind turbine dynamic response. Therefore, the motions of the floating structure are interpolated between the time steps of the wind turbine dynamic response. The interpolation is done by parabolic splines for each position and rotation, because the solution of the positions and rotations in aNySIM is by definition parabolic in time [23].

Chapter 5

Sensitivity Study

This chapter presents a sensitivity analysis of the GustoMSC Tri-Floater, mounted with the 5MW NREL reference wind turbine. The simulations are performed with the use of the fully coupled aero-hydro-servo-elastic simulation software (aNySIM-Phatas), as described in the previous chapter. The following research question is answered in this chapter:

Which physical phenomena, present in fully coupled aero-hydro-servo-elastic simulations, need to be taken into account in a simplified model?

At first, the sensitivity methodology is described, followed by the description of the available physical phenomena and relevant model outputs. At last, the results are given and conclusions and recommendations are presented.

5.1 Methodology

A sensitivity study is performed to identify the most influential physical phenomena on the mean and maximum motions and mooring loads of the GustoMSC Tri-Floater, using the fully coupled model as described in Chapter 4. The approach of the sensitivity study is based on a hierarchical multi-layered framework, in which the fully coupled aero-hydro-servo-elastic simulation model is decomposed and grouped into a framework of multiple layers. The first layer consists of the four typical physical contributors: aerodynamics, hydrodynamics, control system and structural dynamics. Each physical main contributor comprises different physics. These physics can be excluded from the simulations. As a result, various simulations are constructed each with its own variation. These simulations are then compared to a base case simulation with respect to the mean and maximum motions and mooring loads. The base case simulation is constructed by including all available physical phenomena in the fully coupled aero-hydro-servo-elastic simulation model, marked in green in Fig. 5.1. This base case model is regarded as most accurate in terms of its results, i.e. closest to a real scenario. Thus, the base case model includes a controller adjusted to avoid negative damping, plus all aerodynamic, structural and hydrodynamic effects.

As a simple example, to examine the effect of the floater drag loads on the mean platform surge excursion, two simulations are compared. The first simulation is the base case simulation. The second simulation is constructed by excluding the floater drag in the base case simulation (by setting the drag coefficients to zero). This approach is done for all physical phenomena present in the base case simulation.

5.2 Physical phenomena

In this section, a brief explanation is given on each of the physical phenomena grouped by the main contributor, as presented in the hierarchical sensitivity framework, Fig. 5.1. The section starts with the aerodynamics, followed by the controllers and structural dynamics and at last the hydrodynamics are discussed.

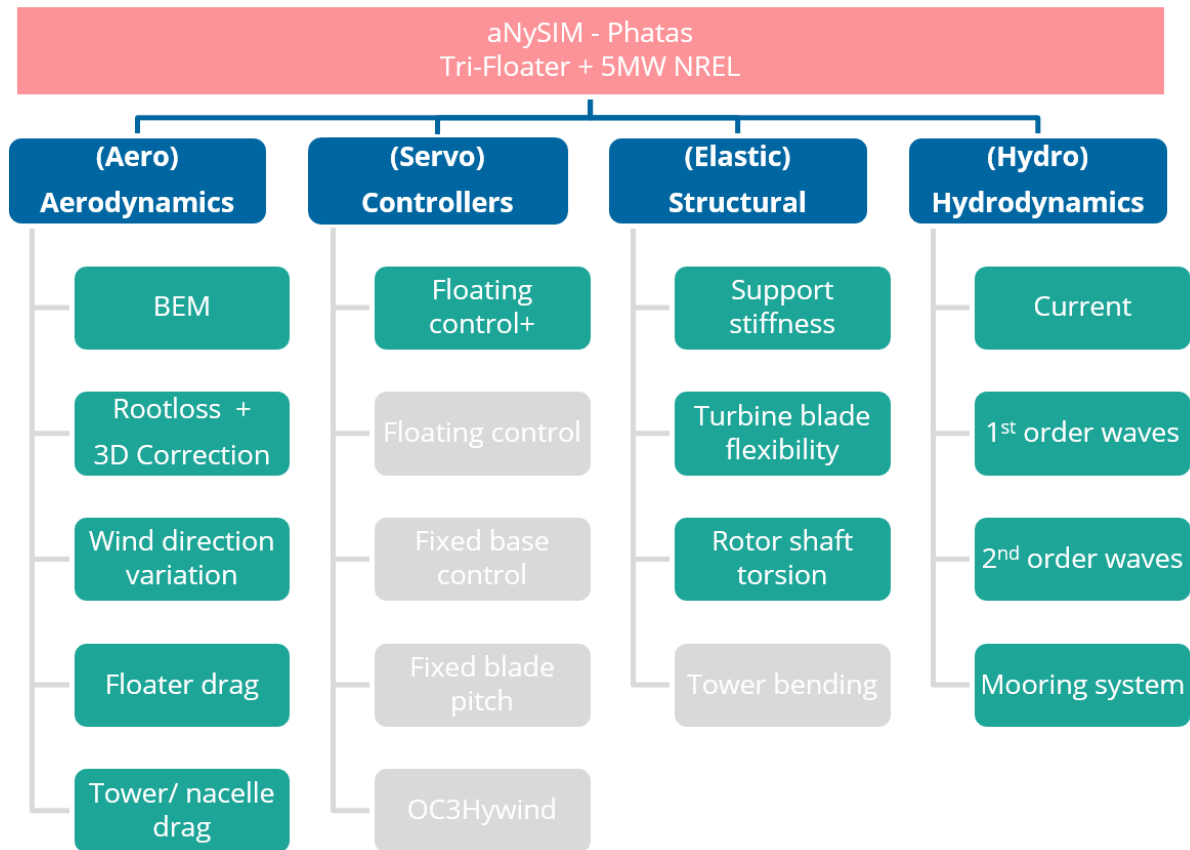


Figure 5.1: Hierarchical sensitivity framework of the fully coupled aero-hydro-servo-elastic simulation model of the Tri-Floater mounted with the 5MW NREL wind turbine. The physical phenomena marked in green are considered to be included in the base case simulation.

5.2.1 Aerodynamics (aero)

Here the aerodynamic physical model inputs are discussed. The aerodynamic loads on the rotor, tower, nacelle and floater are calculated by Phatas.

Blade Element Momentum (BEM) The BEM theory is the governing theory which calculates the aerodynamic loads on the rotor blades. When excluded, no aerodynamic loads on the rotor are calculated and as a result no thrust excitation is present. For more information on BEM theory, the reader is referred to Section 2.5.1.

Root/ tip loss When looking at the radial distribution of a wind turbine blade (starting inwards), the blade is connected to the hub. The hub carries the loads of the blades to the main shaft. The first part of the blade, starting from the root, is generally not shaped as an airfoil in order to minimize the stress concentrations at the blade root. Going radially outwards, the wind turbine blades have a tapered geometry, with the aim to reduce the forces on the blade tip and the moments in the blade root. Root and tip vortices are generated when the airflow slips from a high pressure region to a low pressure region around the blade root and tip. These root and tip vortices trail downstream into the wake and causes downwash. The downwash changes the local direction of the flow, leading to a change in the local angle of attack. The downwash reduces the aerodynamic thrust on the local blade elements. The *root/ tip loss* physical effects are related to this loss of the rotor aerodynamic performance. In Phatas, the loss of aerodynamic thrust loss due to the root and tip vorticity is modelled with the Prandtl factor. The Prandtl factor is a fraction less than one, which indicates a loss. The Prandtl factor is accounted for in the blade element theory, and modifies the local induced flow along the blade after setting the blade element theory equal to the momentum theory.

3D correction A wind turbine blade generally consists of several segments with different NACA airfoils. These NACA airfoil shapes are developed for aircraft wings. A fundamental difference in the inflow of the air of an aircraft wing compared to a wind turbine blade is the rotation of (generally) three wind turbine blades. The blade rotation positively affects the lift coefficients of the blade sections. The *3D correction* due to the rotation implemented in Phatas is based on the method derived by Snel et al. [39].

Wind direction variation The wind loads on the rotor are calculated using a generated turbulent wind field by the program SWIFT, following the Kaimal spectral model. The program generates a cylindrical grid with on each point of the grid a wind velocity vector. The direction of the vector can be either three dimensional, two dimensional or one dimensional. The *wind direction variation* is included in the model to investigate the dependency of the local change in the wind direction. The pre-generated turbulent wind fields are read by Phatas.

Floater drag Floating offshore structures and ships with a large area above the waterline are subjected to wind loads. Dependent on the wind speed, wind direction, surface area and shape, the wind loads may vary on the structure above the waterline. The *floater drag* is calculated as a coefficient based load, using

$$F_{\text{wind}} = \frac{1}{2} \rho C A v^2, \quad (5.2.1)$$

with the air density (ρ), the wind load coefficient (C), the frontal area (A) and the wind speed (v). For each wind direction a set of wind load coefficients is defined for each of the DoFs of the floater. Wind speeds at the height of the floater are less than the wind speeds at the hub, due to wind shear effects.

Tower & nacelle drag For the calculation of the total wind loads on a FOWT, the *tower & nacelle drag* also need to be included. The same coefficient based formula (Eq. (5.2.1)) is used for the determination of the wind load on the nacelle and tower. The tower is generally cylindrical shaped, while the nacelle is more or less box shaped.

5.2.2 Wind turbine controllers (servo)

The controllers, which controls the rotor speed and blade pitch of the wind turbine, are developed separately and included as DLLs in a Phatas input file. This section elaborates on the various controllers included in the simulations.

Floating control+ The *Floating control+* is the most advanced wind turbine controller. It includes floating support damping in the above rated conditions as well as wave induced load reduction, specifically developed for the GustoMSC Tri-Floater.

Floating control The *Floating control* is an extension to the *Fixed base control* and includes the floating support damping in the above rated conditions. This wind turbine controller is adjusted for floating wind turbines.

Fixed base control The *Fixed base control* used in the fully coupled simulations is a wind turbine controller without modifications for floating wind. The controller is used on fixed bottom foundations and does therefore not include floating support damping and wave induced load reduction.

Fixed blade pitch In case the blade pitch is set to a fixed value, a simulation with *fixed blade pitch* is achieved. The fixed blade pitch angle is set to the value corresponding to the wind speed considered. This implies that turbine blades remain at a fixed blade pitch in the below and above rated condition.

OC3Hywind Floating wind turbine controllers are adjusted for specific floater configurations, as the floaters have different motion characteristics. The *OC3Hywind* controller is specifically developed for the Hywind spar buoy of Statoil.

5.2.3 Structures (elastic)

Here the available structural physics are described. The structural dynamic modelling is included in Phatas.

Support stiffness Onshore and offshore wind turbines are generally placed on a foundation in the ground. Dependent on the location and soil properties, stiffness characteristics may vary which results in flexibility of the foundation. The support stiffness on the Tri-Floater is characterised by the steel construction at the tower base.

Turbine blade flexibility Wind turbine blades are slender and have a tapered shape. The main reason for this is to reduce high loads at the tip, resulting in lower bending moments at the blade root. As a consequence, the mass and stiffness distribution along the radial direction of the turbine blades varies. Blade bending deformation can be either an out-of-plane or in-plane displacement. Both DoFs are combined because rotors with a strong blade twist and rotors with pitch control have a strong coupling between in and out-plane bending [24].

Rotor shaft torsion An important element in the drive train of a wind turbine is the main shaft. It transfers the loads from the rotor to the generator. The shaft torsion is subjected to high torsional loads, and can deform elastically.

Tower bending For aero-elastic calculations, tower bending is an important contributor to the structural loads. The flexibility of the wind turbine tower is included based on a modal approach following the Craig-Bampton theory. However, due to numeric instability, the tower bending option was not available and therefore not included in the sensitivity analysis.

5.2.4 Hydrodynamics (hydro)

Considering a fully coupled aero-hydro-servo-elastic simulation, the contribution of aNySIM and Phatas to the total computational time are in the ratio of 1:9, respectively. So clearly, simplifying the aero-servo-elastic part of the simulations can lead to significant reduction in computational time. Therefore, the hydrodynamic physics are not considered in the sensitivity analysis.

5.3 Simplified aerodynamic models

The total set of simulations constructed based on the physical phenomena described in the previous section, is expanded with a set of simulations with simplified aerodynamic models. In these simplified aerodynamic models, Phatas is excluded and the aerodynamic loads are replaced by means of a point force at rotor height. By adding these simplified simulations, a first step is taken towards the exploration of simplified aerodynamic models.

Constant thrust In this simplified simulation, a *constant thrust* is applied at rotor hub height in aNySIM. The magnitude of the constant thrust corresponds to the value found in the steady state thrust curve depending on the mean wind speed, see Fig. 5.2.

Thrust approximation An extension to the constant thrust simplified simulation is achieved by coupling aNySIM with Python. This coupling allows an external force (calculated by Python) to be inserted in the time-integration loop of aNySIM. The external force at rotor hub height in the *thrust approximation* simulation is calculated according to the steady state thrust curve. From the steady state thrust curve, the external force is looked up depending on the relative wind speed. Basically, the external force follows the steady state thrust curve.

Constant C_t This simplified aerodynamic simulation is also constructed by coupling aNySIM with Python. For a given mean wind speed and mean thrust, a dimensionless thrust coefficient is calculated using,

$$Ct = \frac{T}{1/2\rho v^2 \pi R^2}, \quad (5.3.1)$$

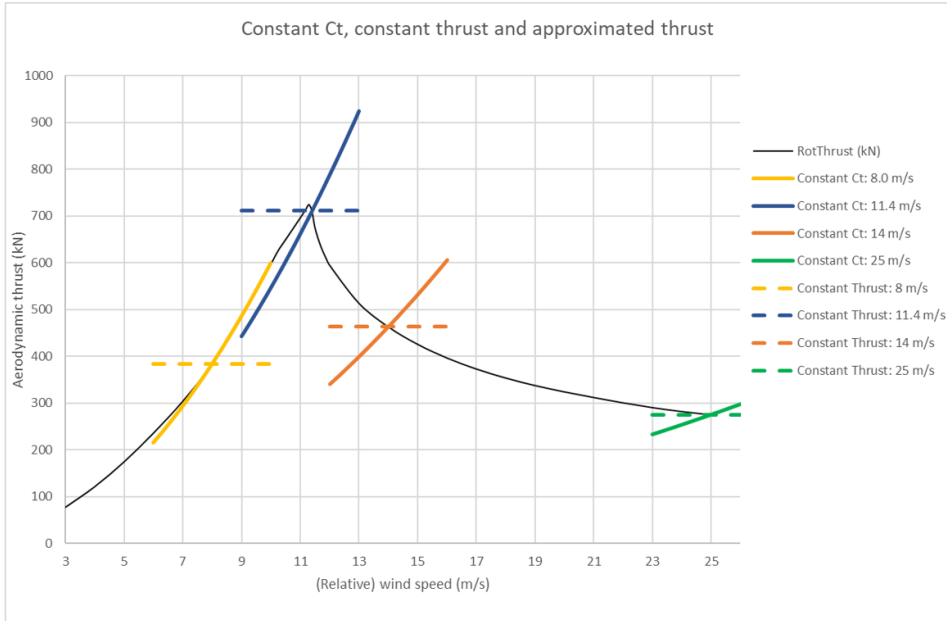


Figure 5.2: Implemented aerodynamic thrust of the simulations with thrust approximation, constant thrust and constant thrust coefficient.

with the aerodynamic rotor thrust (T), the air density (ρ), the relative wind speed (v) and the rotor disk radius (R), see Table 5.1. With the constant thrust coefficient, a thrust force is calculated (in Python) using the same equation as given Eq. (5.3.1) as function of the relative wind speed. Then, the thrust force is applied at the rotor hub height. The relation of the constant thrust coefficient to the steady state thrust curve is displayed in Fig. 5.2.

Table 5.1: Aerodynamic rotor thrust and thrust coefficients for given wind speeds used in the simulations

Average wind speed [m/s]	Aerodynamic thrust [kN]	C_t [-]
8.0	384	0.79
11.4	711	0.72
14.0	464	0.31
25.0	275	0.06

5.4 Model outputs

In early conceptual design phases, the motions and mooring loads of the floater need to be assessed for different environmental conditions to dimension the floating platform (including mooring system). Therefore, a selected set of model outputs are defined. In the analysis, the differences in the mean and maximum of the model outputs for each simulation relative to the base case simulation has been investigated. All model outputs that are selected for the analysis are summarised in Table 5.2.

The motions of the floater are all determined at the same position on the floater, i.e. the Center of Gravity (CoG). The tension in the mooring lines are given at the fairlead positions. Since simulations in the time-domain are used, the results of the model outputs are in the time-domain as well. The time-domain data of the model outputs are first analysed in terms of the mean and the maximum value. The computational time is only given as a percentage of the base case simulation.

Table 5.2: Overview of the model outputs with a short description

Model output	Unit	Description
Platform surge	[m]	Total surge offset of the platform
Platform pitch	[deg]	Total pitch of the platform
Fairlead tension	[kN]	Total tension in the fairlead
Rotor aerodynamic thrust	[kN]	Total aerodynamic load due to the incoming wind
Resultant tower-base bending moment	[Nm]	Resultant tower bending moment in the floating support of the wind turbine
CPU time	[sec]	Total computational time

Power Spectral Density (PSD)

Each simulation is calculated in irregular waves and stochastic wind. To indicate the contribution of different frequency components, a power spectral analysis is used. The spectra of the time series are derived using Fast Fourier Transform (FFT) techniques. In order to distinguish the various frequency components of the model outputs, the frequency regions, as given in Table 5.3, are considered.

Low frequency effects of the turbulent wind are visible below 0.3 rad/s, whereas the effect of the waves can be observed between 0.3 rad/s and 2.0 rad/s. The table also provides important natural frequencies of the floating wind turbine. The frequency axis in the PSDs are plotted on a logarithmic scale, to allow clear visualisation of the low, wave and high frequency variations in one plot.

Table 5.3: Overview of frequency regions together with natural platform surge and natural platform pitch frequency

Frequency region	Frequency [rad/s]
Low Frequency (LF)	< 0.30
Wave Frequency (WF)	0.30 - 2.00
High Frequency (HF)	> 2.00
Platform surge natural frequency	0.084
Platform pitch natural frequency	0.21

5.5 Environmental conditions

The environmental conditions which are assessed in the fully coupled simulations for the sensitivity analysis are presented in Table 5.4. The environmental conditions have been reduced to a set of four typical conditions, and are in accordance with the conditions as presented in Huijs et al. [12].

A Jonswap wave spectra is used for the simulations with a peak enhancement factor of 3.3. A Kaimal wind spectrum is used with a wind shear profile exponent of 0.10. The current is assumed constant over the draft of the floating structure. The wave, current and wind directions are assumed to act collinear with a direction of 180 degrees. Therefore, the upwind mooring line was selected for this study since it is aligned with the incoming wind and wave direction. As a result, this mooring line is subjected to the highest loads.

5.6 Sensitivity results

This section elaborates on the results obtained from the sensitivity analysis. Only rated (11.4 m/s) and cut-out wind speed (25 m/s) are presented, as these two wind speeds are considered to be the most control sensitive wind speeds. The results of the under (8 m/s) and above rated wind speed (14 m/s) can be found in Appendix A.

Table 5.4: Environmental conditions for the simulations used in the sensitivity analysis.

		Operational at under rated wind speed	Operational at rated wind speed	Operational at above rated wind speed	Operational at cut-out wind speed
Significant wave height	[m]	4.5	4.5	4.5	4.5
Wave peak period	[s]	10	10	10	10
10-minute mean wind speed	[m/s]	8.0	11.4	14.0	25.0
Turbulence Intensity (TI) ¹	[%]	13.0	14.7	14.2	13.1
Current velocity	[m/s]	0.6	0.6	0.6	0.6
Wave, current and wind direction	[deg]	180	180	180	180

¹ TI is derived by the standard deviation divided by the average wind speed over 10 minutes.

5.6.1 Rated wind speed: 11.4 m/s

The rated wind speed is the most sensitive control region, mainly due to the fact that the control system is switching between under and above rated condition. In the above rated condition, the wind turbine blades are pitched to reduce the aerodynamic forces, while under rated wind condition the blade pitch is fixed and generator torque is controlled.

Aerodynamic sensitivity

Table 5.5 presents the relative differences in the mean and maximum values of the model output data between the base case and the simulations in which the aerodynamic physics are alternately excluded. At first glance, the simulation with all aerodynamics off indicates the importance of the aerodynamic forces on the motion and mooring loads of the floater. Also, it is seen that the aerodynamics are responsible for large computational time. In case the floater drag or tower & nacelle drag are excluded, the platform motions and fairlead tension show relative large differences. All other aerodynamic physics show to have no significant effect on the model output data.

Table 5.5: Relative differences between the base case and the simulations in which the aerodynamic physics are alternately turned off with respect to the base case

	CPU time	Surge		Pitch		TFairlead		Rotor thrust		Bending moment	
	[%]	Mean	Max	Mean	Max	Mean	Max	Mean	Max	Mean	Max
Aerodynamics OFF	-72	-71	-80	-124	1605	-40	-44	-100	-100	-85	-60
Floater drag OFF	19	-7	-5	3	-3	-4	-6	0	-1	1	1
Tower & nacelle drag OFF	7	-2	-2	-2	13	-1	-2	0	0	-2	1
YZ-direction wind OFF	2	0	-1	0	-55	0	0	0	-1	0	1
Z-direction wind OFF	3	0	0	0	-27	0	0	0	-1	0	0
3D correction OFF	7	0	0	0	-5	0	0	0	0	0	1
Rootloss OFF	4	0	0	0	-6	0	0	0	0	0	2

Figures 5.3a and 5.3b show PSD plots of the aerodynamic thrust and surge excursion for the aerodynamic sensitivity, respectively. Looking at the aerodynamic thrust, it is seen that all aerodynamic physics have no significant effect on the aerodynamic rotor thrust excitation, except when all aerodynamics are excluded (no aerodynamic loading, as expected). The contribution of the floater and tower & nacelle drag to the surge offset is clearly visible in Fig. 5.3b.

Control sensitivity

The relative differences in the mean and maximum values of the model output data between the base case and the simulations in which different controllers (including simplified models) are included, are presented in Table 5.6. From the results, it is seen that the simulations with *constant* C_t , *constant*

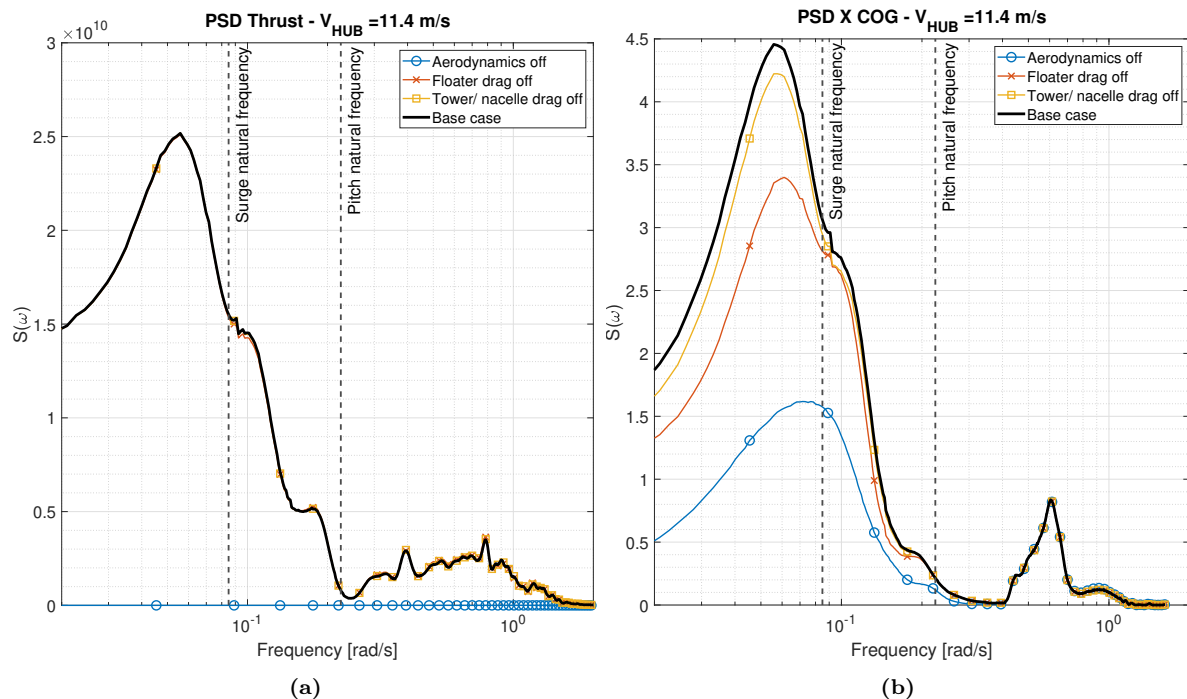


Figure 5.3: PSD of the aerodynamic thrust excitation (left) and platform surge excursion (right) at rated wind speed in 180 deg wave, current and wind direction in which the aerodynamic sensitivity is displayed.

thrust and *thrust approximation* do significantly reduce the computation time. However, the differences in the mean and maximum values of the model output data are significant, especially for the simplified models with constant C_t and constant thrust. The reason for the large differences can be attributed to the thrust deviating from the steady state thrust curve. The simulation of the approximated thrust however, shows promising results compared to the base case simulation. Also, large differences are seen in the output when the blade pitch is not controlled. No large differences are found in the mean and maximum values of the Floating Control, since this controller is almost identical to the base case controller. When simulations are performed with the Fixed Base Control, the unstable platform pitch behavior is clearly observed in the maximum difference.

Table 5.6: Relative differences between the base case and the simulations in which different controllers are included (together with the simplified models)

	CPU time [%]	Surge [%]		Pitch [%]		TFairlead [%]		Rotor thrust [%]		Bending moment [%]	
		Mean	Max	Mean	Max	Mean	Max	Mean	Max	Mean	Max
Constant C_t	-92	-57	-66	-120	1547	-35	-37	32	70	n/a	n/a
Constant thrust	-58	17	44	49	-1302	17	16	30	-10	-62	-43
Thrust approximation	-93	3	9	5	159	2	10	5	-8	n/a	n/a
Fixed Blade Pitch	15	6	-4	20	11	6	24	17	276	18	42
OC3Hywind	10	3	4	142	0	1	6	4	4	4	8
Fixed Base Control	4	0	4	1	-163	0	2	1	0	1	3
Floating Control	10	0	0	0	-13	0	0	0	8	0	2

The PSD plots of the aerodynamic thrust excitation and platform pitch for the control sensitivity are depicted in Figs. 5.4a and 5.4b, respectively. As already concluded from Table 5.6, the simulations with constant C_t and Fixed Blade Pitch indeed show large differences in the aerodynamic thrust excitation and platform pitch response. Taking a close look to the aerodynamic thrust spectrum for the Approximated Thrust simulation, it is seen that the thrust excitation is predicted quite reasonable in the low frequency region. Also, the thrust excitation peak around the natural platform pitch frequency is

clearly visible, which results in significant platform pitch motion as seen in the platform pitch spectrum. The wind turbine controller in the base case simulation lowers the energy around the pitch natural frequency, as expected.

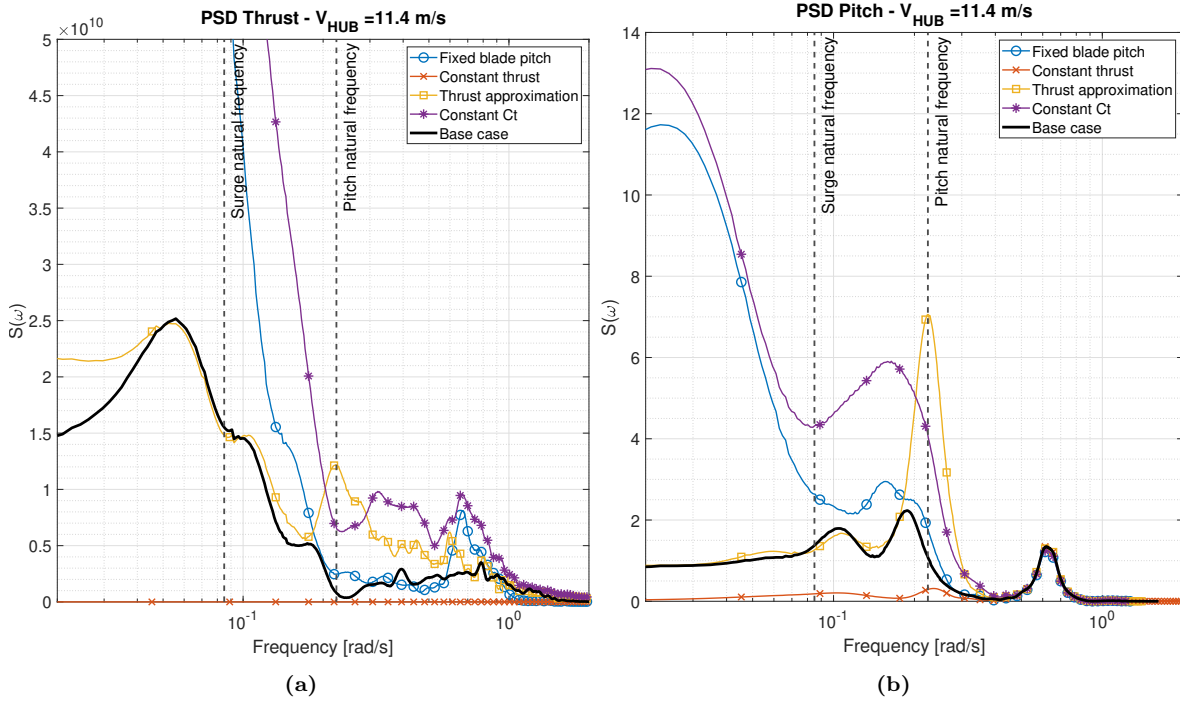


Figure 5.4: PSDs of the aerodynamic thrust excitation (left) and platform pitch (right) at rated wind speed in 180 deg wave, current and wind direction in which the control sensitivity is displayed.

Structural sensitivity

Table 5.7 presents the relative differences in the mean and maximum values of the model output data between the base case and the simulations in which the structural physics are alternately excluding. By excluding the structural physics, the computational time is significantly reduced while all differences are very small, compared to the base case simulation. Interestingly, a significant reduction in computational time is seen in case the shaft torsion deformation is excluded. Slow convergence is expected in the drive train flexibility, as stated in the Phatas manual [24]. Therefore, the computational time significantly reduces while having small differences in the model output data.

Table 5.7: Relative differences between the base case simulation in which the structural physics are alternately turned off with respect to the base case

	CPU time [%]	Surge [%]		Pitch [%]		TFairlead [%]		Rotor thrust [%]		Bending moment [%]	
		Mean	Max	Mean	Max	Mean	Max	Mean	Max	Mean	Max
Structures OFF	-60	2	3	4	-2	1	2	4	9	3	3
Blade flexibility OFF	-62	1	3	4	0	1	2	3	6	4	2
Shaft torsion OFF	-40	0	0	0	-2	0	0	0	-1	0	1
Support stiffness OFF	8	0	0	0	4	0	0	0	0	-1	-1

Figures 5.5a and 5.5b show PSD plots of the aerodynamic thrust excitation and platform pitch response, respectively. Only small differences are visible in the low frequency region.

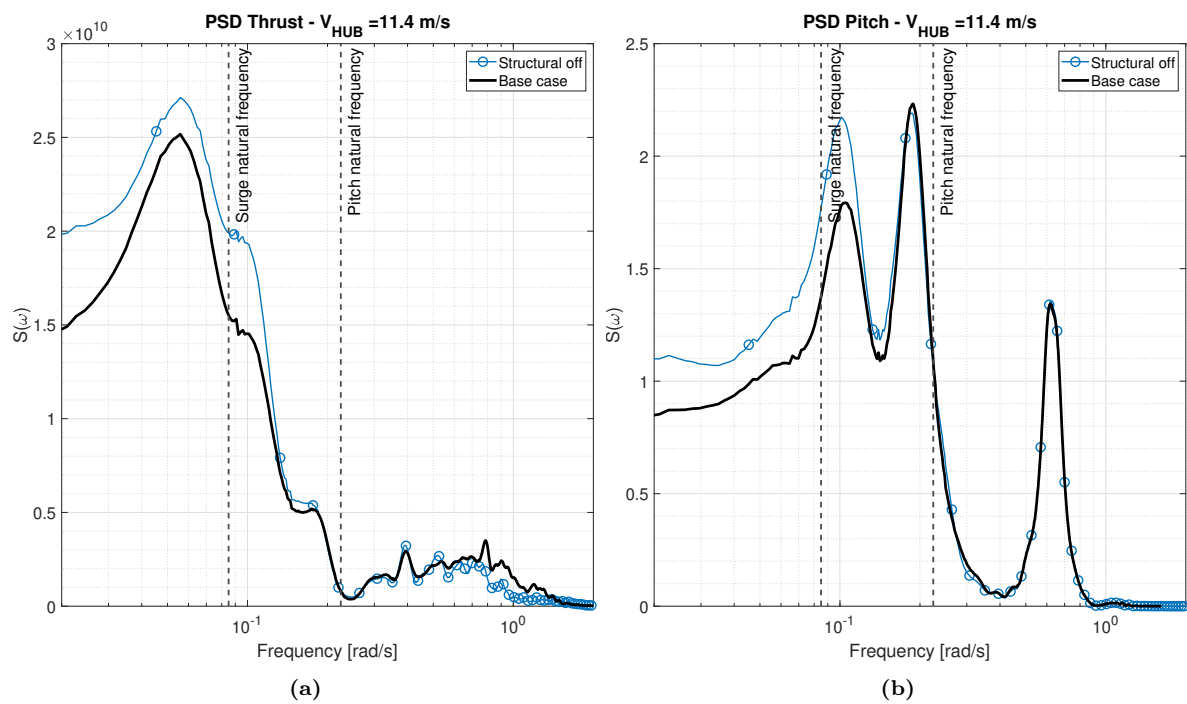


Figure 5.5: PSDs of the aerodynamic thrust excitation (left) and platform pitch motion (right) at rated wind speed in 180 deg wave, current and wind direction in which the structural sensitivity is displayed.

5.6.2 Above rated wind speed: 25 m/s

Another control sensitive region is the region close to the cut-out condition, where the turbine is about to shut-off. Here the wind speed of 25 m/s wind speed is considered which is the cut-out wind speed. At this wind speed, the turbine blades are pitched to almost 24 degrees.

Aerodynamic sensitivity

Table 5.8 presents the relative differences in the mean and maximum values of the model output data between the base case and the simulations in which the aerodynamic physics are alternately excluded. As at rated wind speed, the importance of the aerodynamics on the floater motions and mooring loads are seen and the aerodynamics are responsible for large computational time. In absence of the floater and tower & nacelle drag loads, large differences arise in the platform surge motion, platform pitch motion and forward fairlead tension. For a wind speed of 25 m/s, the contribution of the drag loads on the floater and tower & nacelle are simply higher than for a lower wind speed due to the squared relationship with wind load and wind speed.

Table 5.8: Relative differences between the base case and the simulations in which the aerodynamic physics are alternately turned off with respect to the base case

	CPU time	Surge		Pitch		TFairlead		Rotor thrust		Bending moment	
	[%]	[%]		[%]		[%]		[%]		[%]	
		Mean	Max	Mean	Max	Mean	Max	Mean	Max	Mean	Max
Aerodynamics OFF	-75	-74	-82	-158	49	-41	-51	-100	-100	-76	-70
Floater drag OFF	7	-31	-28	34	-43	-19	-29	0	-1	7	4
Tower& nacelle drag OFF	-8	-8	-8	-24	4	-7	-10	0	-2	-12	5
YZ-direction wind OFF	-6	0	-2	1	-6	0	-1	1	-6	-1	1
Z-direction wind OFF	-7	0	-1	0	-4	0	-1	0	-3	0	0
3D correction OFF	-5	0	0	0	-2	0	0	0	-2	0	1
Rootloss OFF	-5	0	0	0	-2	0	-1	0	-2	0	1

Figs. 5.6a and 5.6b show PSD plots of the aerodynamic thrust excitation and the platform surge excursion for the aerodynamic sensitivity, respectively. As for the rated wind speed, the effect of the aerodynamic physics on the aerodynamic thrust excitation is negligible. However, large thrust fluctuations are seen and a clear thrust attenuation around the natural platform pitch frequency is observed, as a result of the wind turbine controller. From the platform surge PSD, the contribution of the floater and tower & nacelle drag are clearly seen. In case the floater drag is turned off, the spectra almost corresponds to the simulation with all aerodynamics off. At 25 m/s wind speed, the aerodynamic thrust contribution is lower compared to 11.4 m/s rated wind speed.

Control model inputs

The relative differences in the mean and maximum values of the model output data between the base case and the simulations in which different controllers (including simplified models) are included, are presented in Table 5.9. As for the rated wind speed, it is seen that the simulations with constant C_t , constant thrust and thrust approximation significantly reduces the computational time. The differences in the model outputs of the constant thrust are relative small. The reason is found to be in the gradient of the steady state aerodynamic thrust at 25 m/s. The thrust follows almost a constant line with a small negative gradient. Therefore, the horizontal thrust line as implemented in the constant thrust, better predicts the aerodynamic thrust at 25 m/s wind speed compared to the 11.4 m/s rated wind speed. The same goes for the constant C_t simulation. The approximated thrust simulation shows again promising results.

The PSD plots of the aerodynamic thrust excitation and platform pitch for the control sensitivity are depicted in Figs. 5.7a and 5.7b. As already concluded from Table 5.9, the simulations with Fixed Blade Pitch showed large differences in the aerodynamic thrust excitation and platform pitch response. The simulation with constant C_t shows large differences in the low frequency range, due to the positive gradient of the applied thrust. Again, a clear aerodynamic thrust attenuation is seen around the natural platform pitch frequency. No clear instability of the platform pitch is seen around the platform pitch natural frequency, which is directly related to the gradient of the thrust curve.

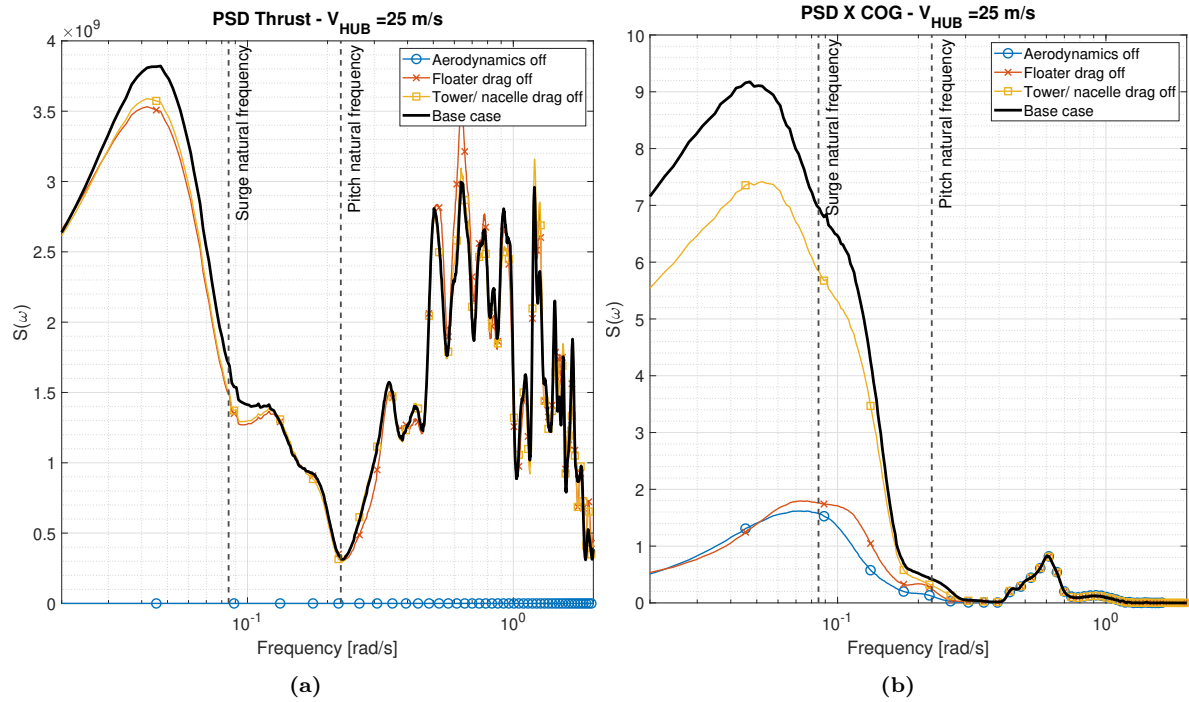


Figure 5.6: PSD of the aerodynamic thrust excitation (left) and platform surge excursion (right) at cut-out wind speed in 180 deg wave, current and wind direction in which the aerodynamic sensitivity is displayed.

Table 5.9: Relative differences between the base case simulation and simulations in which different controllers are included (together with the simplified models)

	CPU time [%]	Surge [%]		Pitch [%]		TFairlead [%]		Rotor thrust [%]		Bending moment [%]	
		Mean	Max	Mean	Max	Mean	Max	Mean	Max	Mean	Max
Constant Ct	-91	2	-9	-34	10	1	9	3	-15	n/a	n/a
Constant Thrust	-66	0	2	5	-36	0	-5	1	-56	-73	-67
Thrust Approximation	-94	3	10	-29	-27	1	-2	6	-38	n/a	n/a
Fixed Base Control	1	0	0	1	12	0	-1	0	-7	0	-7
OC3Hywind	0	0	-5	0	-2	0	1	0	7	1	-6
Fixed Blade Pitch	-3	-16	-34	-122	80	-14	-14	-81	-32	-46	-5
Floating Control	-4	0	0	1	-4	0	-2	0	-2	0	-1

Looking at the Fixed Blade Pitch simulation in the aerodynamic thrust PSD, it is seen that the energy is much less compared to the rated condition. This is as a result of the pitch angle of the blades at the cut-out condition. The turbine blades are pitched by almost 24 degrees. Nevertheless, from the platform pitch PSD it is seen that the platform pitch motion is highly over estimated.

While the mean and maximum values of the constant thrust and thrust approximation simulations do match relatively well, the PSD plots show that they underestimate the thrust and the platform pitch response. As they do follow the same trend as the base case simulation, and have high computational speed, it is worth looking into.

5.6.2.1 Structural model inputs

Table 5.10 presents the relative differences in the mean and maximum values of the model output data between the base case simulation and the simulations in which the structural physics are alternately excluded. By excluding the structural physics, the computational time is significantly reduced, as for the rated wind speed. The differences with respect to the base case simulation remain very small. As

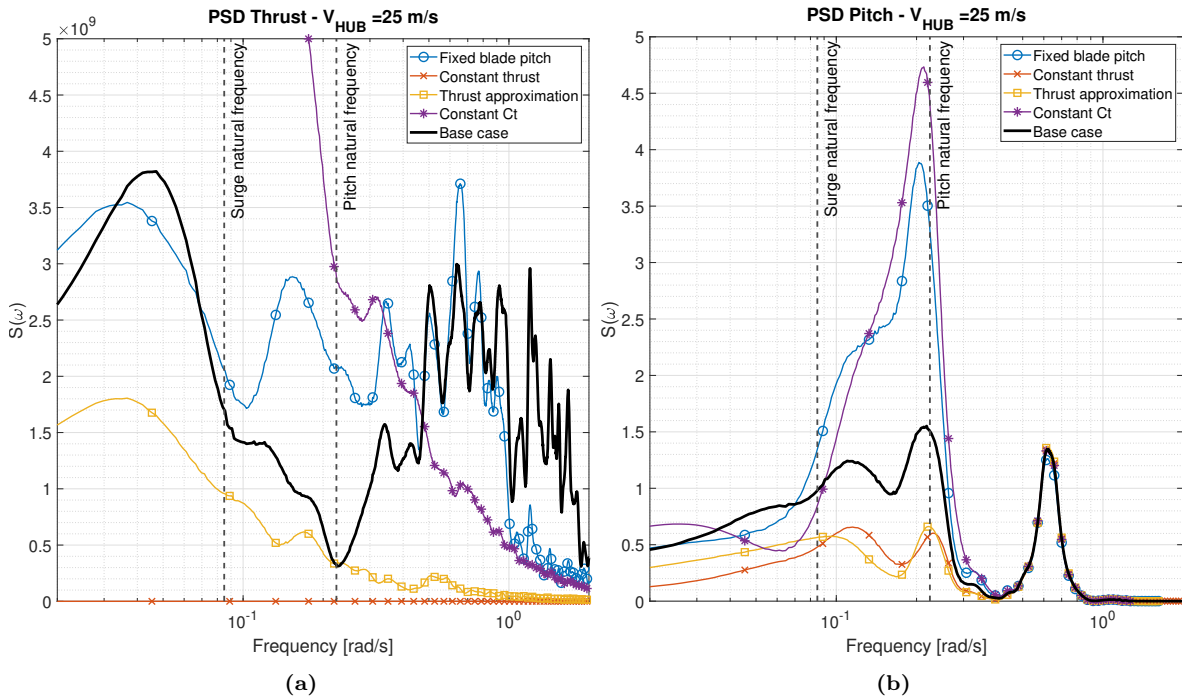


Figure 5.7: PSDs of the aerodynamic thrust excitation (left) and platform pitch motion (right) at cut-out wind speed in 180 deg wave, current and wind direction in which the control sensitivity is displayed.

for the rated condition, the shaft torsion deformation results in significant reduction in computational time due to slow convergence [24].

Table 5.10: Relative differences between the base case simulation and simulations in which the structural physics are alternately turned off with respect to the base case

	CPU time [%]	Surge [%]		Pitch [%]		TFairlead [%]		Rotor thrust [%]		Bending moment [%]	
		Mean	Max	Mean	Max	Mean	Max	Mean	Max	Mean	Max
Structures OFF	-71	-1	-1	-7	2	-1	-1	-4	-4	-4	2
Blade flexibility OFF	-68	-1	-1	-6	0	-1	-1	-4	-5	-4	2
Shaft torsion OFF	-45	0	0	0	0	0	0	0	-3	0	2
Support stiffness OFF	-3	0	0	-1	0	0	0	0	1	-1	0

Figures 5.8a and 5.8b show PSD plots of the aerodynamic thrust excitation and platform pitch response, respectively. The plots confirm the small differences observed Table 5.10.

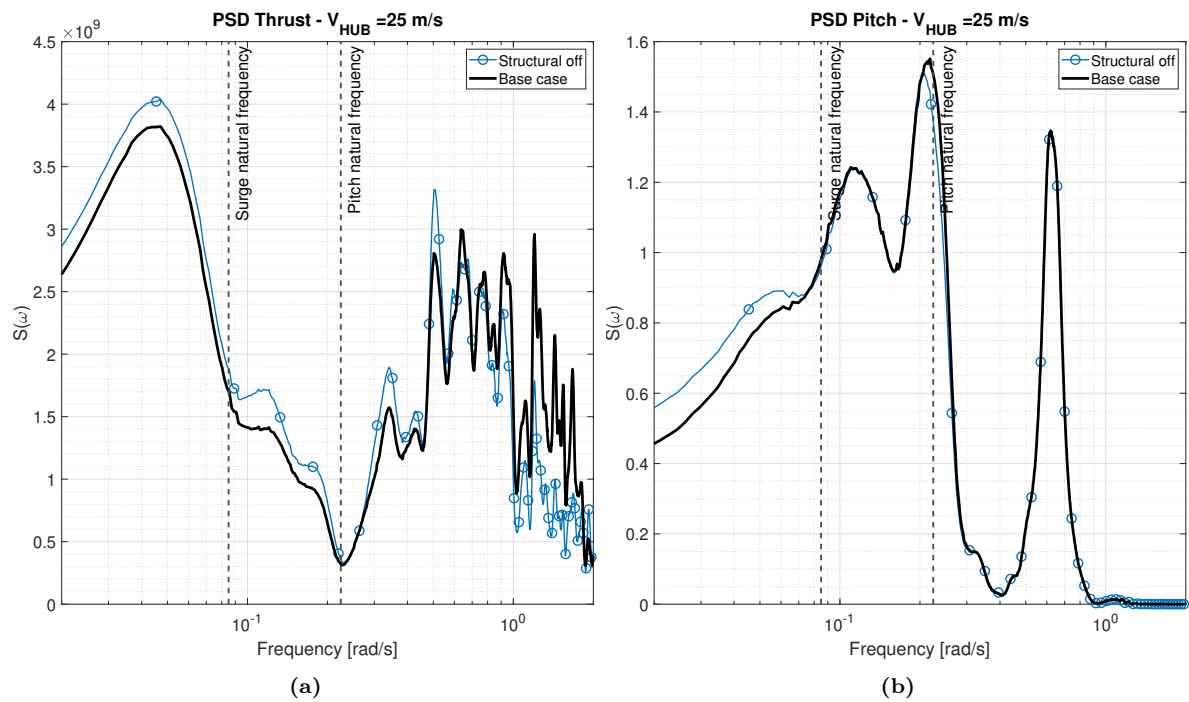


Figure 5.8: PSDs of the aerodynamic thrust excitation (left) and platform pitch motion (right) at cut-out wind speed in 180 deg wave, current and wind direction in which the structural sensitivity is displayed.

5.7 Conclusions and recommendations

The research question formulated at the start of this chapter was:

Which physical phenomena, present in fully coupled aero-hydro-servo-elastic simulations, need to be taken into account in a simplified model?

To answer the research question, a sensitivity analysis is performed. The sensitivity analysis is used to identify the most influential physical phenomena present in fully coupled simulations of the GustoMSC Tri-Floater. The floater, mounted with the 5MW NREL reference turbine, is modelled in aNySIM-Phatas. Simulations are constructed by excluding physics in the fully coupled simulations. Then, these simulations are compared to a base case simulation. Mean and maximum motions and mooring loads of the Tri-Floater are compared, together with PSD plots.

From the differences observed in the mean, maximum and PSD plots the most influential physics are selected to include in the simplified model. Overall, the simulations match very good in the wave frequency range. The largest differences are observed in the low frequency range and around the natural platform pitch frequency. In the following section, the conclusions are drawn for the three main contributors in the sensitivity analysis: aerodynamics, controllers, structural.

Aerodynamics

From the analysis, it is concluded that the aerodynamics do have significant effect on the motions and mooring loads of the floating platform. Simulations are performed without any aerodynamic load which resulted in very inaccurate results. From the results, it is obtained that the BEM theory, without corrections like 3D correction and rootloss, together with the floater, tower and nacelle drag are the main contributors to the platform motions and mooring loads. Therefore, the aerodynamic loads on the rotor together with the wind loads on the floater, tower and nacelle need to be taken into account in the simplified model.

Controllers

Simulations are performed with different controllers, and compared to the base case simulation. It is seen that the base case simulation includes floating support damping by reducing the platform pitch motion around the natural frequency. In the controller sensitivity study, simplified models are also included to explore the feasibility of simplified aerodynamics. In the simplified models, aNySIM is coupled to a Python code. The models show to have high potential with respect to predicting the platform motions and mooring loads, with a large reduction in computation time.

Structures

The differences in mean and maximum motions and mooring loads in case the structural physics are excluded, were very small. The structural physics show to have a significant (positive) effect on the computational time. However, as the focus of the simplified model is on predicting motions and mooring loads of the floater, the structural physics are not considered to be important at this stage.

5.7.1 Recommendations

Tower bending was not available at the time this research was conducted, due to numerical instability of the simulations. For future work however, it would be interesting to investigate the effect of the tower bending modes on the response of the floater.

Chapter 6

Simplified model

In this chapter, the description of the simplified model is given. The following research question is answered:

How can the relevant physical phenomena be integrated in a simplified model?

To start, the simplified model in this study is constructed in the time-domain rather than the frequency domain. The main reason is because of the non linearities in the aerodynamics, wind turbine controller and mooring stiffness. The frequency domain is by definition linear.

The chapter starts with the description of the coupling between aNySIM and Python. The coupling serves as the basis of the simplified time-domain model. Then, the implementation of the main inputs to the simplified model is explained: steady state thrust curve, thrust sensitivities and turbulent wind speed filtering.

6.1 Coupling aNySIM - Python

In this section, the setup of the simplified model is given. The simplified model is constructed by using the multi-body time-domain simulation software aNySIM, developed by MARIN. This software is developed for performing time-domain simulations of floating objects, particular in the oil & gas industry. aNySIM allows for the implementation of a Python module inside the integration loop. The Python module is used to account for the aerodynamic wind turbine response and control behavior, in a simple manner. The lay-out of the coupling of aNySIM and Python, together with the inputs and outputs is illustrated in Fig. 6.1.

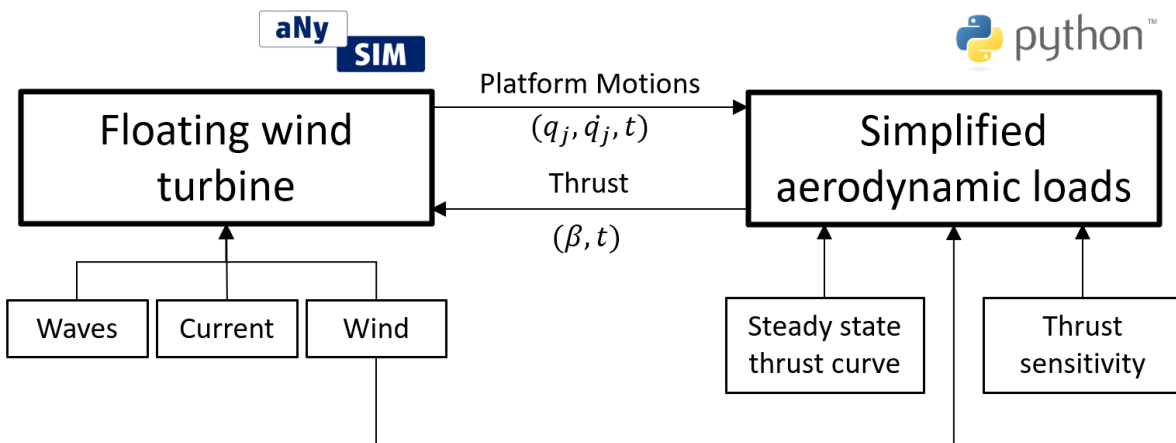


Figure 6.1: Coupling of hydrodynamic software aNySIM with the Python module.

As schematically illustrated in Fig. 6.1, aNySIM outputs the rigid floating platform motions due to wave, wind and current loading. For each DoF, the time dependent motions and velocities are calculated at

the CoG of the platform. The motions and velocities are input for the simplified model, together with the wind speed, steady state thrust curve and thrust sensitivities (which are described later in this chapter). A time dependent thrust is calculated and included into the integration loop of aNySIM. Subsequently, aNySIM solves the equation of motions.

It must be noted that in the current setup of the simplified model, no wind loads on the floater, tower and nacelle are taken into account. However, the inclusion of these wind loads are inevitable in an early concept design phase of a floater. So the remaining force in the simplified model is the simplified aerodynamic thrust, calculated by Python. This simplified aerodynamic thrust is applied at the center of the rotor hub, as depicted in Fig. 6.2.

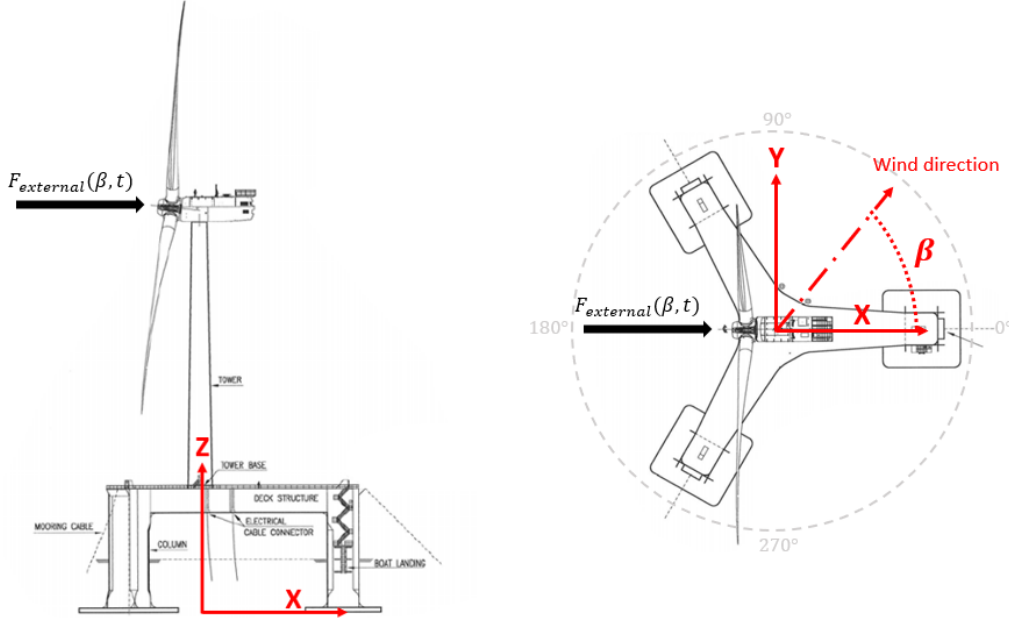


Figure 6.2: Time dependent external force acting as a force vector at the center of rotor, as function of wind direction in the body fixed reference system.

The thrust force is dependent on time and wind direction, and is implemented in aNySIM as a force vector by

$$\mathbf{F}(t) = [T(t) \cdot \cos(\beta) \quad T(t) \cdot \sin(\beta) \quad 0]^T, \quad (6.1.1)$$

where $T(t)$ is the calculated simplified thrust at each time step and β is the (going to) wind direction in the body fixed reference system. The force vector will induce a moment around the CoG of the platform. Subsequently, the resulting platform motions are computed numerically by aNySIM.

6.2 Steady state thrust curve

The steady state thrust curve is the one of the inputs for the calculation of the thrust in the simplified model. The curve of the wind turbine is normally available in the concept design phase of a floater. It represents the relation between steady state aerodynamic forces versus wind speed. The steady state of the thrust implies that transient effects, due to for instance instantaneous increase of wind speed, are not included. In this thesis, the thrust curve of the 5MW NREL reference wind turbine is used. For more information on this reference turbine, the reader is referred to Jonkman et al. [16].

The steady state thrust, reported by Jonkman et al. [16], is obtained from the land-based 5MW baseline wind turbine using FAST. It is compared with the steady state aerodynamic rotor thrust calculated

with the use of fully coupled aNySIM-Phatas simulations, see Fig. 6.3. This is achieved by running a series of constant uniform wind speeds with a fixed floater. A constant and uniform wind speed implies that no wind speed variations exist along the height and width of the rotor. The length of the time period between two successive steady uniform wind speeds was long enough to ensure that all transient have died out. The steady state thrust is then derived from the average over the last 100 seconds, and compared with the curves obtained by FAST, as depicted in Fig. 6.3. It must be noted that the aerodynamic rotor thrust reported by Jonkman et al. [16] is corrected by the axial load component from gravity of the rotor (94 kN).

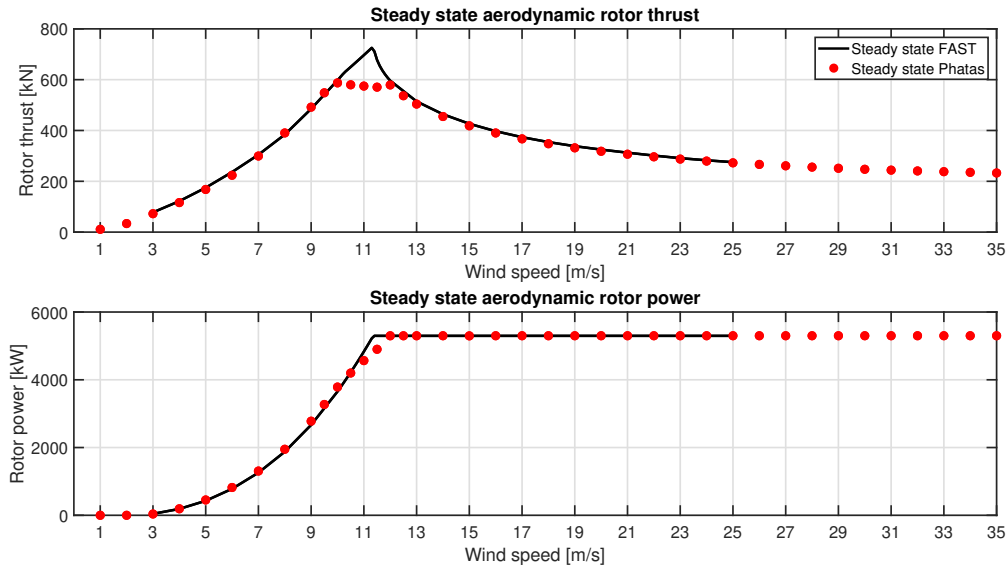


Figure 6.3: Steady state aerodynamic rotor thrust (top) and steady state aerodynamic rotor power (bottom) obtained from fully coupled aNySIM-Phatas simulations, plotted with data reported by Jonkman et al. [16]. The steady state thrust from the fully coupled aNySIM-Phatas simulations are used as input for the simplified model.

From the comparison depicted in Fig. 6.3, it is observed that the aerodynamic thrust obtained from Phatas matches well with the aerodynamic thrust obtained from the analysis with FAST. The steady state rotor thrust from Phatas is slightly lower than the thrust calculated by FAST, due to differences in aerodynamic models. From comparison of the steady state aerodynamic thrust (top figure) it is clearly visible that the wind turbine controller included in Phatas (Floating Control+), reduces the thrust force around rated wind speed significantly. The wind turbine controller starts pitching the turbine blades from 10 m/s and keeps the steady state thrust at a (more or less) constant level up to around 12 m/s. This 'peak-shaving' allows for significant peak thrust force reduction, with negligible energy loss at and around rated wind speed. The effect of the peak-shaving on the rotor power is seen in the bottom figure. In the above rated condition, the aerodynamic thrust is lowered as a result of pitching the wind turbine blades. Moreover, above rated wind speed the wind turbine controller maintains constant power.

The steady state thrust, calculated from FAST, is only given between cut-in (3 m/s) and cut-out (25 m/s) condition. The relative wind speed may exceed these limits, as a result of floater motions or turbulence in the wind. Therefore, the steady state thrust curve is extended over the full wind speed range from 1 to 35 m/s. Finally, the curve obtained over the full wind speed range is converted to a look-up table and used as input to the simplified Python model.

6.2.1 Low-frequency turbulent wind

For slowly varying wind speeds, the wind turbine controller has 'time' to react to slow changes in the wind. Slowly varying wind speeds are applied on the floating wind turbine, to identify the behavior of the Floating Control+ wind turbine controller. Only platform pitch motion is considered.

Turbulent wind speeds with low-frequency turbulence of 0.015 rad/s are considered, which is far below the platform natural pitch frequency. To avoid noise from the blade passing frequencies, the aerodynamic thrust is low-pass filtered and then plotted against the incoming wind speed in the steady state thrust curve. The result are shown in Fig. 6.4.

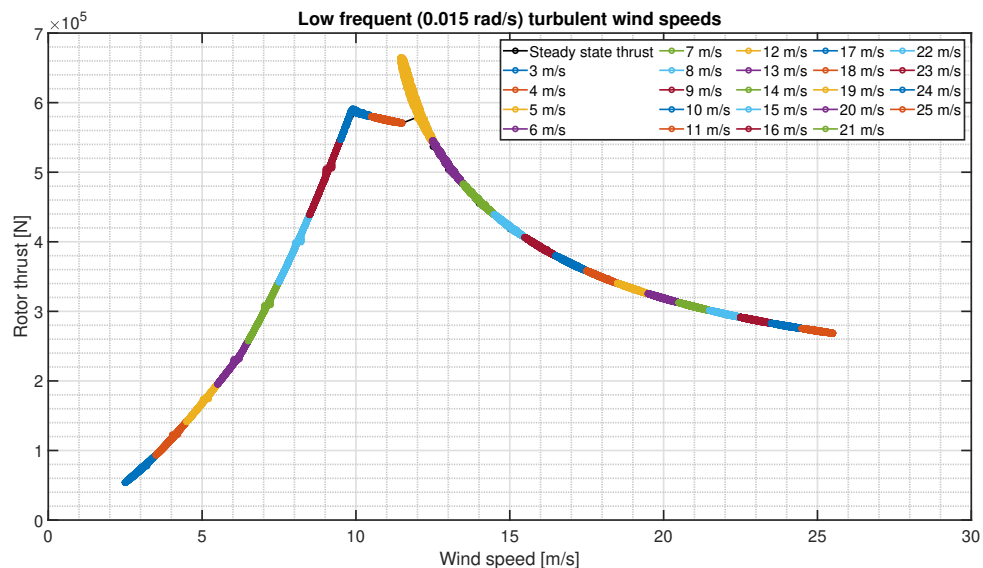


Figure 6.4: Aerodynamic rotor thrust plotted against relative wind speed for a range of wind speeds with low-frequency turbulence (0.015 rad/s).

From the figure, it is seen that the aerodynamic thrust in the low-frequency wind speeds exactly follows the steady state thrust curve. For the low-frequency turbulent wind speeds in the simplified model, the thrust is looked up from the steady state thrust curve. The wind speed of 12 m/s follows the thrust curve without peak shaving, but this effect is ignored in the rest of this thesis.

6.2.2 Platform natural pitch frequency turbulent wind

From several previous studies ([18] and [21]) it was shown that the instability of the wind turbine pitch controller is related to the lightly damped eigenfrequencies of the floating platform within the controller bandwidth. The platform natural pitch frequency is one of these lightly damped eigenfrequencies within the bandwidth of the controller. To overcome the instabilities, ECN developed the Floating Control+ specifically for the Tri-Floater [37].

The effect of the controller on the aerodynamic thrust in platform natural pitch frequency turbulent wind speeds, is depicted in Fig. 6.5. The 'loops' in the aerodynamic thrust between a wind speed of 6 and 16 m/s clearly indicate the non linear effect of the wind turbine controller. Outside this range, the aerodynamic thrust follows a more or less straight line with respect to the relative wind speed. It indicates a linear behavior of the floating wind turbine controller. The inclusion of the thrust behavior for wind speeds with a frequency equal to the platform natural pitch frequency, thrust sensitivities are used. These thrust sensitivities are described later in this chapter.

6.2.3 High and wave frequency turbulent wind

The aerodynamic thrust versus incoming high-frequency turbulent wind speed, is shown in Fig. 6.6. A high-frequency turbulent wind with a frequency of 0.15 rad/s is considered, which is far above the

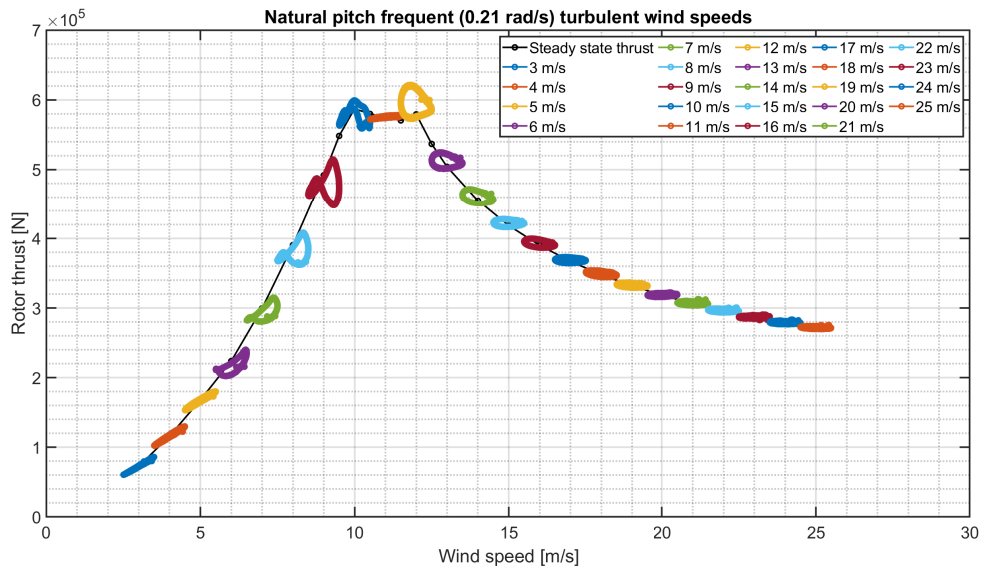


Figure 6.5: Aerodynamic rotor thrust plotted against relative wind speed for a range of wind speeds with platform natural pitch frequency turbulence (0.21 rad/s).

platform natural pitch frequency. The same simulation assumptions as for the low-frequency winds are applied. From the figure, a positive gradient is observed for all wind speeds ranging from 3 to 25 m/s. In the below rated conditions, the wind turbine controller only maintains optimal tip speed ratio indicating that the wind turbine blades are not pitched. Due to an increase in relative wind speed, the aerodynamic thrust increases as well, i.e. the wind turbine blades respond aerodynamically. The same effect is seen in the above rated conditions. The blade pitch controller is unable to react to the fast (high-frequency) changes in the wind speed. For now, the wind speeds with a frequency equal to the high-frequency are looked up from the steady state thrust curve, in the simplified model.

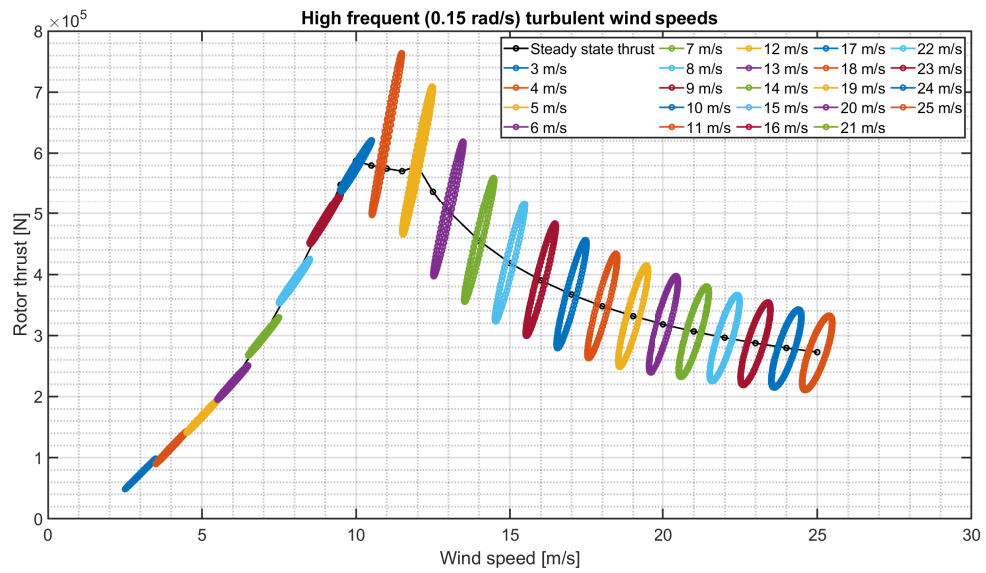


Figure 6.6: Aerodynamic rotor thrust plotted against relative wind speed for a range of wind speeds with high-frequency turbulence (0.15 rad/s).

6.3 Thrust sensitivity

The wind turbine controller for the floating platform is developed such that the system is not negatively damped. The negative damping problem is present around the natural pitch frequency of the platform, as described by Jonkman [18].

To capture the behavior of the floating wind turbine controller on the aerodynamic thrust in the platform natural pitch frequency, thrust sensitivities are defined. These thrust sensitivities relate the change in aerodynamic thrust with respect to the variation in platform motion, and are the second input to the simplified model. Considering constant uniform wind speeds, the simplified aerodynamic thrust is then calculated in terms of a mean aerodynamic thrust plus the variation in aerodynamic thrust (thrust sensitivity) dependent on the platform motions. The total simplified aerodynamic thrust for constant wind speeds in the simplified model is then included by,

$$T(V, t) = T_{\text{mean}} + \frac{\partial T}{\partial \dot{x}} \cdot \dot{x}_{\text{hub}}(t), \quad (6.3.1)$$

with the steady state mean aerodynamic thrust T_{mean} for the specific constant wind speed corrected by the thrust sensitivity $\partial T / \partial \dot{x}$ due to the motion of the platform \dot{x}_{hub} at time t .

6.3.1 Decay simulations

The effect of the wind turbine controller on the aerodynamic thrust force in various constant uniform and turbulent wind speeds has been investigated. This has been done by looking into the variation of the aerodynamic thrust with respect to the variation in relative wind velocity, by performing decay simulations.

Platform pitch decay simulations are performed by applying a (negative) pitch moment at the CoG of the platform. The platform will move in its natural pitch frequency. To ensure the system is only free to move in pitch, all other DoFs are fixed. The pitch moment is then slowly increased until a steady state pitch offset is reached of around four degrees. After a couple of seconds, the pitch moment is released. Then, the platform pitch time trace is analysed under the influence of aerodynamic forces and wind turbine controller.

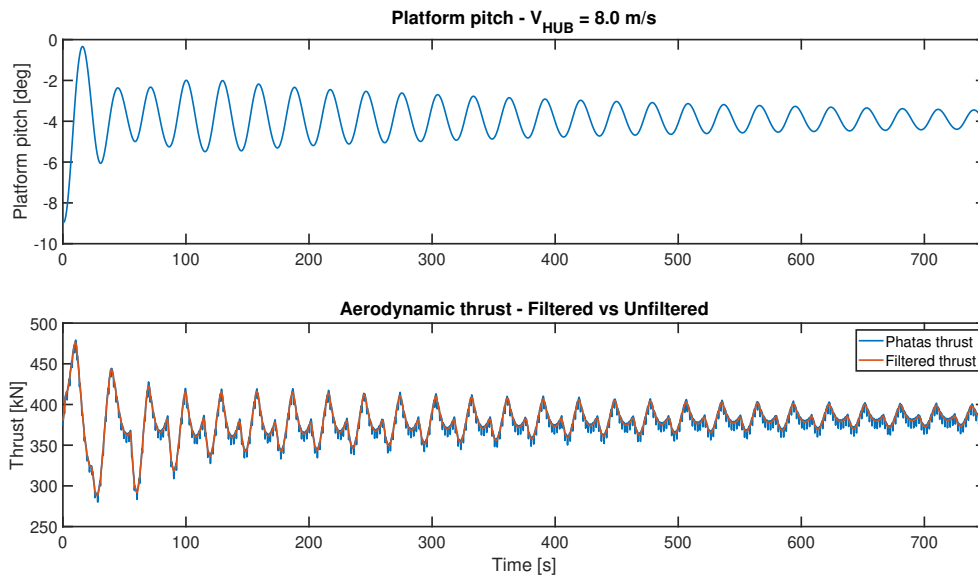


Figure 6.7: Pitch decay in 8 m/s constant wind presenting the aerodynamic thrust due to pitch decay together with the filtered thrust signal.

An example of the aerodynamic thrust after a decay in a constant uniform wind of 8 m/s as function of time is illustrated in Fig. 6.7. From the figure it is seen that after the external platform pitch moment is

released, the decay causes a change in aerodynamic thrust. It is observed that the aerodynamic thrust changes with changing relative velocity, i.e. the aerodynamic thrust calculated from Phatas follows the decay motion in pitch of the floater. However, the aerodynamic thrust calculated from Phatas does not follow a smooth decay motion (high-frequency noise). To get insight in the different frequencies of the aerodynamic thrust, a PSD is obtained, plotted in Fig. 6.8.

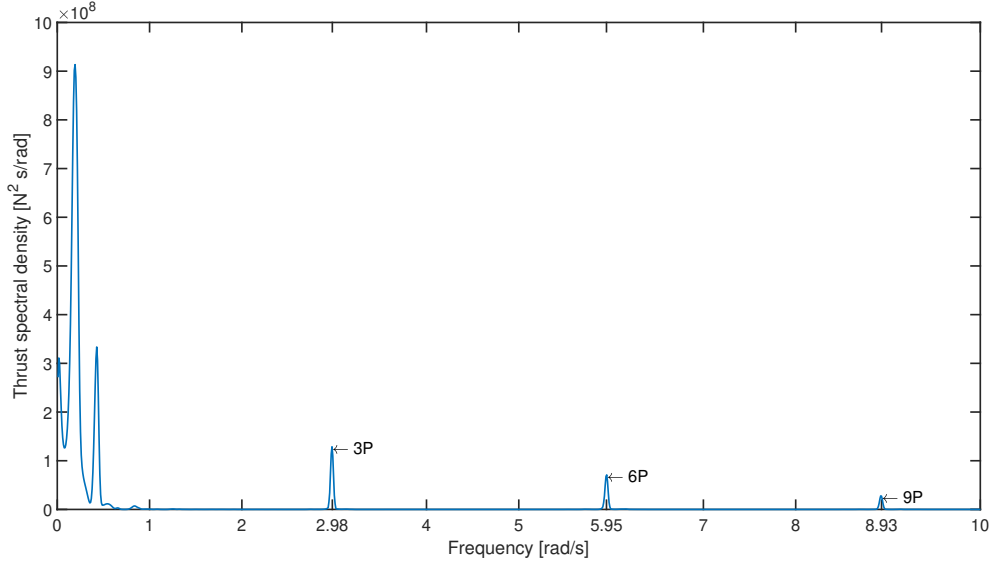


Figure 6.8: Power Spectral Density (PSD) of the aerodynamic thrust of a platform pitch decay simulation in 8 m/s constant uniform wind speed illustrating blade pass frequencies.

Apart from the energy present in the low frequency range, peaks are present in the high frequency range. This high-frequency noise seen in the aerodynamic thrust time trace originates from the turbine blades passing the wind turbine tower. The blade passing (3P) frequency is calculated by,

$$\omega_{3P} = 3 \cdot 2\pi \cdot \frac{\text{RPM}}{60}, \quad (6.3.2)$$

in which the Revolutions Per Minute (RPM) equates 2.97 for a constant uniform wind speed of 8 m/s, such that $\omega_{3P} = 2.98$ rad/s. This value matches the peak in the spectrum around 3 rad/s. The other blade passing (6P and 9P) frequencies are multiples of the blade passing (3P) frequency. Therefore, the noise present in the aerodynamic signal is allocated to the (3P, 6P and 9P) blade pass frequencies. In this thesis, the effect of the blade passing frequencies are neglected by low-pass filtering the aerodynamic thrust such that only the effect of the global motion is included.

To arrive at the determination of the thrust sensitivities, two methods are applied: method A, in which the thrust sensitivity is derived from the correlation of aerodynamic thrust and relative wind speed, and method B, in which the thrust sensitivities are derived from the aerodynamic damping. Both methods are described in the following sections.

6.3.2 Method A: thrust sensitivity from correlation thrust and relative wind velocity

In this section, the first method is described to arrive at the intended thrust sensitivities. The low-pass filtered aerodynamic thrust as a result of the platform pitch decay is plotted. The simulations are carried out in constant uniform winds. By this, the relation between aerodynamic thrust and relative wind speed is studied, see Fig. 6.9. From the relationship, a thrust sensitivity is derived based on a straight line through the data points.

From the figure, it is seen that the cluster of aerodynamic thrust data points is located at the correct value of mean steady state rotor thrust. The aerodynamic thrust data points oscillate around this mean

value. The aerodynamic thrust follow approximately the steady state thrust curve for constant uniform wind speeds below rated of 4, 6 and 8 m/s. Around rated (10 and 12 m/s), the aerodynamic thrust data shows more scattering in relation to the relative wind speed. The scattering in the aerodynamic thrust is a direct result of the non linear behavior of the wind turbine controller, switching between control regions. In the above rated condition, however, it is seen that the aerodynamic thrust almost follows a straight line. When wind speeds are closer to cut-out condition, the relation becomes more evident. This indicates the effect of the controller in the above rated condition.

After plotting a linear fit through the data points, it is concluded that the straight lines are very sensitive to the length of the aerodynamic time trace. Moreover, the linear fit would even more deviate when turbulent winds would be considered. Therefore, the next section describes an alternative derivation of the thrust sensitivities: Method B. The method also includes a derivation in turbulent winds.

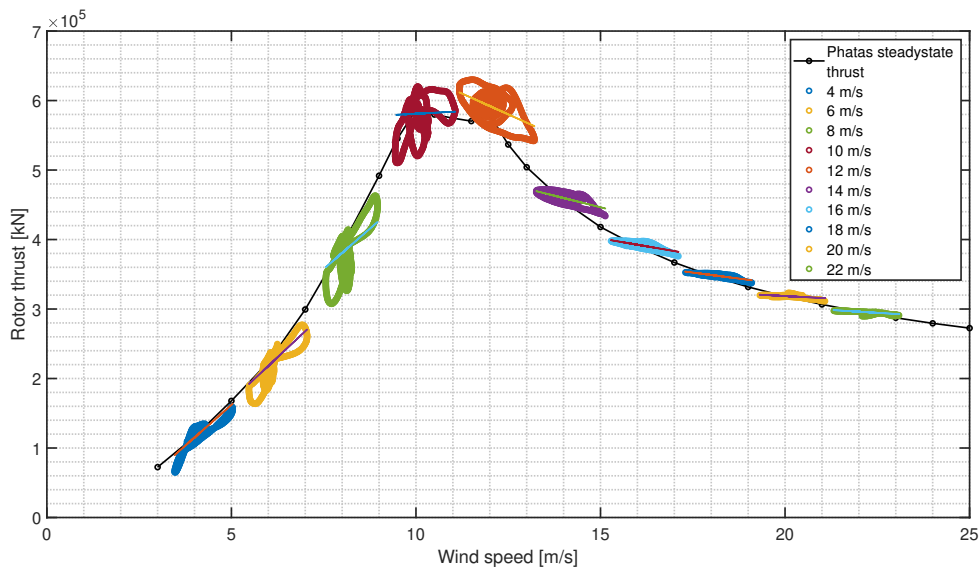


Figure 6.9: Filtered aerodynamic thrust plotted against relative velocity in decay simulations in constant uniform wind speeds, showing trends in the thrust force.

6.3.3 Method B: thrust sensitivity derived from aerodynamic damping

In the previous section, thrust sensitivities were derived from a linear fit through the data points of the aerodynamic thrust. The method was not considered very suitable, as the gradient of the linear fit is very sensitive to the length of the aerodynamic thrust. This section elaborates on an alternative derivation of the thrust sensitivities, which will be used as input to the simplified model, for constant and turbulent winds.

Aerodynamic damping

The linear aerodynamic damping of the Tri-Floater is determined by the analysis of free decay simulations in pitch, using the method as presented in Pegalajar-Jurado et al. [33]. The aerodynamic damping is derived from the platform pitch decay time traces. The decay simulations are performed in calm water under a series of constant uniform and turbulent winds, including a floating wind turbine controller. During the decay simulations, all structural, hydrodynamic and mooring contributions are excluded. Also, the wind loads on the floater, tower and nacelle are not included during the decay simulations, such that aerodynamic damping due to the rotor is the only contributor to the damping of the system.

The structural damping is disabled by considering only rigid body motions (no structural deformation). The exclusion of the hydrodynamic damping is achieved by setting the quadratic damping coefficients in aNySIM to zero. These quadratic damping coefficients are included in the model as they cover the

damping as a result of fluid friction, vortices and flow separation. The quadratic damping coefficients are generally determined by carrying out model tests. The (potential) damping, which is related to the radiation of waves (they take energy from the system as they transport energy), is excluded by setting the potential damping coefficients to zero for each frequency, DoF, and direction. Damping caused by the mooring system is easily excluded by ignoring the mooring system in the model.

Figure 6.10 presents two platform pitch decay time traces, from which the aerodynamic contribution is omitted. This is done by setting the air density in Phatas to zero. The pitch decay excluding hydrodynamic damping, shows no damping of any source. In the determination of the aerodynamic damping using decay simulations, the aerodynamic rotor forces are the only contributor to the damping of the system.

As a result, assuming a system with linear aerodynamic damping only, the logarithmic decrement δ as function of wind speed W is defined by

$$\delta(W) = \frac{1}{n} \log \left(\frac{x_i}{x_{n+i}} \right), \quad (6.3.3)$$

with the i^{th} and $(n+i)^{\text{th}}$ peak of pitch motion.

For a linear system, the logarithmic decrement δ is related to the relative damping ξ_{aero} (i.e. the percentage of the critical damping) by,

$$\xi_{\text{aero}}(W) = \frac{\delta}{\sqrt{4\pi^2 + \delta^2}}. \quad (6.3.4)$$

The following sections present the aerodynamic damping obtained from a series of constant uniform and turbulent winds.

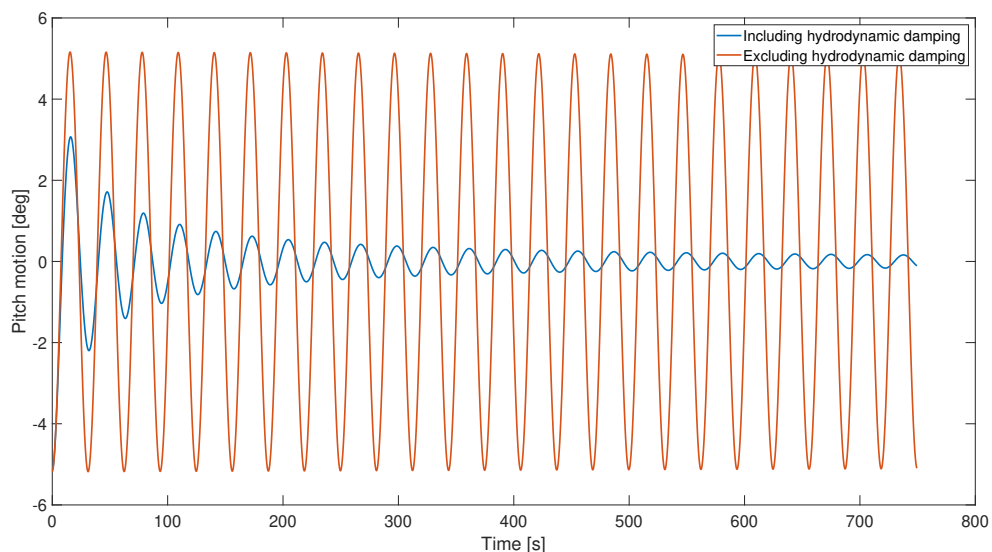


Figure 6.10: Free decay pitch motion of the Tri-Floater in calm water and no wind with and without hydrodynamic (viscous and potential) damping.

Aerodynamic damping in constant wind

In total 23 constant uniform wind speeds are considered for three different wind turbine controllers: Floating Control+, Floating Control and Fixed Base Control. Figure 6.11 shows the platform pitch decay time traces (with Floating Control+) for three constant uniform wind speeds: 5, 10, and 20 m/s. Prior to the determination of the aerodynamic damping coefficient from the time traces, the signals are

corrected by the mean pitch angle. The mean pitch angle is calculated based on the last 200 seconds of the signal, and then subtracted from the complete signal.

The decaying platform pitch motions plotted in Fig. 6.11 are damped under the influence of aerodynamic forces on the blades, only. The difference in aerodynamic damping is a result of the differences in aerodynamic forces induced by the floating wind turbine controller.

From the figure it is clearly visible that the platform pitch decay in 5 m/s constant uniform wind decays fastest to a equilibrium position. This rapid decay indicates a high aerodynamic damping compared to the other decaying signals. Taking a close look to the decay in 10 m/s constant wind, it is becomes clear that the signal decays slowly and shows non linearity in the first three oscillations. The non linearity originates from the control system, switching between torque control and blade pitch control. In 20 m/s constant uniform wind, the wind turbine controller is located in the full load control region, where the wind turbine blades are pitched. As a result, the platform pitch signal decays slow compared to 5 m/s wind, but fast compared to the system in 10 m/s constant uniform wind.

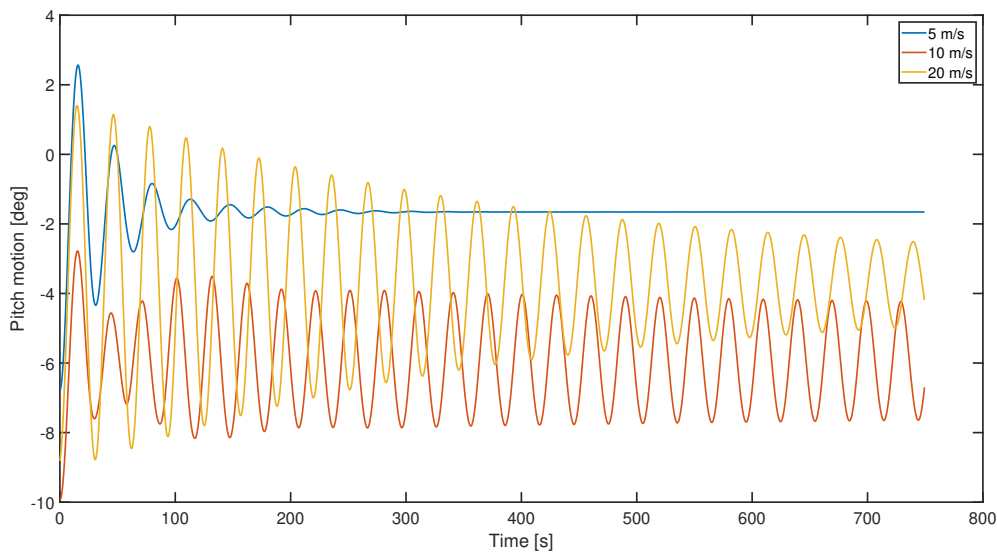


Figure 6.11: Free decay of pitch motion in three constant wind speeds without correction with the mean value of the steady state condition.

The aerodynamic damping ratios as function of constant uniform wind speed for three different ECN controllers are depicted in Fig. 6.12. The aerodynamic damping for the Floating Control+ is largest in magnitude at 5 m/s constant uniform wind. As from 5 m/s, the aerodynamic damping ratios become smaller up to 9 m/s. From 9 m/s the aerodynamic damping increases slightly. A local peak is seen at rated wind speed (11.4 m/s). In the above rated region, the aerodynamic damping ratios remain at a more or less constant value. The same trend in the aerodynamic damping ratios is noticed for the Floating Control controller. The Floating Control and Floating Control+ wind turbine controllers behave essentially the same, but the latter includes adjustments for wave induced load reductions.

Big differences in the aerodynamic damping ratios are seen for the Fixed Base Control, with respect to the Floating Control+. The Fixed Base Control is a land based controller, i.e. no modifications for floating structures. The aerodynamic damping ratios increase with wind speeds up to 7 m/s, and remains at a more or less constant level from 7 m/s to 9 m/s. A significant drop is found in aerodynamic damping from 9 m/s and becomes even negative from 12 m/s. The negative aerodynamic damping is a direct result of the land-based wind turbine controller. Still, the total system damping is not negative, as the sum of the aerodynamic damping ratio plus the potential and viscous damping ratios has a value greater than zero. From 20 m/s constant uniform wind speed, the aerodynamic damping ratios become positive again, which is due to the smaller gradient of the thrust curve. The gradient of the thrust curve

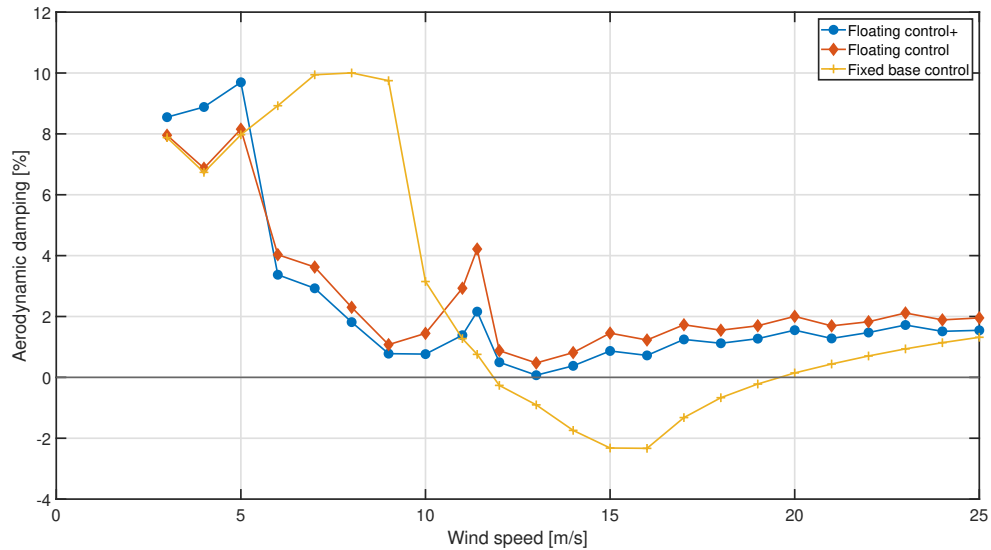


Figure 6.12: Aerodynamic pitch damping ratios determined using logarithmic decrements from decay simulations for three different control approaches in constant uniform wind.

is largest and negative just above rated, resulting in the largest negative damping ratios.

Aerodynamic damping in turbulent wind

The aerodynamic damping ratios are also determined for a series of turbulent wind speeds. To be able to calculate the aerodynamic damping ratios using Eqs. (6.3.3) and (6.3.4), free decay simulation are performed with and without an external platform pitch moment. The platform pitch decay signal for which the analysis is applied, is obtained by subtracting the simulation without external pitch moment from the simulation with external pitch moment.

Three different realisations of the platform pitch decay in the same turbulent wind are considered by releasing the external pitch moment at three different moments. By this, the platform is exposed to various wind time traces of the same turbulent wind speed realisation. An example of a pitch decay time trace in a 10 minute mean wind speed of 4 m/s is shown in Fig. 6.13. From the figure, a clear difference is seen between the pitch motions of the simulation with and without the external pitch moment. After subtraction, a neat decay motion remains from which the aerodynamic damping ratio is derived. The same approach is carried out for all other turbulent wind speeds. The aerodynamic damping ratios as function of turbulent wind speeds for three different wind turbine controllers, are presented in Fig. 6.14. Each point in the plot represents an aerodynamic damping ratio estimated from one time-domain simulation. Then, a line is plotted through the average values of the three data points at the specific turbulent wind speed.

Comparison of aerodynamic damping in steady and turbulent wind

The comparison of the aerodynamic damping ratios, from the simulations with the Floating Control+, in constant uniform and turbulent winds is depicted in Fig. 6.15. From the figure, it becomes clear that the aerodynamic damping ratios follow a similar trend. Small differences are observed in the under rated and above rated conditions. Around rated wind speeds, however, relative larger differences are observed. From this analysis, it is concluded that the damping ratios derived from the constant winds are applicable to the simulations in turbulent winds.

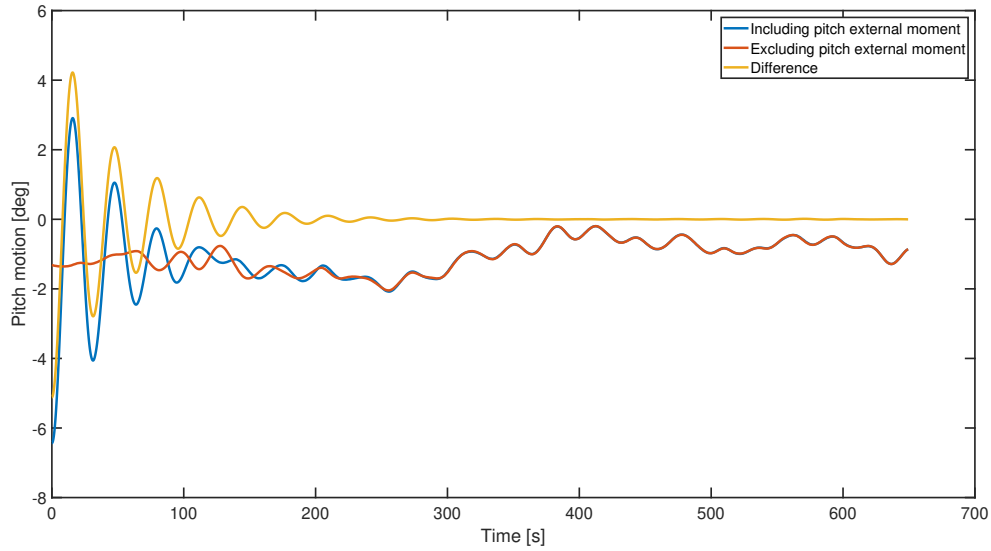


Figure 6.13: Free decay of pitch motion under 8 m/s turbulent wind (one seed) showing differences between decay motion with and without external moment, for which the aerodynamic damping ratio is determined.

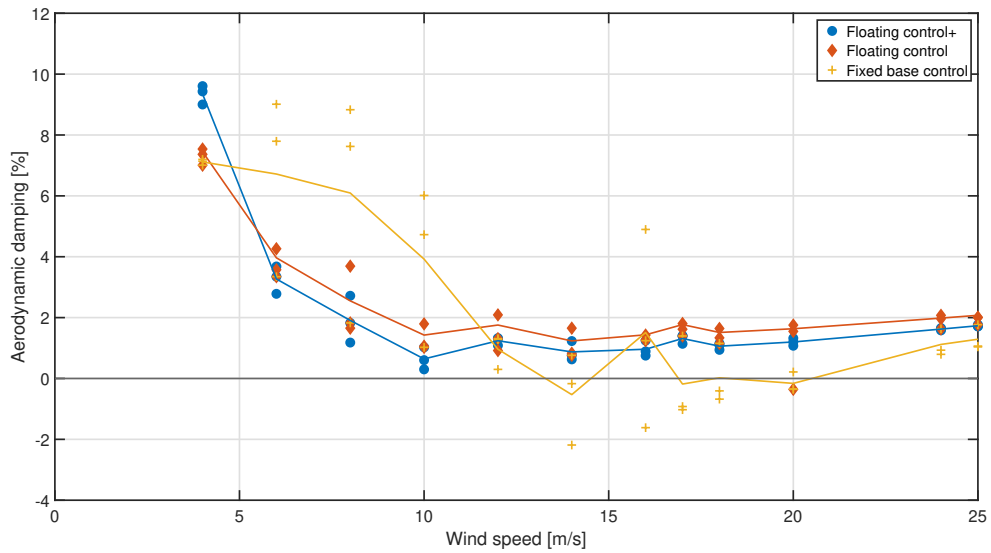


Figure 6.14: Aerodynamic pitch damping ratios determined using logarithmic decrements from decay simulations for three different control approaches and different seeds in turbulent wind.

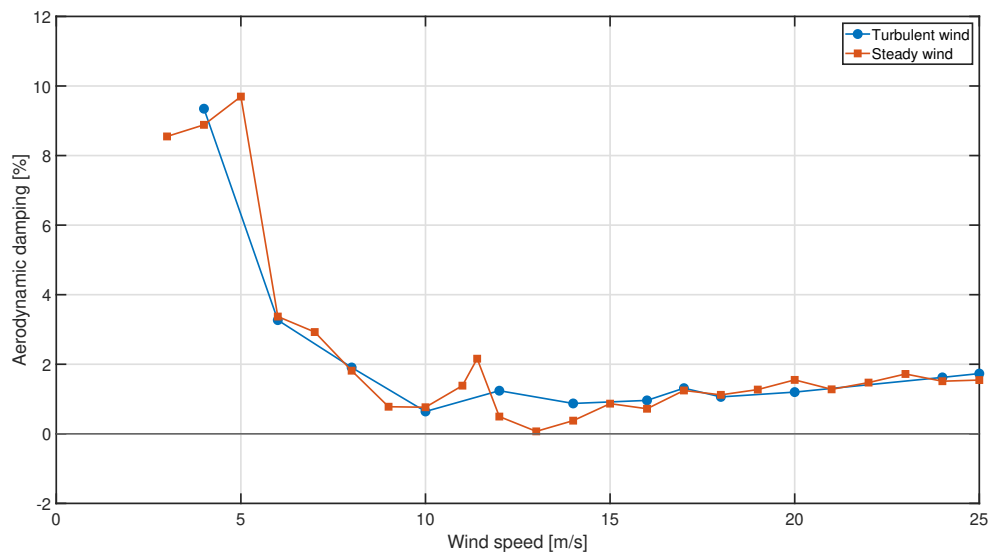


Figure 6.15: Difference in aerodynamic pitch damping ratios determined using the logarithmic decrements from pitch decay simulations in constant uniform wind and turbulent wind.

Translation of aerodynamic damping to thrust sensitivity

So far, no clear relationship is provided between the aerodynamic damping ratios and thrust sensitivities. Therefore, this section considers the translation between the aerodynamic damping ratios to thrust sensitivity.

The theoretical relationship between the aerodynamic damping and thrust sensitivity is explained by means of a rigid body platform pitch motion as a single DoF. The platform pitch equation of motion for this single DoF system, without mooring, is given as

$$(I_{yy} + A)\ddot{\theta} + B_{\text{hydro}}\dot{\theta} + C\theta = L_{\text{hub}}T, \quad (6.3.5)$$

where $\ddot{\theta}$ is the platform pitch rotational acceleration, $\dot{\theta}$ the platform pitch rotational velocity, θ the platform pitch angle, I_{yy} is the pitch moment of inertia of the complete system, A is the added mass coefficient associated with pitch, B_{hydro} is the hydrodynamic damping coefficient including potential damping and viscous damping associated with pitch, C is the pitch hydrodynamic restoring coefficient, L_{hub} is the hub height from the CoG, and T is the aerodynamic rotor thrust applied at the center of the hub.

To gain insight into the behavior of the damping caused by the aerodynamic thrust, Eq. (6.3.5) is rewritten in terms of the translational motion of the hub x by considering small pitch angles ($\sin(\theta) \approx \theta$) by,

$$x = L_{\text{hub}}\theta. \quad (6.3.6)$$

The aerodynamic thrust T is dependent on relative wind speed variation, as a result of the hub motion. Actually, the aerodynamic thrust is dependent on the rotational speed of the rotor and blade pitch angle, but here only the thrust variation caused by the hub motion is considered. Therefore, the aerodynamic rotor thrust is written as,

$$T = T_0 - \frac{\partial T}{\partial \dot{x}}\dot{x}, \quad (6.3.7)$$

in which T_0 is the mean aerodynamic thrust at a given mean wind speed from the steady state rotor thrust and \dot{x} is the velocity of the hub. In case of a zero degree (going to) direction of the wind, together with a positive platform motion, the hub translates from the wind. This results in a decrease in total thrust T . Vice versa, if the platform moves into the direction of the wind, thus a negative platform motion, the relative wind speed increases leading to an increase in the total thrust. This leads to a minus sign in front of the thrust sensitivity term in Eq. (6.3.7). Combining Eqs. (6.3.5) to (6.3.7), the equation of motion of the platform pitch can be written as,

$$(I_{yy} + A)\ddot{x} + (B_{\text{hydro}} + B_{\text{aero}})\dot{x} + Cx = L^2T_0, \quad (6.3.8)$$

with

$$B_{\text{aero}} = \frac{\partial T}{\partial \dot{x}}L^2. \quad (6.3.9)$$

Aerodynamic damping ratio

From the equation of motion, the aerodynamic damping ratio is determined, which is the aerodynamic damping as a fraction of the system's critical damping,

$$\xi_{\text{aero}}(W) = \frac{B_{\text{aero}}}{2\sqrt{(I_{yy} + A)C}}. \quad (6.3.10)$$

The aerodynamic damping ratio in Eq. (6.3.10) can become negative only if the damping coefficient B_{aero} is negative. The system parameters I_{yy} , A and C are positive by definition. The thrust sensitivity can be expressed in terms of the aerodynamic damping ratios (derived from the decay simulations) by combining Eqs. (6.3.9) and (6.3.10),

$$\frac{\partial T}{\partial \dot{x}} = \frac{\xi_{\text{aero}}(W) \cdot 2\sqrt{(I_{yy} + A)C}}{L^2}. \quad (6.3.11)$$

6.3.4 Comparison of method A and method B

In this section, the results of method A and method B are compared. To summarize, method A was used to derive the gradient ($\partial T/\partial \dot{x}$) of the linear fit through the data points of the aerodynamic thrust and relative wind speed. As method A was considered to be inaccurate, method B was carried out to derive $\partial T/\partial \dot{x}$ from the aerodynamic damping ratios.

Fig. 6.16 shows the thrust sensitivities using both methods. From the figure it is seen that the thrust sensitivities, derived from both methods, follow a similar trend. However, the results do not agree sufficiently. In the below rated region, both damping ratios are positive, but show some (significant) discrepancies. Above rated condition, however, the aerodynamic damping ratios derived from the thrust sensitivities are negative. Why this value is negative, while the decay motion shows positive damping, needs some further investigation.

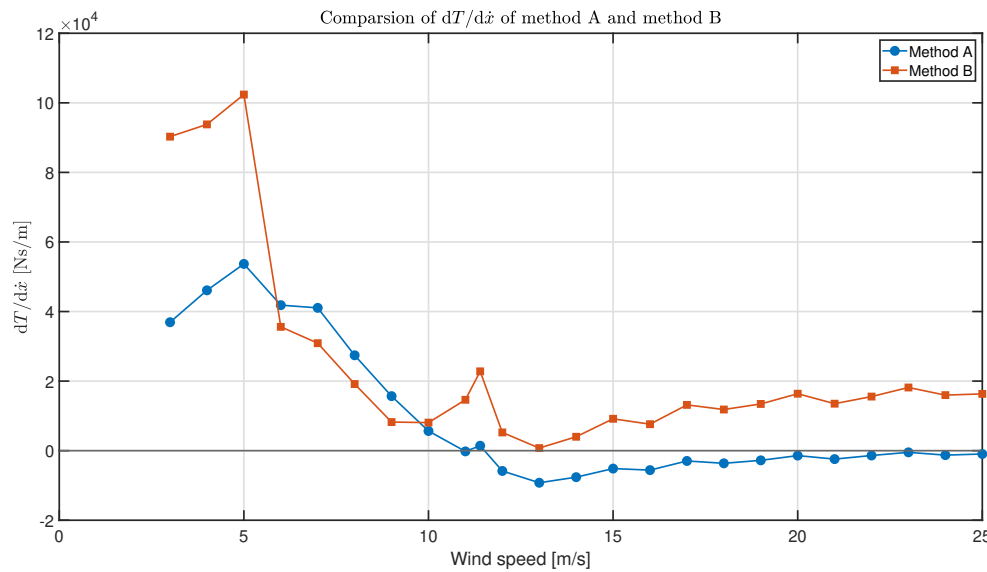


Figure 6.16: Comparison of $\partial T/\partial \dot{x}$ derived from method A and method B. Where method A tries to capture the thrust sensitivity from correlation of aerodynamic thrust and relative wind speed, method B determines the thrust sensitivity from the aerodynamic damping.

6.3.5 Selected method

Two different approaches were used to determine the thrust sensitivity term $\partial T/\partial \dot{x}$: method A, in which the gradient is estimated from the aerodynamic thrust versus relative wind speed, and method B in which the term is derived from the aerodynamic damping. Although both methods are different, both methods should result in more or less the same value. In the development of the simplified model, the thrust sensitivities derived by the aerodynamic damping are used. From the decay analysis, it was shown that the decay motions were positively damped. Using the negative thrust sensitivities in the simplified model would result in unstable platform motions.

6.4 Turbulent wind speed filtering

Turbulent wind has a stochastic character and is therefore not constant over time at a specific offshore site. The variations of the wind speed over time is considered as turbulence. Turbulent wind covers a range of time scales, from seconds to hours and even seasonal. Turbulence on a smaller time scale and closer to shore is a result of the topography of land (mountains, hills and buildings). Also, the wind generated waves have an effect on the turbulence of the wind. Turbulence is expressed as the standard deviation of the variation around the mean.

In the previous sections, the steady state thrust curve and the thrust sensitivities were introduced

as input for the simplified model. The steady state thrust curve is included as a look-up table acting on the incoming wind speed. The thrust sensitivities are calculated from the aerodynamic damping ratios to capture the behavior of the wind turbine controller. In this section, the turbulent wind speed filtering is explained, which is one of the inputs to the simplified model.

6.4.1 Aerodynamic thrust excitation

The reason wind speed filtering is applied, is explained by looking at the aerodynamic thrust excitation of the fully coupled simulations. Figure 6.17 shows PSD plots of the platform pitch (left) and aerodynamic thrust (right), for a turbulent wind speed of 14 m/s. From the aerodynamic thrust PSD, a peak around the platform natural pitch frequency is observed. This peak is a result of the Fixed Base Control. The aerodynamic thrust PSD of the Floating Control+, shows a clear attenuation in the aerodynamic thrust around the platform natural pitch frequency. As a result, the fully coupled simulation with the Fixed Base Control shows significant larger response in the platform pitch PSD around platform natural pitch frequency, compared to the fully coupled simulation with the Floating Control+.

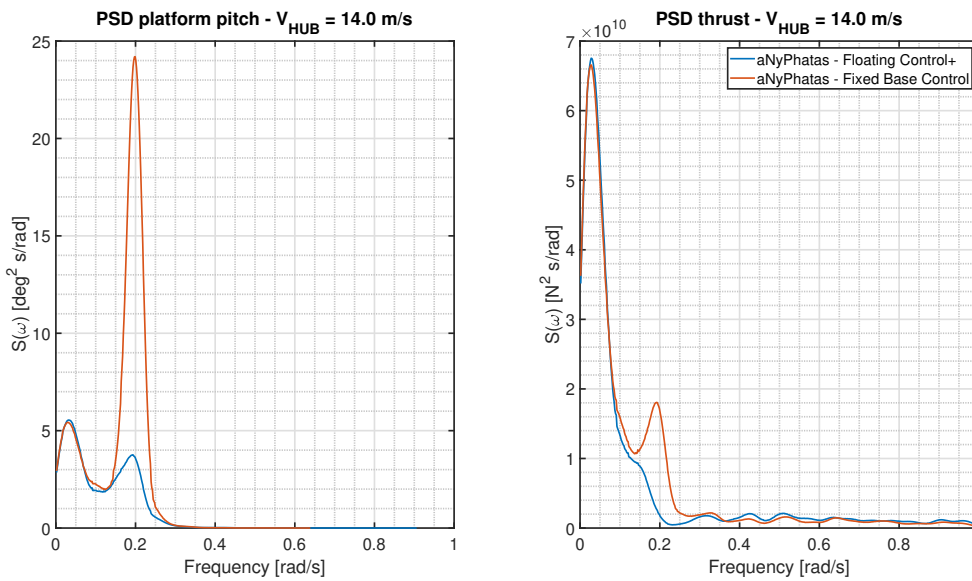


Figure 6.17: PSD of platform pitch and aerodynamic thrust in a turbulent wind speed of 14 m/s, showing the negative damping effect induced by Fixed Base Control compared to the fully coupled simulation with the Floating Control+.

In the simplified model, the effect of the floating wind turbine controller (attenuating the thrust excitation around the platform natural pitch frequency), is included as a band-stop filter on the incoming wind speed.

6.4.2 Filter type

For the investigation of the most suitable band-stop filter type, the incoming turbulent wind is filtered by three different filters: FFT band-stop filter, windowed-sinc filter and a notch filter. Below, a brief description on the working principle of each filter is given.

FFT band-stop filter

This type of band-stop filter uses Fast Fourier Transform (FFT) to filter an input signal. The input signal is transformed from the time-domain into the frequency domain, by using FFT. Before transformed back to the time-domain, the frequencies of the signal between the specified bandwidth are set to zero.

Windowed-sinc filter

A windowed-sinc filter is constructed by a filter kernel derived from a ideal frequency response. After some modification to the filter kernel, the filter can be applied as a band-stop filter. For detailed information on how the filter works and implementation, the reader is referred to Smith [38].

Notch filter

A band-stop filter can be regarded as a combination of a low and high pass filter, such that the filter passes all frequencies with the exception of the frequencies within the stop band. A notch filter is a special type of band-stop filter which is mainly used to reject a single or very small band of frequencies.

The results of the different band-stop filters for a turbulent wind speed of 14 m/s, are presented in Fig. 6.18.

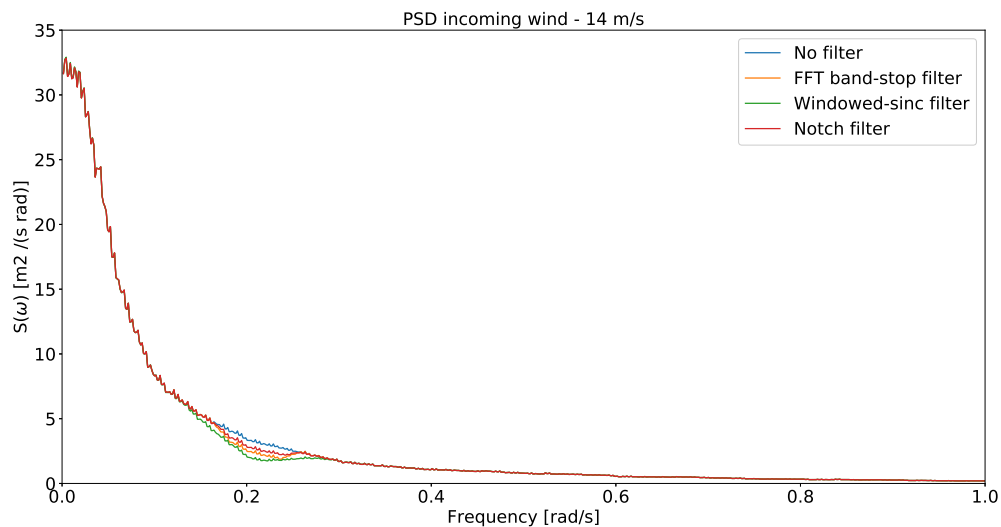


Figure 6.18: Spectral density of an incoming turbulent wind field of 14 m/s, filtered around the natural pitch frequency with different filters with a stop-band of 0.18 to 0.23 rad/s.

From the PSD plot depicted in Fig. 6.18, it is observed that the turbulent wind speed contains frequencies up to 1 rad/s. Most of the energy of the turbulent wind is present in the low frequency region. Therefore, the motion response of the platform for this specific wind speed will be dominated by the low frequency aerodynamic thrust excitation.

All filters are constructed with a stop band of 0.21 to 0.23 rad/s. However, a different effect of the filters on the attenuation of the frequencies in the stop band of the turbulent wind speed is seen in Fig. 6.18. Also, it is observed that the filters do not fully attenuate the frequencies around the natural pitch frequency. As a result, the floating platform in the simplified model is still excited in its pitch natural frequency. From the various filters the FFT band-stop is selected, because this filter attenuates most of the frequencies around the platform natural pitch frequency, together with the smallest bandwidth. The simplicity of the filter is an additional advantage.

Effect of wind speed filtering on aerodynamic thrust excitation

The FFT band-stop filtered wind speed is used as input to the simplified model. As a result, the thrust applied at the rotor center, contains lower energy around the pitch natural frequency. Fig. 6.19 shows the effect of the FFT band-stop filter on the aerodynamic thrust excitation, which is a result of an incoming turbulent wind speed of 14 m/s in calm water. From the figure, it is clearly observed that the platform pitch motion is overestimated significantly, in case no filter is applied. The excitation of the aerodynamic thrust around the platform natural pitch frequency is effectively lowered when the FFT band-stop is applied. The differences seen in the low frequency region of the aerodynamic thrust PSD

is a result of the peak shaved steady state thrust curve, which is used in the simplified model.

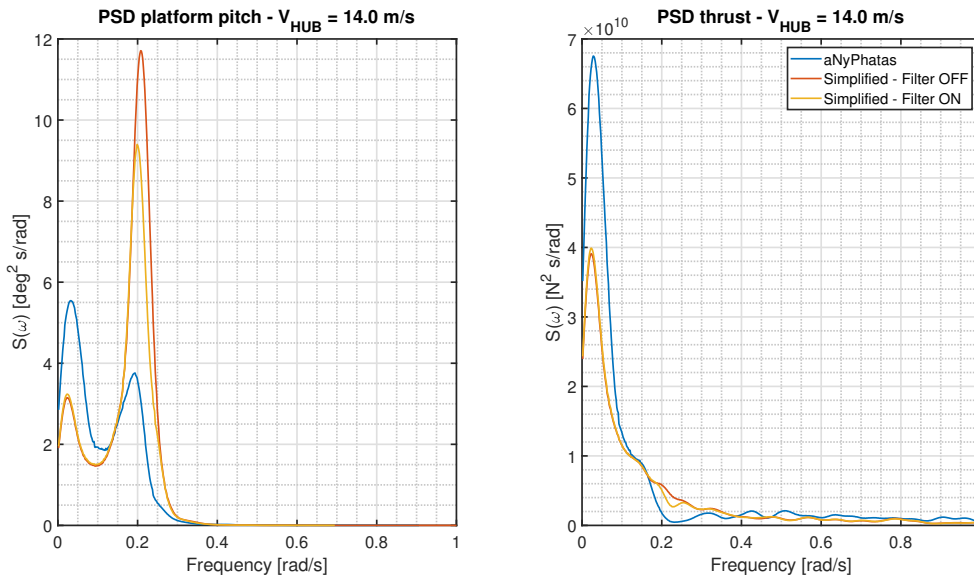


Figure 6.19: Comparison of the platform pitch and aerodynamic thrust between the fully coupled model and the simplified model with and without a simple FFT filter applied on the incoming wind speed. The filter is constructed with a stop-band of 0.21 to 0.23 rad/s, lowering the aerodynamic thrust response at the natural platform frequency.

6.5 Overview of complete simplified model

The three main external inputs to the simplified model were introduced: the steady state thrust curve, the thrust sensitivities and the turbulent wind speed filtering. In this section, the complete overview of the simplified model is given in Fig. 6.20.

From the flowchart it is seen that the turbulent incoming wind speed is filtered with the FFT band-stop filter. The filtered wind speed is used to determine the thrust from the steady state thrust look-up table. The tower top velocity, which is a result of the aerodynamic loading and wave loads, acts on the thrust sensitivity curve and contributes to the damping of the system. Both forces are added and result in the thrust which is applied at the rotor center.

6.6 Conclusions and recommendations

In the beginning of the chapter, the following research was formulated:

How can the relevant physical phenomena be integrated in a simplified model?

The simplified model has been constructed using aNySIM and Python. The Python module allows a user-defined script to be executed within the time-integration loop of aNySIM. In this thesis, the Python script is constructed by using the steady state thrust curve, thrust sensitivities and a filtered turbulent wind speed as input.

From the analysis in a low-frequency turbulent wind, it is found that the aerodynamic thrust excitation follows the steady state thrust curve exactly. For high-frequency turbulent wind, it is seen that the gradient of the aerodynamic thrust with respect to the relative wind speed is always positive. Nevertheless, in this thesis the turbulent incoming wind field acts on the steady state thrust look-up table.

For the platform pitch motion around the natural pitch frequency, thrust sensitivities are derived.

The thrust sensitivities include information of the aerodynamic thrust as function of the relative wind speed. Two methods are used for a range of wind speeds to determine the thrust sensitivities: Method A and Method B. In method A, the aerodynamic thrust is plotted against relative wind speed after which the gradient of the linear fit through the data points is calculated. In method B, aerodynamic damping ratios are determined (from the platform pitch decay simulations) which are then translated into thrust sensitivities. From the comparison it becomes clear that the thrust sensitivities have different signs in the above rated conditions. The reason for this difference is expected to be the result of the wind turbine controller. From the decay analysis it is seen that even in the above rated conditions the system was positively damped (due to aerodynamic damping). Therefore, in the simplified model, the thrust sensitivities of method B are selected and included in the simplified model.

From the aerodynamic thrust PSDs obtained from fully coupled simulations, it was observed that the aerodynamic thrust is attenuated around the platform natural pitch frequency (0.21 rad/s). The attenuation of the aerodynamic thrust around the platform natural pitch frequency in the simplified model, is achieved by applying a FFT band-stop filter on the incoming wind speed. The filter showed that the aerodynamic thrust around the platform natural pitch frequency could be attenuated efficiently. As a result, the aerodynamic thrust excitation and platform response around the platform natural pitch frequency, was lowered.

6.6.1 Recommendations

To use the simplified model for early concept design stages, the wind loads on the floater, tower and nacelle need be included.

Also, the reason for the difference in the gradient of the linear fit in the aerodynamic thrust versus relative wind speed in the above rated conditions, should be investigated. It was found that the gradient of the thrust versus wind speed in the fully coupled simulations were negative, while from the aerodynamic damping ratios the thrust sensitivities were obtained positive.

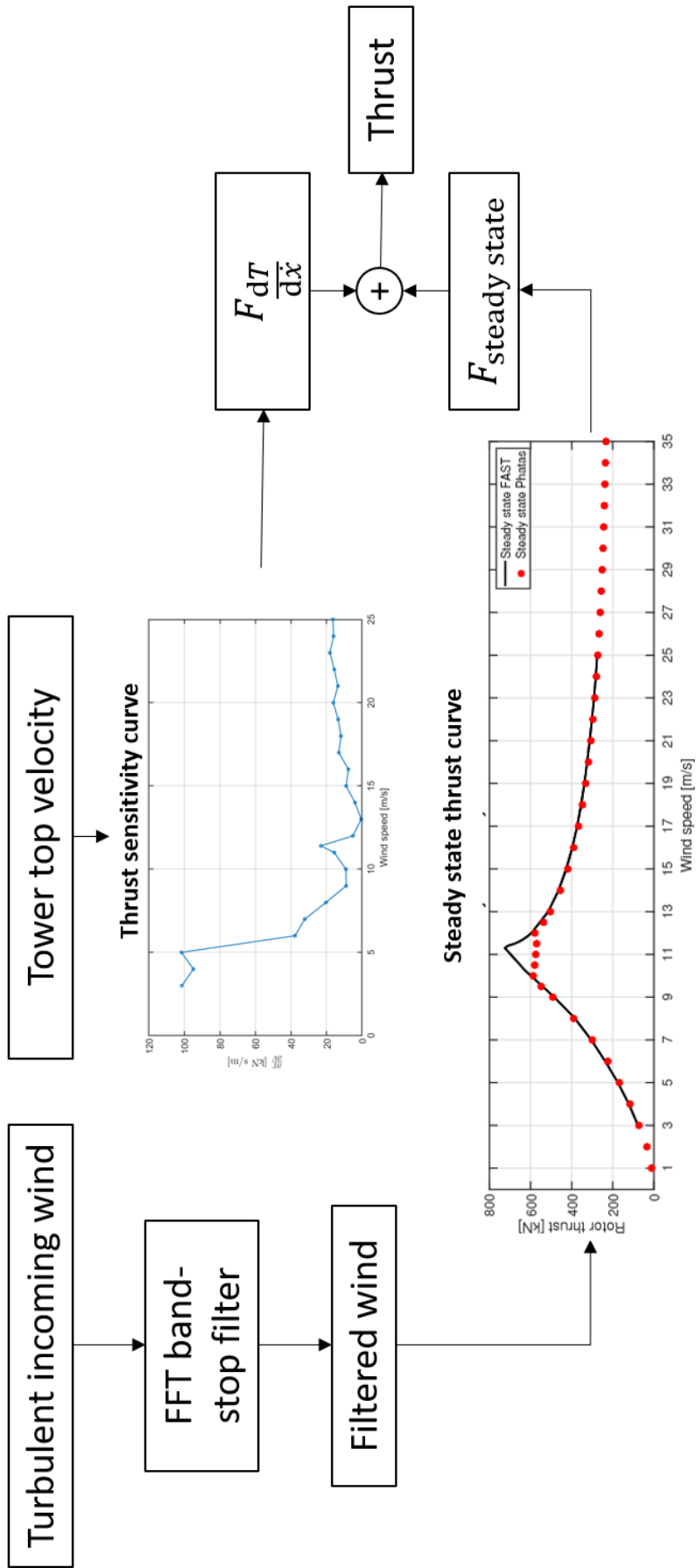


Figure 6.20: Flowchart showing the steps taken in the Python script to calculate the thrust.

Chapter 7

Verification simplified model

This chapter describes the verification and presents the results of the simplified model, compared to the fully coupled aNySIM-Phatas simulations. Here the following research question is answered:

To what extent does the simplified model compare to fully coupled aero-hydro-servo-elastic time-domain simulations?

The chapter starts with the verification of the steady state aerodynamic thrust curve implementation, using a stair case wind field. Then, the simplified model is verified in constant winds after which a low-frequency, natural pitch frequency and high-frequency turbulent wind speed is investigated, followed by fully turbulent winds. The previously mentioned verification steps are all performed for the platform only free to move in pitch. Moreover, the wind loads on the floater, tower and nacelle are not included in both the simplified model and fully coupled model. Also the current forces are not taken into account for both models. At last, an ultimate test is performed for a free floating platform.

7.1 Stair case wind verification

The implementation of the look-up table, derived from the steady state aerodynamic thrust curve (Fig. 6.3), is investigated in this section. The verification is done by considering a stair case wind field, ranging from 3 to 25 m/s, with a direction of 180 degrees. The aerodynamic thrust curve verification is performed in calm water (i.e. no waves and current). Furthermore, the mooring system is included. In the stair case wind simulations, the thrust sensitivities which contribute to damping of the system, as derived in the previous chapter, are included for completeness.

For the verification, the differences in the aerodynamic rotor thrust and the platform pitch motion between the fully coupled model and the simplified model are investigated, as depicted in Figs. 7.1 and 7.2. The numerical mean values are shown in Table 7.1, derived from the time traces of the last 200 seconds of each step in the wind, after the majority of the transient effects are dissipated.

Aerodynamic rotor thrust

The aerodynamic thrust calculated in the simplified model, for the wind speed range between 3 and 13 m/s is depicted in Fig. 7.1. A good agreement is shown compared with the fully coupled model. As wind speed increases, the blade pass frequencies in the fully coupled model become more pronounced (larger fluctuations in the aerodynamic thrust). For the wind speeds ranging from 15 to 25 m/s, the blade passing frequencies are also clearly visible. The fully coupled model shows high thrust peaks after each step in the wind, which might be due to the aerodynamic response of the blades. The wind turbine controller has a small time lag and responds a fraction later to this (rapid) increase in the wind speed by maintaining optimal tip speed ratio, or by pitching the blades. Looking at the differences in the mean values of each wind speed in Table 7.1, it is concluded that the aerodynamic thrust values agree very well.

Platform pitch

The platform pitch motions, as depicted in Figs. 7.1 and 7.2, are a result of the aerodynamic force on the rotor and show some (damped) oscillations after each step in the wind. Although, the simplified model shows positive damping at each wind speed, it is seen that the pitch decay of the platform after a step in the wind is not fully captured by the simplified model. Looking at the platform pitch mean values between 3 and 13 m/s in Table 7.1, it is concluded that the differences are within 3.3 %, compared to the fully coupled model. For the wind speeds from 15 to 25 m/s the differences in the mean values do not exceed 5.4%.

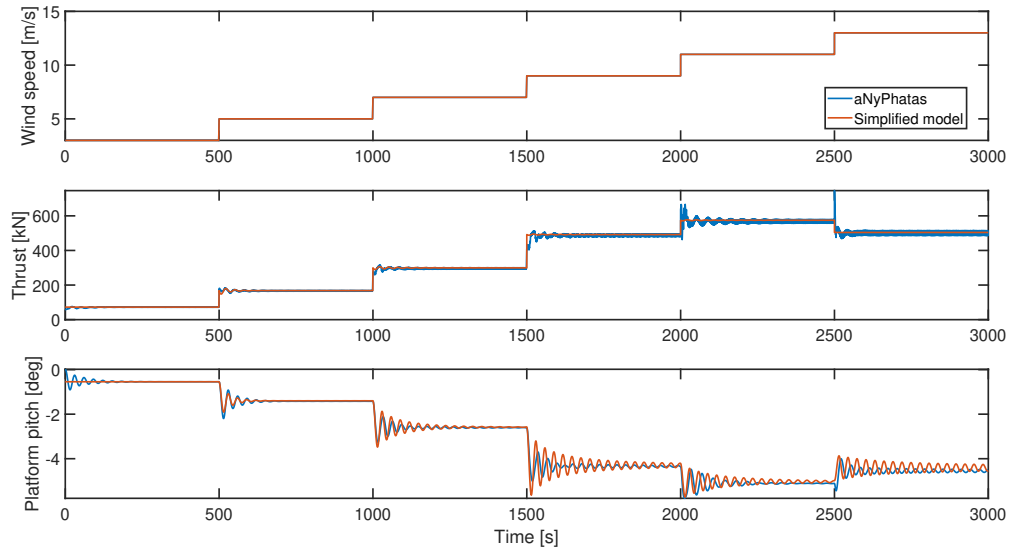


Figure 7.1: Stair case wind simulation from 3 to 13 m/s in steps of 2 m/s of the simplified model compared to the fully coupled simulation model. The aerodynamic thrust force is plotted (middle) together with the platform pitch (bottom).

Table 7.1: Mean (taken from the last 200 seconds of a wind step) comparison of aerodynamic thrust and platform pitch between simplified and aNySIM-Phatas simulations in a stair case wind field from 3 to 25 m/s.

Wind speed [m/s]	Aerodynamic thrust [kN]			Platform pitch [deg]		
	aNySIM-Phatas	Simplified model	Error [%]	aNySIM-Phatas	Simplified model	Error [%]
3	72.6	72.5	-0.2	-0.5	-0.5	-0.01
5	167.8	167.9	0.0	-1.4	-1.4	-1.5
7	298.6	299.4	0.3	-2.6	-2.6	-0.9
9	491.5	491.8	0.1	-4.3	-4.3	-1.0
11	575.0	574.7	-0.1	-5.1	-5.0	-1.6
13	510.0	504.0	-1.2	-4.6	-4.4	-3.3
15	421.6	418.0	-0.8	-3.8	-3.7	-3.2
17	368.4	367.0	-0.4	-3.3	-3.2	-3.5
19	332.5	331.8	-0.2	-3.0	-2.9	-3.9
21	306.7	306.6	-0.0	-2.8	-2.6	-4.3
23	287.1	287.4	0.1	-2.6	-2.5	-4.8
25	271.9	272.5	0.2	-2.5	-2.3	-5.4

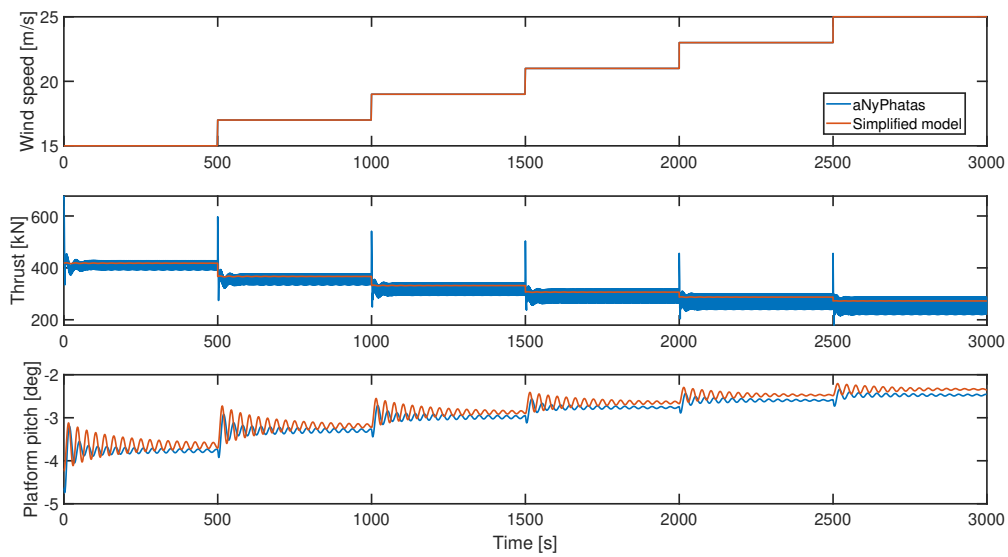


Figure 7.2: Stair case wind simulation from 15 to 25 m/s in steps of 2 m/s of the simplified model compared to the fully coupled simulation model. The aerodynamic thrust force is plotted (middle) together with the platform pitch (bottom).

7.2 Constant uniform wind verification

In this section, the simplified model is verified in constant uniform winds, with a direction of 180 degrees. It starts with the comparison of the platform pitch decay in calm water between the fully coupled and simplified simulations for a range of constant uniform wind speeds. By this, the implementation of the (relative) wind speed dependent thrust sensitivities, derived in the previous chapter, are assessed. Subsequently, irregular waves are added to the simulations, where only first order wave forces are taken into account. Furthermore, the mooring system is included.

7.2.1 Platform pitch decay - constant uniform wind

First, platform pitch decay simulations are performed for the investigation of the correct hydrodynamic and aerodynamic damping properties. Simulations of 1000 seconds are performed where the first 250 seconds are used to impose a fixed offset by applying an external pitch moment around the CoG of the floater. After the external pitch moment is released, the time period is sufficient long to ensure that the system reaches an equilibrium condition and (almost) all transient effects are dissipated.

Before any wind is added to the simulations, the similarity of the hydrodynamic properties of the fully coupled model is compared to the simplified model. This is done by carrying out a decay simulation excluding the mooring system, such that the potential and viscous damping are the only contributors to the damping of the platform. The platform is only free to move in pitch, by setting all other DoFs fixed.

Decay without wind

Figure 7.3 shows the platform pitch decay time traces of the fully coupled and simplified model in absence of wind and excluding the mooring system. From the figure it is seen that a slowly increasing platform pitch moment around the CoG causes a pitch offset, which is then released at 250 seconds. After 250 seconds, the platform starts oscillating around the zero degree position.

From the figure, the dependence of the Rotor-Nacelle Assembly (RNA) orientation is clearly visible. The total mass distribution of the floating platform is calibrated in case the RNA is oriented in negative x-direction, which results in a small CoG offset in the mass distribution of -0.03 m. This orientation of the RNA corresponds to a wind (going to) direction of zero degrees. For clarification on wind speed direction, the reader is referred to Fig. 6.2. The decay simulations in this section are performed for a wind direction 180 degrees, resulting in a (yaw) rotation of the RNA of 180 degrees as well (assuming the RNA perfectly aligns with the wind direction). The yawing of the RNA results in a small shift of the CoG towards the positive x-direction. The fully coupled model takes the shift in CoG into account by communicating from Phatas to aNySIM. In the simplified model however, the shift in the CoG is not automatically taken into account.

The comparison with the fully coupled simulations is satisfactory in case the simplified model is corrected by the CoG shift ($x_{\text{COGfloater}} = +0.03$). Only a small phase shift is observed, which might be due to the small differences in the inertia values communicated from Phatas to aNySIM. In addition, a platform pitch natural period of around 29 seconds is found from the both decay analysis, which is in accordance with values derived from model tests.

Decay in constant uniform wind

Decay simulations in constant winds allow assessing the effect of the thrust sensitivities on the platform pitch motion. The thrust sensitivities, as derived in Section 6.3.3, are included in the simplified model. The decay simulations of the simplified model are compared with the fully coupled simulations.

The comparison of the time traces between the simplified and fully coupled simulations of the platform pitch and aerodynamic thrust for various constant wind speeds, is given in Fig. 7.4. The aerodynamic thrust calculated in the fully coupled model is low-pass filtered to attenuate the blade pass frequencies, for clarity. From the figure, it becomes clear that the platform pitch motions of the simplified and fully coupled simulations are in good agreement, with respect to the mean pitch value and decay rate. For the constant uniform wind speed of 8 m/s, a clear (non linear) effect is seen on the platform pitch motion.

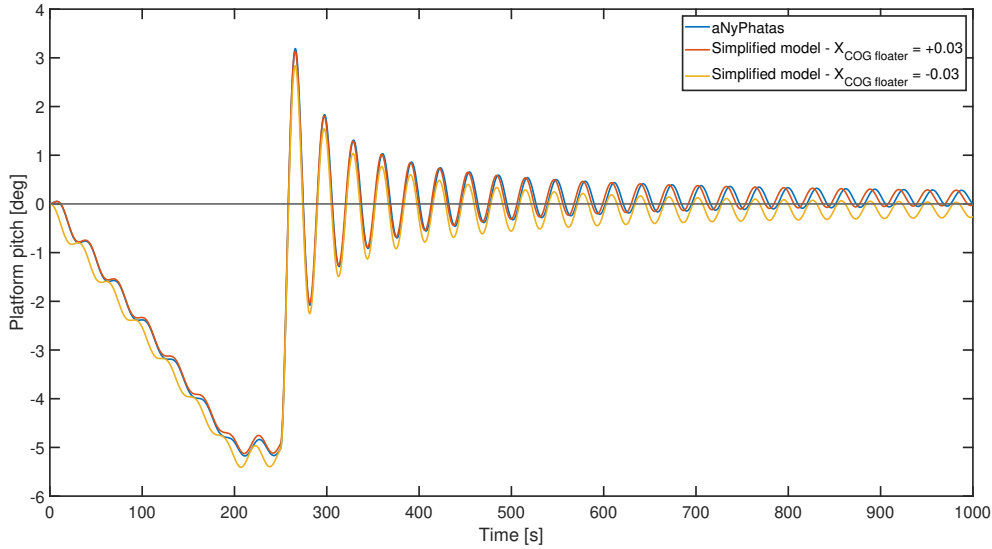


Figure 7.3: Platform pitch decay simulations of the fully coupled simulations and simplified model, showing the influence of the nacelle orientation.

This non linearity is caused by the effect of the wind turbine controller on the aerodynamic thrust. For this wind speed, the decay motion causes the relative wind speed to exceed the rated wind speed of 11.4 m/s, leading to blade pitch control action. The blade pitch action done by the wind turbine controller results in non linear aerodynamic thrust response, and consequently to non linear platform pitch response. The simplified model, which is constructed by the use of the thrust sensitivities, is by definition not able to capture this non linear behavior.

For the above rated constant wind speeds of 14 m/s and 20 m/s, the wind turbine control action on the aerodynamic thrust is also clearly visible. At the time the external platform pitch moment is released, the platform pitches into the wind, resulting in an increase in relative wind speed. From the figure it is seen that this increase in relative wind speed results in aerodynamic thrust decrease, by the action of the controller (pitching the turbine blades). This effect is however not seen in the platform pitch motion. This specific thrust behavior is a result of the construction of the Floating Control+, developed by ECN. The aerodynamic thrust of the simplified model shows positively damped behavior, i.e. an increase in aerodynamic thrust due to an increasing relative wind speed, which is expected by definition.

Quantitative decay comparison

To investigate the similarities between the pitch decay time traces of the simplified and fully coupled model, a quantitative comparison is carried out. The first quantification is in terms of the absolute differences of the logarithmic decrement over the first 4 oscillations. The second quantification is done by looking at the mean period (differences between two zero-crossings), over the first 4 oscillations. The results are shown in Fig. 7.5.

From Fig. 7.5, it is seen that for wind speeds under rated condition (< 12 m/s), the absolute differences in the logarithmic decrement δ are the largest compared to the wind speeds in the above rated condition. In the above rated wind speeds, the differences in the logarithmic decrement become smaller, indicating a similar decay. From this, it can be concluded that the decay simulations of the simplified model for constant uniform wind speeds above rated wind speed, compare relatively well with the decay simulations of the fully coupled model. The reason for this is explained by the behavior of the wind turbine controller. Above rated wind speed, the aerodynamic thrust behavior follows almost a horizontal straight line with respect to the relative wind speed. In contrast to the above rated conditions, the rated and below rated conditions show more variation in the aerodynamic thrust behavior when plotted

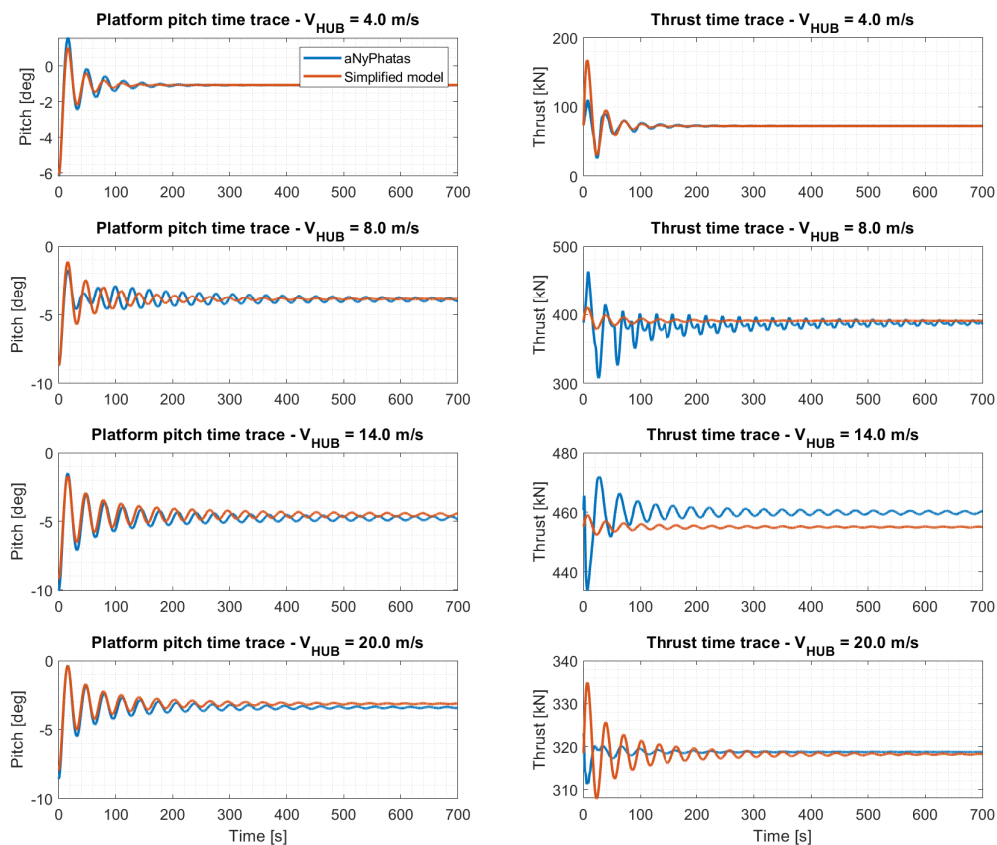


Figure 7.4: Comparison of time traces of a pitch decay in a 4 m/s constant uniform wind for a fully coupled and simplified simulations.

in the steady state thrust curve. The large aerodynamic thrust variation at and below rated result in differences in the platform pitch motion.

The difference in the mean platform pitch period shows the same trend as the differences seen in the logarithmic decrement. In the below rated conditions, the differences are the largest while the differences become smaller in the above rated condition. As explained for the differences in the logarithmic decrement, the differences in the mean platform pitch period can also be attributed to the variations in the aerodynamic thrust at and below rated conditions, caused by the wind turbine controller.

7.2.2 Response to irregular waves - constant uniform wind

This section elaborates on the verification of platform pitch motion response and aerodynamic thrust by simulations in irregular waves and constant uniform winds. The thrust sensitivities derived from the decay simulations are applied on the motion induced wind speeds. Again, the floating platform is constrained in all its DoFs, except for pitch. The simulations are performed in a Jonswap wave spectrum with a significant wave height H_s of 4.5 m, and a wave peak period T_p of 10 s. Only first order waves forces are considered, and no current and drag forces on the tower, nacelle and floater are taken into account. In all cases, wind and waves are assumed to act collinear with an environmental direction of 180° . Again, four wind speeds are investigated: far below (4 m/s), below (8 m/s), above (14 m/s) and far above (20 m/s) rated wind speeds.

Typical spectra of the platform pitch motion and aerodynamic thrust from the time-domain simulations

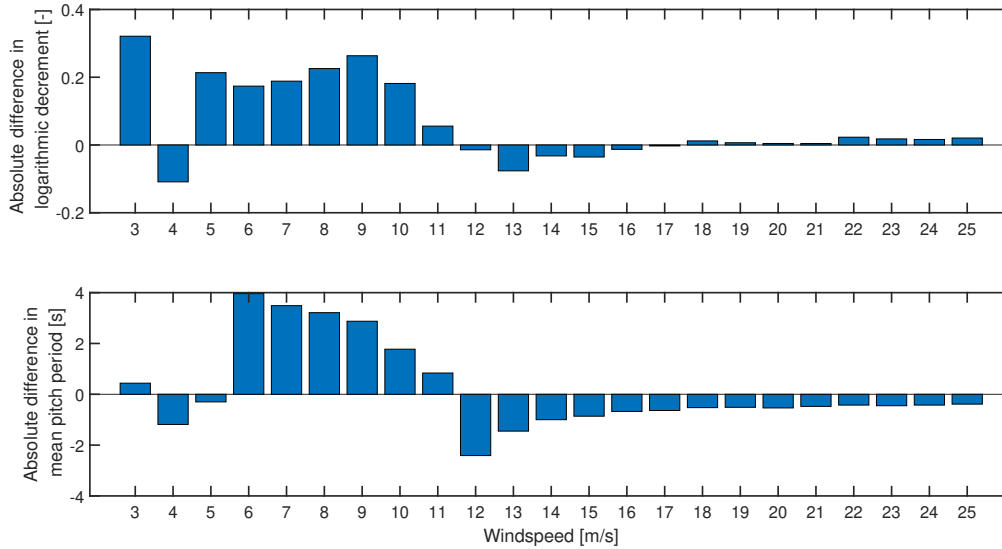


Figure 7.5: Absolute difference of the logarithmic decrement over the first 4 oscillations of the decay (top), and absolute differences of the mean platform pitch period over the same first 4 oscillations.

are presented in Fig. 7.6. From the figure it is clearly observed that the platform pitch spectra are well predicted by the simplified model in the wave frequency region. The spectrum of the aerodynamic thrust in a constant wind of 4 m/s, shows that the thrust response of the simplified model is approximately 9 times larger than the fully coupled simulations. This is caused by a relative too large thrust sensitivity, obtained from the decay analysis, see Fig. 7.7. While the difference in the aerodynamic thrust spectrum is significant, no effect is seen on the platform pitch. As the focus is on predicting the platform motions, the difference in aerodynamic thrust around the wave frequency is not of interest.

For a constant uniform wind speed of 8 m/s, the effect of the thrust sensitivity is the other way around. The smaller gradient of the thrust sensitivity, derived from the decay simulations, result in an underestimation of the aerodynamic thrust calculated by the simplified model compared to the fully coupled simulations, see Fig. 7.7. Moreover, the aerodynamic thrust spectrum of the fully coupled model shows energy in the low and high frequency regions. This is a direct result of the wind turbine controller, which is developed for wave load reduction at the rated wind speeds. This behavior is also clearly visible in Fig. 7.7. Obviously, the simplified model is unable to capture this aerodynamic thrust behavior.

The differences observed in the aerodynamic thrust spectrum in a constant uniform wind speed of 14 m/s are a result of the non linear behavior of the wind turbine controller. From Fig. 7.7, larger thrust variations are seen in the fully coupled model compared with the simplified model. The simplified model only introduces thrust variation based on the relative small thrust sensitivity. Due to this small gradient of the thrust sensitivity, the aerodynamic thrust variations are small. After transforming the time-domain signal into the corresponding PSDs, only a small amount of energy in the wave frequency region is observed. Again, the platform pitch spectrum is not affected by the significant difference in aerodynamic thrust.

Contrary to the aforementioned constant wind speeds, the aerodynamic thrust spectrum for a wind speed of 20 m/s show a good agreement between the simplified model and the fully coupled model. Despite that the thrust sensitivities have opposite signs, the aerodynamic thrust in the simplified and fully coupled model do show similar behavior.

Aerodynamic thrust versus relative wind speed

Fig. 7.7 shows the relation between the (filtered) aerodynamic thrust and the relative wind speed of the simplified model and the fully coupled model in irregular waves and constant wind. The simplified model includes the thrust sensitivities obtained from the decay simulations, while the aNySIM-Phatas model is equipped with the Floating Control+. From the figure it is clearly seen that the slope of the aerodynamic thrust versus relative wind of both models are quite different. As mentioned earlier, the differences in the aerodynamic thrust spectra observed in Fig. 7.6, are directly related to the differences between the slopes of the aerodynamic thrust and relative wind speed, for the various constant wind speeds.

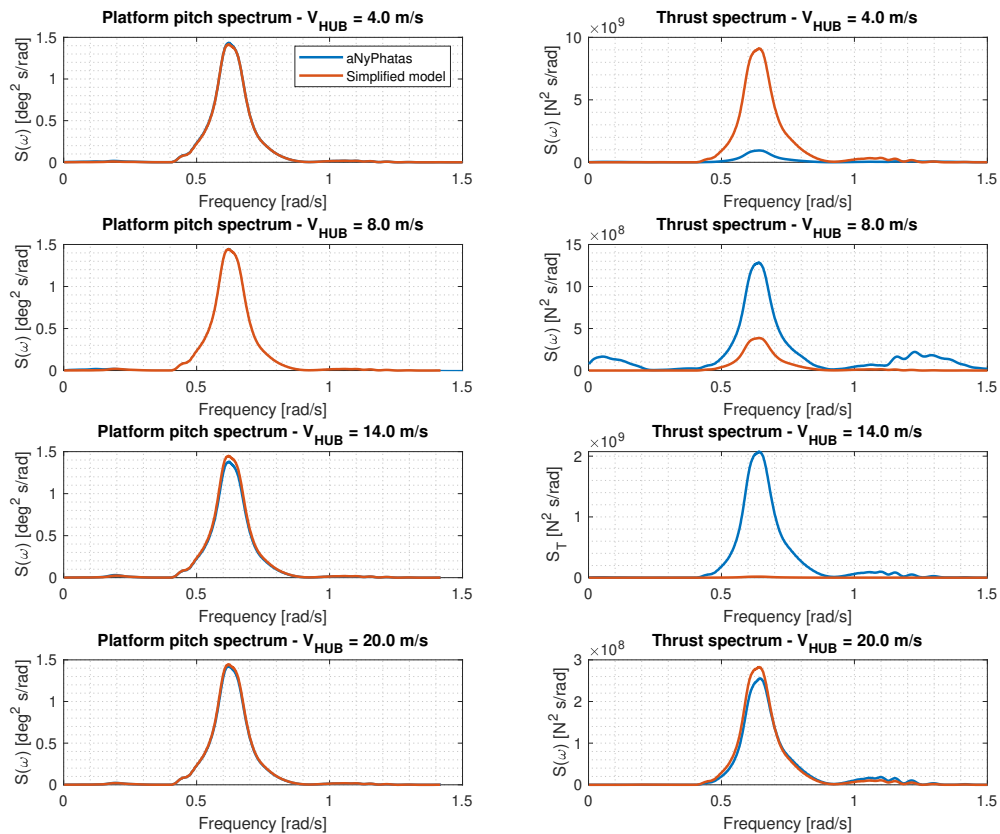


Figure 7.6: Comparison of platform pitch and aerodynamic thrust spectra between fully coupled and simplified simulations in irregular waves and constant (below and above rated) winds.

Effect of aerodynamic thrust on platform pitch

From the analyses in irregular waves and constant winds, it was seen that the aerodynamic thrust spectra, obtained from time-domain simulations, showed relative large variations in under and above rated conditions. However, the differences in the aerodynamic thrust did not seem to have a significant effect on the platform pitch. This is explained by the fact that aerodynamic thrust forces (causing a platform pitch moment around CoG) are dominated by the first order wave forces in pitch. Figure 7.8 presents the platform pitch wave forces together with the platform pitch moment induced by the aerodynamic thrust force in a constant wind speed of 12 m/s. At this wind speed the aerodynamic thrust forces are the largest, leading to the largest contribution of the aerodynamic forces on the platform pitch motion. From the comparison, it becomes clear the wave forces are around 300 times larger than the pitch moment induced by the aerodynamic thrust.

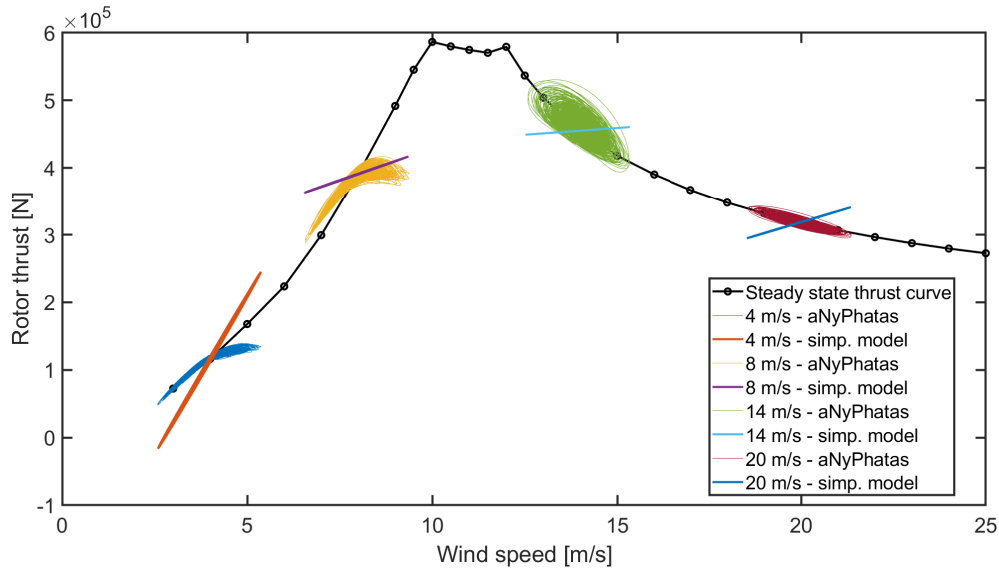


Figure 7.7: Differences in gradients of aerodynamic thrust versus relative wind for various constant wind speeds of the simplified model and fully coupled model.

Wave forces are linearly dependent on the wave height. Thus, by reducing the wave height by a factor 10 (resulting in a wave height of approximately 0.5 m), the platform pitch wave forces also reduce by a factor 10. As a consequence, the motions induced velocities will also go down, leading to a similar reduction in the aerodynamic moment. It can be concluded that the platform pitch response in the wave frequency region is dominated by the wave forces.

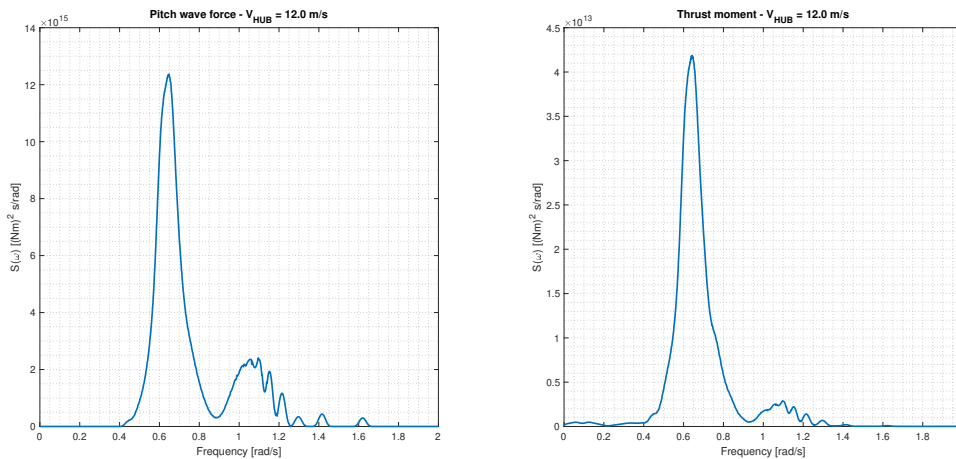


Figure 7.8: Platform pitch wave forces compared to pitch moment cause by aerodynamic thrust for a constant uniform wind speed of 12 m/s.

7.3 Low, natural pitch and high-frequency turbulent wind loading

In this section, a (small) step is taken towards a fully turbulent wind field. The correct implementation of the steady state thrust curve and thrust sensitivities is assessed. This is done by investigating the results of the platform pitch response under a wind loading with three different frequencies: 0.015, 0.21 and 1.5 rad/s. In the simplified model, the velocities components associated with the low frequency part of the wind, follow the steady state thrust curve in both the below and above rated condition. The velocity components associated with the natural platform pitch frequency include the thrust sensitivities. At this stage, the high frequency components of the turbulent wind field follow the steady state thrust curve as well.

7.3.1 Low-frequency turbulent wind

The PSDs for wind speeds of 8 and 12 m/s, containing only low frequency turbulence, are depicted in Fig. 7.9. As for most wind speeds, including 8 m/s, the PSD corresponds very well. In the above rated conditions, the platform pitch spectra show energy content around the natural pitch frequency of the platform, while the aerodynamic thrust spectrum does not show any energy around this frequency. For the fully coupled simulations, this energy content might be a result of the initial blade pitch angle before starting the calculation. An initial blade pitch angle of 31 degrees is set, which is not the optimal blade pitch angle for wind speeds in the above rated conditions, after which the blade pitch angle is adjusted by the control system. Therefore, relative high aerodynamic loads on the blades occur at the start of the simulation, resulting in platform motion at the natural (pitch) frequency. Moreover, as the aerodynamic damping is relatively low in the above rated condition, energy is present at the natural pitch frequency. When the simulations are run for a longer time period, these transients effects will be dissipated. The large aerodynamic damping which is present in the under rated conditions leads to damping of these platform motions at the natural pitch frequency after the platform is excited.

For a wind speed of 12 m/s however, some differences are observed in the low frequency region. As already shown in Fig. 6.4, the aerodynamic thrust in the fully coupled model for a wind speed of 12 m/s, does not follow the steady state thrust curve, while the simplified model does follow the curve. As a result, the aerodynamic thrust forces in the simplified model deviate significantly, as shown in Fig. 7.10, leading to a relative large error in the platform pitch. The behavior of the aerodynamic thrust of the fully coupled model at 12 m/s, should be investigated whether this is the desired behavior. If so, it is easy to include.

7.3.2 Natural pitch frequency turbulent wind

The PSDs of wind speeds of 8 and 12 m/s, containing only turbulence in the frequency range around the natural frequency of platform pitch of 8 and 12 m/s, are shown in Fig. 7.11. For 8 and 12 m/s, it is seen that the fully coupled model generates much more aerodynamic thrust than the simplified model. The wind speeds considered are located around the rated wind speed, where the aerodynamic thrust versus relative wind show large non linearities. The simplified model, which is constructed only with the thrust sensitivities, is not able to capture the correct aerodynamic thrust loads. The highly non linear behavior of the thrust is illustrated for a wind speed of 10 m/s in Fig. 7.12. The effect of the wind turbine controller on the aerodynamic thrust is clearly observed, as well as the small contribution of the aerodynamic thrust in the simplified model. It is seen that the simplified model is not able to capture aerodynamic thrust around the rated wind speed. In the above rated conditions, the thrust sensitivities in the simplified model are too large, leading to large motions.

7.3.3 High-frequency turbulent wind

In the simplified model, the high-frequency turbulence in the wind speed acts on the thrust curve. Fig. 7.13 shows spectra of the platform pitch and aerodynamic thrust for 8 and 14 m/s high-frequency wind speed. For a wind speed of 8 m/s, it is seen that the high-frequency thrust is relative well predicted by the simplified model. For the above rated condition however, the high-frequency aerodynamic thrust is significantly larger than the simplified model. This is because the simplified model follows the thrust curve, which has a negative gradient, while the fully coupled model follows a strongly positive gradient.

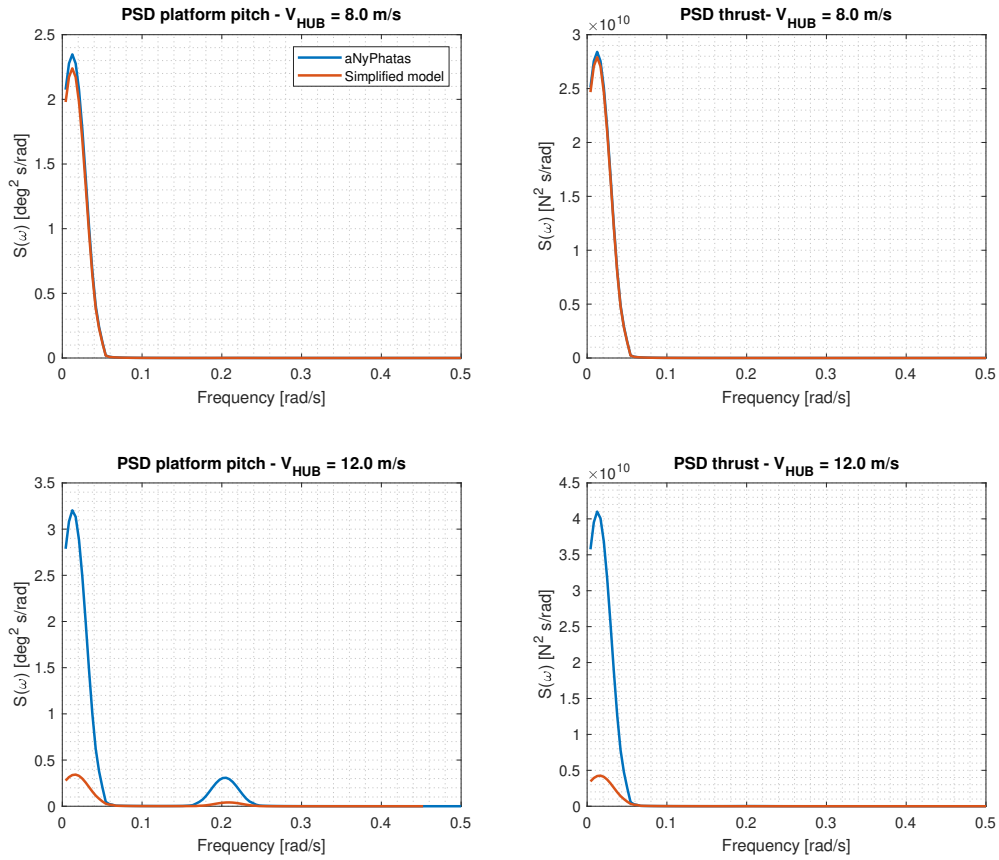


Figure 7.9: Comparison of the platform pitch and aerodynamic thrust between the fully coupled and simplified model, showing PSDs for wind fields of 8 and 12 m/s, containing only low-frequency turbulence.

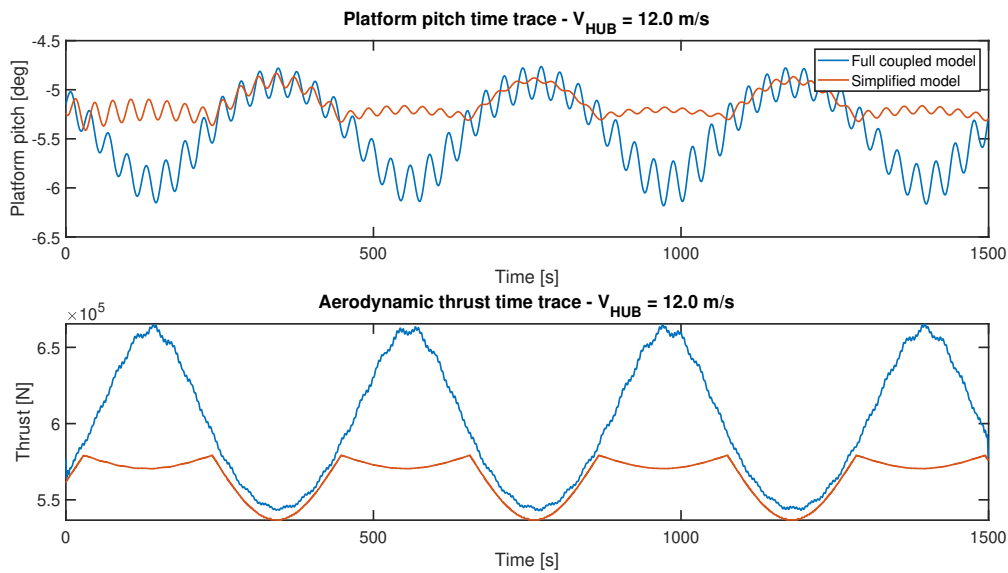


Figure 7.10: Comparison of the platform pitch and aerodynamic thrust time trace between the fully coupled and simplified model, showing time traces for a wind field of 12.0 m/s, containing only low-frequency turbulence.

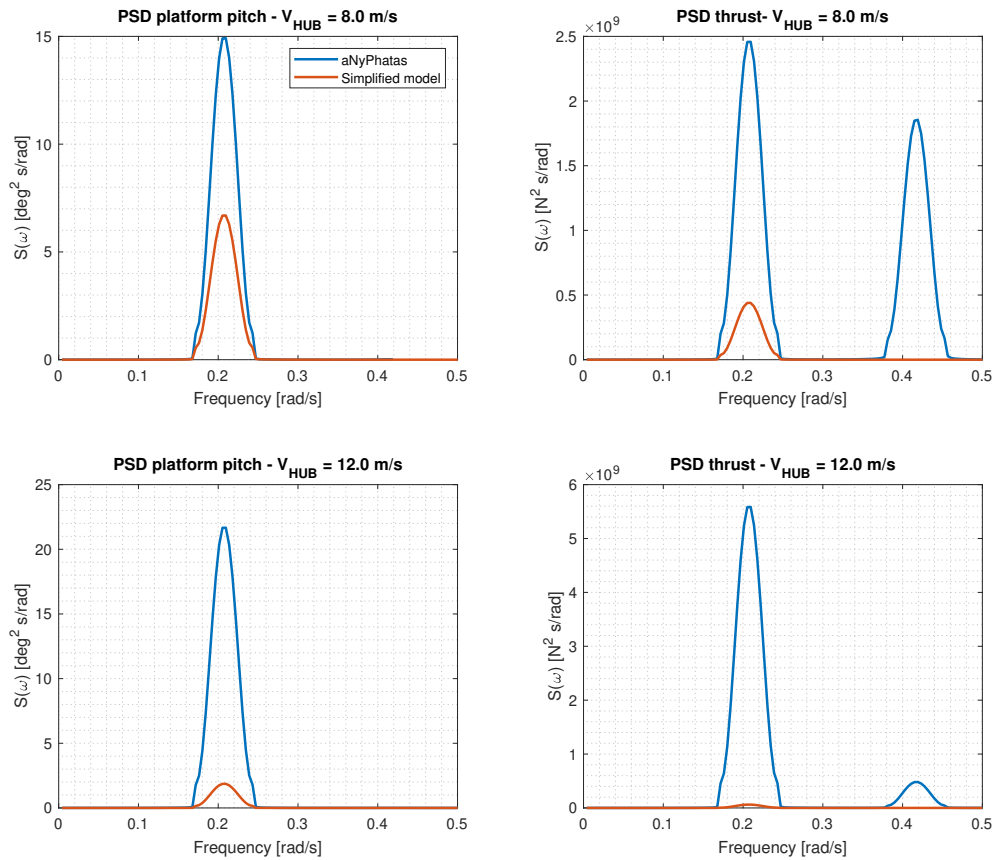


Figure 7.11: Comparison of the platform pitch and aerodynamic thrust between the fully coupled and simplified model, showing PSDs for wind fields of 8 and 12 m/s, containing only turbulence in the frequency range around the natural platform pitch frequency.

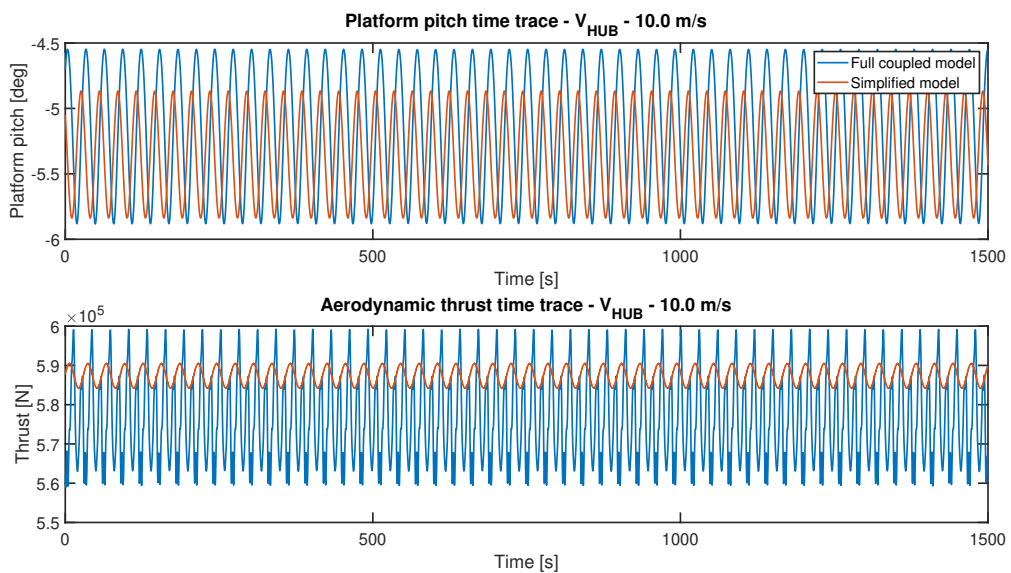


Figure 7.12: Comparison of the platform pitch and aerodynamic thrust between the fully coupled and simplified model, showing time traces for a wind field of 10 m/s, containing only turbulence in the frequency range around the natural platform pitch frequency.

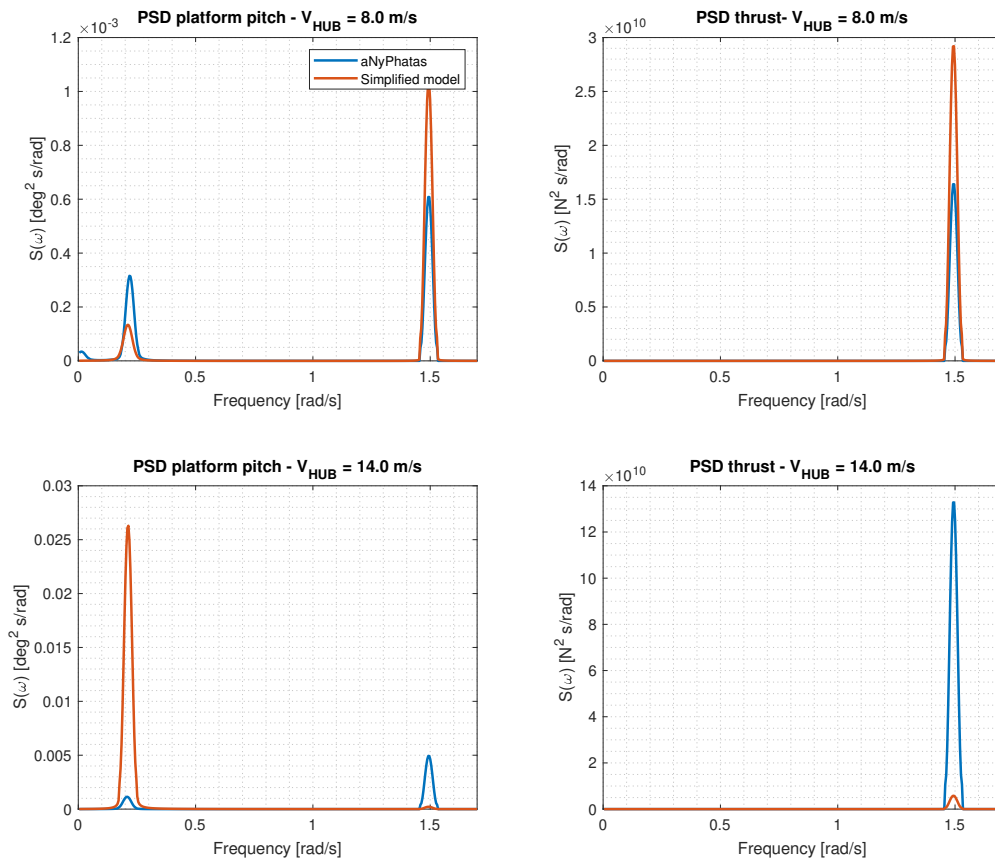


Figure 7.13: Comparison of the platform pitch and aerodynamic thrust between the fully coupled and simplified model, showing PSDs for wind fields of 8 and 14 m/s, containing only high-frequency turbulence.

7.4 Turbulent wind verification - platform pitch only

In this section, the simplified model is verified in turbulent wind. As described in Chapter 6, the simplified model filters the incoming wind speed with a FFT band-stop filter, to attenuate the aerodynamic thrust excitation around the natural platform pitch frequency.

The turbulent wind verification starts with the comparison of the platform pitch decay in calm water between the fully coupled and simplified model for a range of turbulent wind speeds. By this, the implementation of the thrust sensitivities, derived in the previous chapter, are assessed. Also, the incoming wind filtering is tested. Subsequently, a calm water condition with turbulent wind is investigated. Then, irregular waves are added to the simulations for the same range of turbulent wind speeds as used in the decay simulations. In the verification, only first order wave forces are taken into account.

7.4.1 Platform pitch decay - turbulent wind

Decay simulations are performed in turbulent wind conditions. The same thrust sensitivities as used in constant wind conditions are used, as confirmed in Section 6.3.3. The thrust sensitivities are applied on the platform induced wind speed, while the turbulent wind speed is filtered around the platform natural pitch frequency. The look-up table as derived from the steady state thrust curve is included and is applied on the incoming (filtered) wind field.

Quantitative decay comparison

To investigate the similarities between two pitch decay time traces in turbulent wind, again a quantitative comparison is done, as for the constant uniform winds. The first quantification is in terms of the absolute differences of the logarithmic decrement over the first 4 oscillations. The second quantification is done by looking at the mean period (differences between two zero-crossings), over the first 4 oscillations. The results are shown in Fig. 7.14.

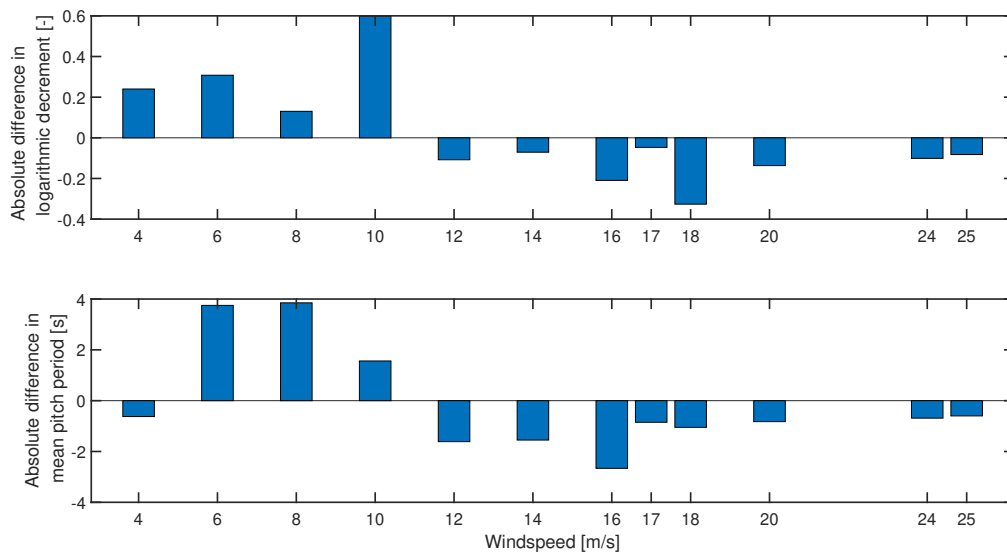


Figure 7.14: Results of decay simulations in turbulent wind, showing the absolute difference of the logarithmic decrement over the first 4 oscillations (top), and absolute differences of the mean platform pitch period over the same first 4 oscillations in turbulent wind.

From Fig. 7.14, it is seen that for wind speeds under rated condition (< 12 m/s), the absolute differences in the logarithmic decrement δ are the largest compared to the wind speeds in the above rated condition. In the above rated wind speeds, the differences in the logarithmic decrement become smaller, indicating a similar decay. From the analysis, it can be concluded that the decay simulations of the simplified model for turbulent wind speeds follow the same trend as the decay in constant winds. The largest

difference, with respect to the logarithmic decrement, is seen for an under rated turbulent wind speed of 10 m/s and a above rated of 18 m/s. The platform pitch time traces showing the comparison of the two wind speeds between the fully coupled and simplified model are depicted in Fig. 7.15.

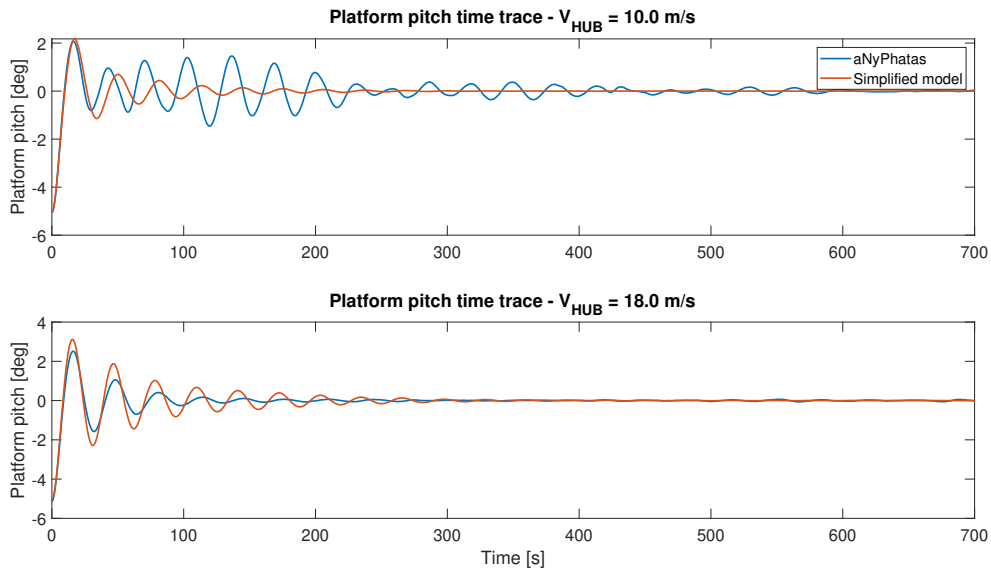


Figure 7.15: Platform pitch and aerodynamic thrust time trace for a turbulent wind speed of 10 m/s (after the results of a decay without external force is subtracted from the results of a decay with external force), showing non linearity of the aerodynamic thrust of the fully coupled model.

From the figure, it is seen that for a turbulent wind speed of 10 m/s the wind turbine controller induces non linear behavior for the platform pitch in the fully coupled model. Around rated, the wind turbine controller shifts between two different control regimes: optimal tip speed ratio control and blade pitch control. Especially the blade pitch control causes relative large (non linear) variations in the aerodynamic thrust, resulting in non linear platform pitch response. Obviously, this non linearity is not captured by the simplified model.

For the far above rated turbulent wind speed of 18 m/s, the platform decay show less non linearity. The same reasoning as for the constant uniform winds can be applied, i.e. the aerodynamic thrust follows a almost horizontal straight line. This is mainly due to the small gradient of the thrust curve, indicating low wind turbine action.

7.4.2 Calm water - turbulent wind

In this section, the simplified model is verified in a fully turbulent wind in calm water (i.e. no wave and current).

Mean, standard deviation and maximum

The mean, standard deviation and maximum values of the platform pitch motion are given in Table B.1 in Appendix B.1. For visualisation, the tabulated results are illustrated in Fig. 7.16. The results in calm water are plotted together with results with waves. The results from waves are discussed in the next section. From the results in calm water, it is concluded that the differences in the mean are within 11% and 6%, for the under and above rated condition, respectively. In terms of the absolute differences, the differences do not exceed 0.32 degrees. The differences in the standard deviation are within 32% and 45%, for the under and above rated condition, respectively. The largest differences are found for the wind speeds: 8, 24 and 25 m/s, which is clearly seen in the figure. The differences in the maximum values of the platform pitch do not exceed 32% and 13%, for the under and above rated condition, respectively. The differences in the maximum value do not exceed 0.90 degrees, in terms of absolute values.

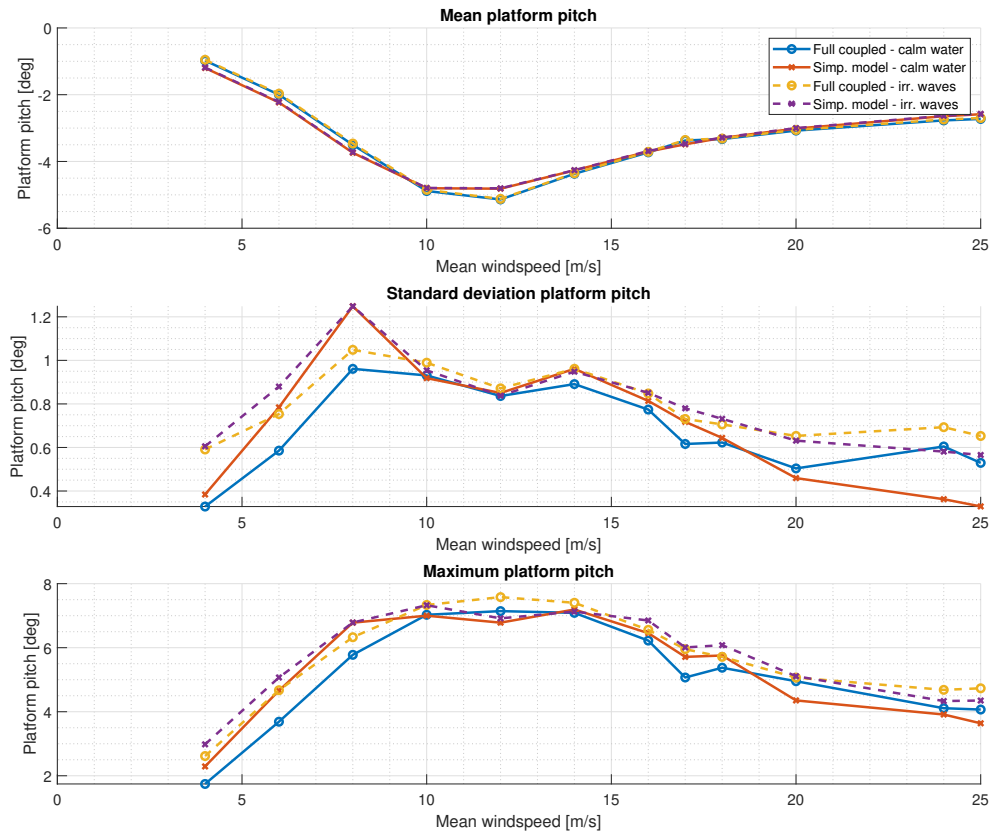


Figure 7.16: Comparison of platform pitch mean, standard deviation and maximum values between fully coupled and simplified simulations in calm water and turbulent wind.

Platform pitch and aerodynamic thrust spectra

From Fig. 7.16, it was observed that the largest differences were seen at turbulent wind speeds of 8, 24 and 25 m/s. Figure 7.17 shows spectra of the platform pitch and aerodynamic thrust for two under rated and two above rated turbulent wind speeds, including 8 and 24 m/s.

Only the low-frequency part is shown in the spectra. From the figure it becomes clear that the platform pitch motions are dominated by the low-frequency motions. For a turbulent wind speed of 8 m/s, it is seen the low-frequency part is well predicted by the simplified model. However, around the pitch natural frequency, the differences are significant. The first reason is that the filter on the wind speed, resulting in lower aerodynamic thrust around 0.22 rad/s, has a negligible effect. This is because the platform pitch frequency for a wind speed of 8 m/s, is not located exactly at 0.22 rad/s. The second reason is explained by the fact that the simplified model overestimates the aerodynamic thrust over the full frequency range. Also, the relative small thrust sensitivity seems to be unable to damp the pitch motion sufficiently.

For a turbulent wind speed of 16 m/s, the platform pitch spectra are in relative good agreement. The low-frequency response is now dominated by the natural pitch frequency response. The main differences in the platform pitch response can be attributed to the differences seen in the aerodynamic thrust spectrum. However, the filter effect is noticed in the aerodynamic thrust, around 0.22 rad/s.

The low frequency part in the platform pitch spectrum for a turbulent wind speed of 24 m/s is predicted well by the simplified model. However, the platform pitch response of the fully coupled model dominates the response of the simplified model. The effect of the wind speed filter on the aerodynamic thrust of

the simplified model is clearly seen around 0.22 rad/s. However, the aerodynamic thrust of the fully coupled model contains more energy around 0.22 rad/s, which results in more platform pitch response. The reason that the simplified model contains less energy around the natural platform pitch frequency, might be caused by the aerodynamic thrust acting on the incoming wind speed instead of the relative wind speed.

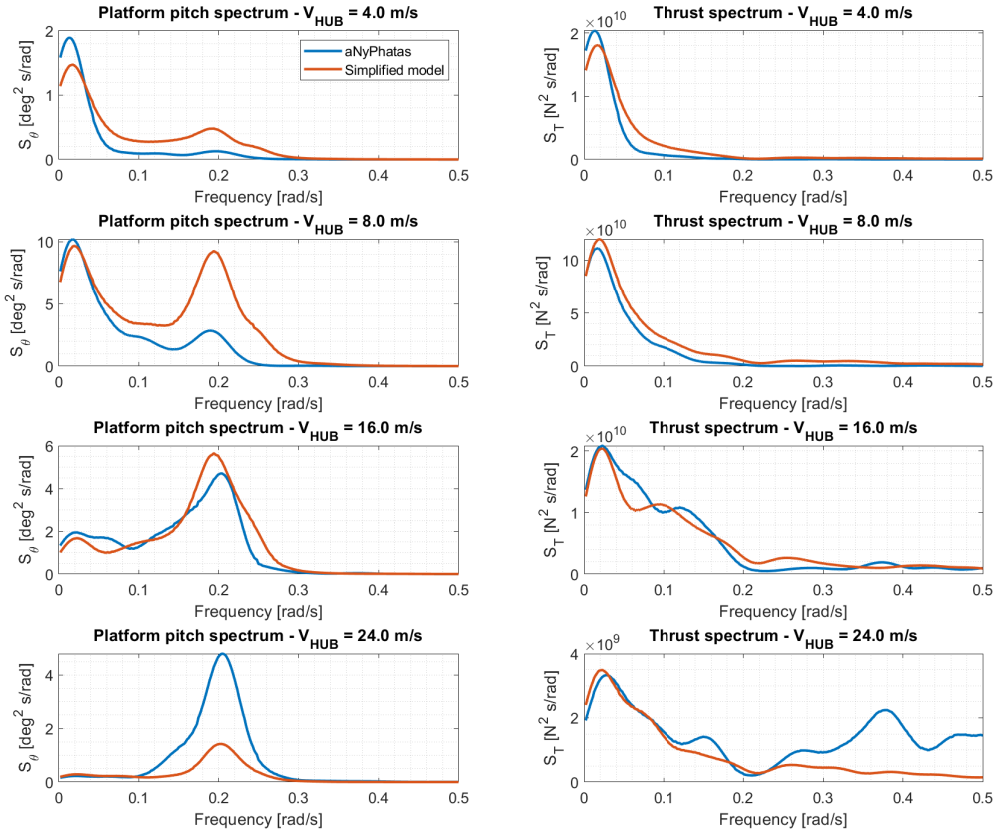


Figure 7.17: Comparison of pitch and aerodynamic thrust spectrum between fully coupled and simplified simulations in calm water and turbulent wind.

Aerodynamic thrust versus relative wind speed in thrust curve

The large differences can also clearly be seen when the aerodynamic thrust of both the fully coupled and simplified model are plotted versus the relative wind speed in the steady state thrust curve, see Fig. 7.18. For both wind speeds, it is seen that the simplified model follows the thrust curve, indicating the large contribution of the low-frequency turbulence. The fully coupled model shows less scattering for the wind speed of 8 m/s, as the high frequency contribution in the wind is smaller compared to 24 m/s. From this plot it can be concluded that the variations in the aerodynamic thrust with respect to the relative wind speed in the fully coupled model are dominated by the wind turbine controller. Clearly, the simplified model is unable to capture the wind turbine control behavior.

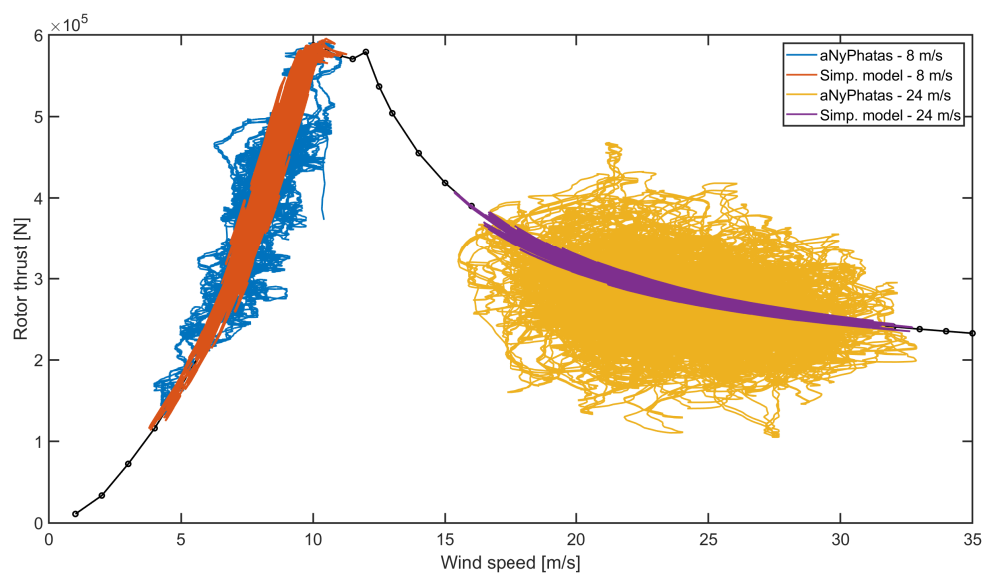


Figure 7.18: Aerodynamic thrust plotted versus relative wind speed for 8 m/s and 24 m/s for the simplified and fully coupled model in turbulent wind without waves.

7.4.3 Response to irregular waves - turbulent wind

For the same range of turbulent wind speeds as in the previous section, irregular waves are added. As described at the start of this section, only first order wave forces are considered.

Mean, standard deviation and maximum

The mean, standard deviation and maximum values of the platform pitch in irregular waves and turbulent winds are given in Table B.1 in Appendix B.1. The tabulated results are graphically shown in Fig. 7.16, together with the results in calm water. From the figure it is clearly observed that the addition of irregular waves does have a negligible effect on mean values of the platform pitch. The differences in the standard deviation and maximum values become somewhat smaller.

From the results in irregular waves, it is concluded that the differences in the mean are within 13% and 6%, for the under and above rated condition, respectively. In terms of the absolute differences, they do again not exceed 0.32 degrees. The differences in the standard deviation are within 19% and 16%, for the under and above rated condition, respectively. The largest differences are again found for the wind speeds: 8, 24 and 25 m/s, which is also observed in the figure. The differences in the maximum values of the platform pitch do not exceed 14% and 9%, for the under and above rated condition, respectively. The absolute differences in the maximum value do not exceed 0.70 degrees.

Platform pitch and aerodynamic thrust spectra

From Fig. 7.16, it was observed that the largest differences were seen at turbulent wind speeds of 8, 24 and 25 m/s. Figure 7.19 shows spectra of the platform pitch and aerodynamic thrust for two under and two above rated conditions, including 8 and 24 m/s. To illustrate the effect of the thrust sensitivity, a third line is plotted in the figure. From the figure, the wave frequency response is clearly visible and matches in all cases. This match is attributed to the dominating first order wave forces over the aerodynamic forces in this region.

From the spectra in 4 m/s turbulent wind, it is observed that the platform pitch response in the wave frequency is approximately of the same order as the response in the low frequency region. Still, the low frequency response dominates the response around the platform pitch natural frequency. A large effect of the thrust sensitivity at the natural platform pitch frequency is seen, which dampens to response. Overall, the agreement is satisfactory.

For a turbulent wind speed of 8 m/s, the low frequency motions are dominant, but are well predicted by the simplified model. However, as for turbulent wind and calm water, the effect of the filter on the platform pitch response is small. The response around the natural pitch frequency is over predicted by the simplified model, and a small effect of the thrust sensitivity is seen.

For a turbulent wind speed of 16.0 m/s, the platform pitch spectrum shows again a relative good agreement. The effect of the wind speed filter is clearly visible in the aerodynamic thrust spectrum. The filter results in a lowering of the pitch response. The thrust sensitivity however, contributes little to the damping of the response.

The low frequency part in the platform pitch spectrum for a turbulent wind speed of 24 m/s is significantly dominated by the pitch natural frequency response, in the fully coupled model. However, the response of the simplified model is significantly lower. This is attributed to the same effect as in the calm water condition. The simplified model calculates the aerodynamic thrust on the incoming wind speed instead of the relative wind speed, resulting in low thrust excitation around the natural platform frequency. As for a turbulent wind speed of 16 m/s, the thrust sensitivity contributes little to the damping of the platform pitch response.

Aerodynamic thrust versus relative wind speed in thrust curve

The large differences can also clearly be seen when the aerodynamic thrust of both the fully coupled and simplified model are plotted versus the relative wind speed in the steady state thrust curve, see Fig. 7.20. For both wind speeds, it is seen that the simplified model follows (almost) the thrust curve. For the wind speed of 8 m/s, the aerodynamic thrust of the fully coupled model is less scattered compared to

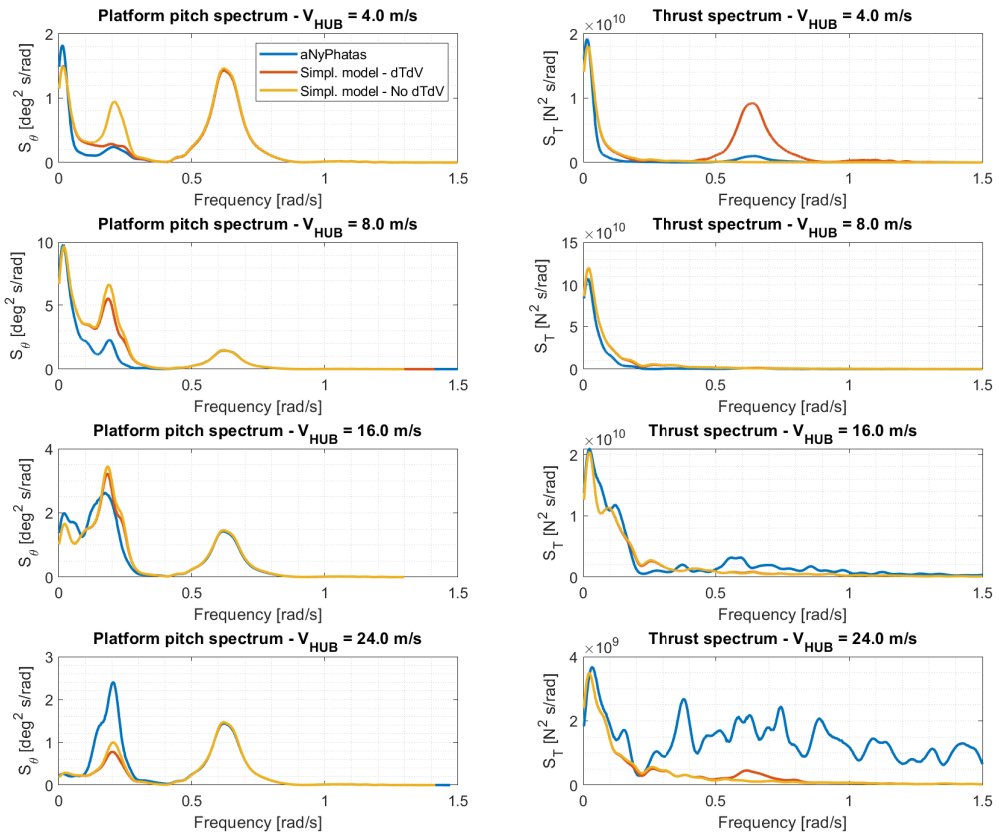


Figure 7.19: Comparison of pitch and aerodynamic thrust spectrum between fully coupled and simplified simulations with waves and turbulent wind.

24 m/s, as the high frequency contribution in the wind is smaller. From the plot it can be concluded that the variations in the thrust with respect to the relative wind speed are dominated by the wind turbine controller, and that the thrust sensitivity in the simplified model has a negligible effect.

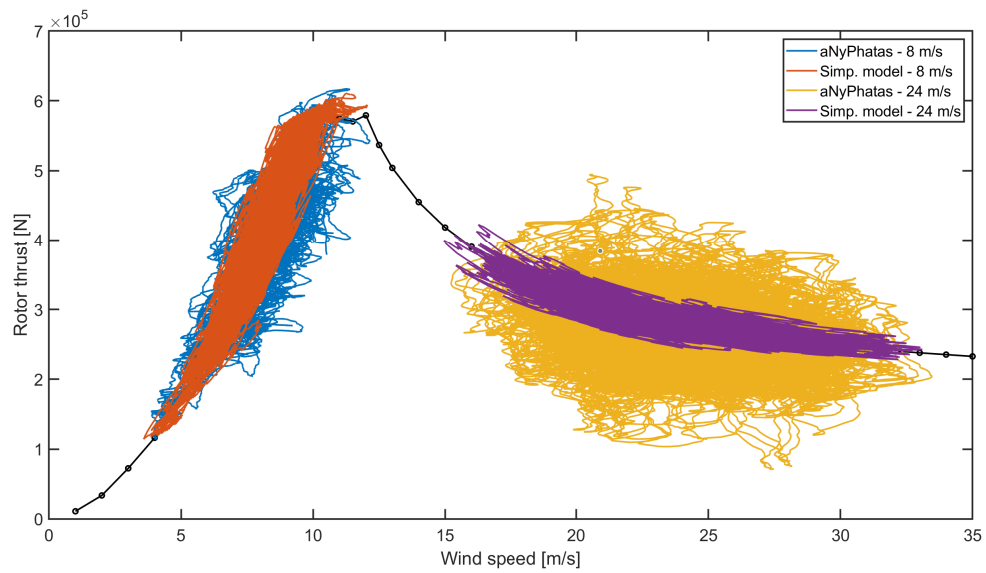


Figure 7.20: Aerodynamic thrust plotted versus relative wind speed for 8 m/s and 24 m/s for the simplified and fully coupled model in turbulent wind with waves.

7.5 Response to irregular waves in all DoF - turbulent wind

Until now, only platform pitch motion has been studied, while all other DoFs were fixed. Also, only first order waves forces were considered. In this section, the system is free to float in all its directions, and second order wave forces are added. However, no wind loads on the floater, tower and nacelle are considered, and also no current load is taken into account.

This step, with all DoFs activated, serves as the ultimate test concerning platform motions, fairlead tension and computational time.

7.5.1 Floater motions

Especially the floater motions which are a result of the combined effect of the hydrodynamics, aerodynamics and the control system are important. The floater motions which are lightly damped and with their natural frequency within the wind turbine controller bandwidth, are of interest. Therefore, the platform surge and pitch are discussed in this section. The mean and maximum response values, for both DoFs, are presented. The wind and waves are assumed to have a direction of 180 degrees. Also, motion spectra are shown.

Mean, standard deviations and maximum

The mean floater motions are tabulated in Table B.2 in Appendix B.2. The results, as illustrated in Fig. 7.21, are promising. From the results in irregular waves with all DoF enabled, it is concluded that the differences in the mean of platform surge are within 5%. The mean absolute differences do not exceed 0.23 meter. The differences in the standard deviation show an accuracy of maximum 17% and 12%, for the under and above rated condition, respectively. The largest differences are found around the rated wind speed, as observed in the figure. The differences in the maximum values of the platform surge do not exceed 10% for all wind speeds. In terms of the absolute differences, the maximum value does not exceed 0.90 meter.

The differences in the mean of platform pitch are within 10%. The mean absolute differences do not exceed 0.25 degrees. The differences in the standard deviation show an accuracy of maximum 23%. The differences in the maximum values of the platform pitch do not exceed 15% for all wind speeds. In terms of the absolute differences, the maximum value does not exceed 0.52 degrees. Overall, the results are very satisfactory.

Motion spectra

The surge and platform pitch motion spectra at CoG, together with the aerodynamic thrust are shown in Figs. 7.22 and 7.23. Looking at the platform surge spectra, it is seen that the spectra of the simplified simulations match the fully coupled simulations very well, for all wind speeds. The platform surge response is dominated by low frequency response as a result of the low frequency wind loads.

The response of the platform pitch around the wave frequency region are in very good agreement for all wind speeds. The largest differences are seen around the natural platform pitch frequency, and can directly be related to the differences seen in the aerodynamic thrust spectra. For 8 m/s, the simplified model over predicts the pitch response around the natural platform pitch frequency. This is a result of the small effect of the FFT band-stop filter of the wind speed on the aerodynamic thrust, as seen in the figure. For 16 m/s, the platform pitch response of the simplified model is relatively in good agreement compared to the fully coupled model. For 24 m/s, the simplified model under predicts the platform pitch motion with respect to the fully coupled model. As the effect of the FFT band-stop filter is clearly seen in the aerodynamic thrust around 0.22 rad/s, the fully coupled model contains significantly larger thrust excitation compared to the simplified simulations.

7.5.2 Fairlead tension

The floating structure is moored with three mooring lines. The wave, current and wind directions are assumed to act collinear with a direction of 180 degrees. Among all three mooring lines, the upwind mooring line was selected for this study since it is aligned with the incoming wind and wave direction. As a result, this mooring line is subjected to the highest loads. The tension in the mooring line is

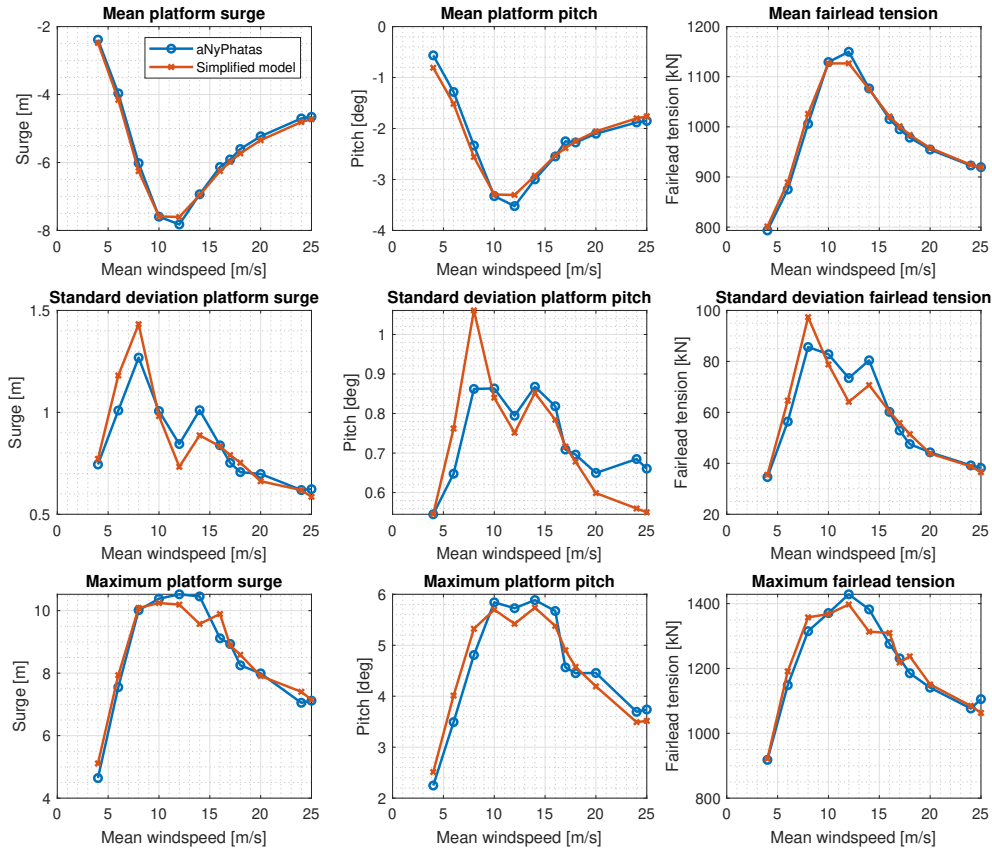


Figure 7.21: Comparison of mean, standard deviation and maximum values between fully coupled and simplified simulations in platform surge, pitch and fairlead tension when the platform is free to float in all directions with waves and under turbulent wind.

determined at the fairlead position. The tensions in the fairlead are one of the main design criteria.

Mean, standard deviation and maximum of forward fairlead tension

The mean values, standard deviation and maximum values of the forward fairlead tensions are shown in Table B.3 in Appendix B.2, and the results are plotted in Fig. 7.21. The differences in the mean of forward fairlead tension are within 2%, which comes down to a maximum absolute difference of 20 kN, which is very satisfactory. The relative differences in the standard deviation show an accuracy within 15%, while the absolute differences do not exceed 12 kN. The differences in the maximum values of the fairlead tension do not exceed 5% for all wind speeds, which is again very satisfactory. In terms of the absolute differences, the maximum value remains within 70 kN. From the results in the differences in the tension of the forward fairlead, it is concluded that the simplified model is capable of predicting the tension very well.

Fairlead tension spectra

The forward fairlead tension spectra are shown in Fig. 7.24. The spectra of the simplified simulations compare very well with the spectra obtained in the fully coupled simulations. The fairlead spectra clearly show that the low frequency responses of the floating platform are dominant.

7.5.3 Computational time

The computational time is one of the limiting factors in the concept design phase of the floater. Fully coupled simulations are time consuming. The simplified model is developed to simplify the aerodynamics

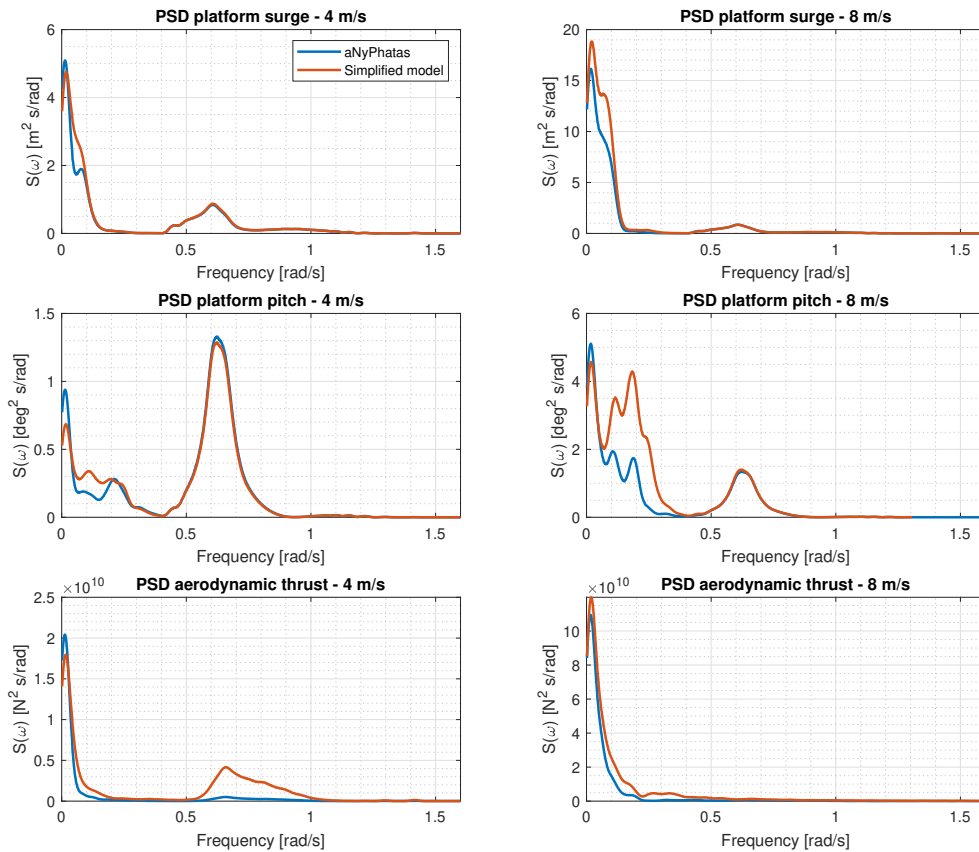


Figure 7.22: Platform surge, pitch and aerodynamic thrust spectra for two under rated wind speeds when the platform is free to move in all its directions.

with the aim to lower the computational time, while still acceptable accuracy is maintained in the calculation of the motions and mooring loads of the platform. The total calculation time for a free floating system per turbulent wind speed is presented in Table 7.2. From the results, it is seen that the total time (in minutes) for the fully coupled model, for all turbulent wind speeds, is equal to almost 277 minutes. The simplified model reaches a total computational time of 56 minutes. From the comparison, it can be concluded that the simplified model is around 5 times faster than the fully coupled model.

Not only computational time is of interest. Also, preparation time is considered to be an important parameter. Once the hydrodynamic data base is constructed, the aerodynamics can easily be simplified by the use of the steady state thrust curve. The fully coupled model needs a full description of the wind turbine, including blade characteristics and wind turbine control system.

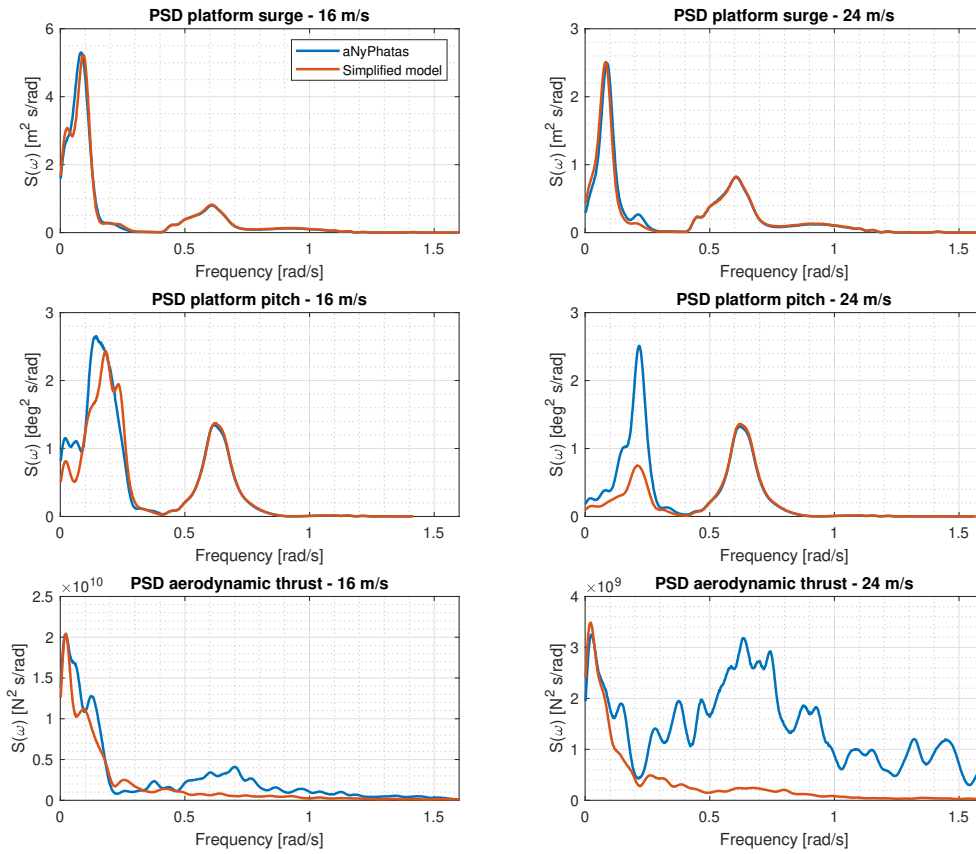


Figure 7.23: Platform surge, pitch and aerodynamic thrust spectra for two above rated wind speeds when the platform is free to move in all its directions.

Table 7.2: Computational time of the fully coupled model and simplified model for a range of turbulent wind speeds.

Wind speed [m/s]	Computational time [min]	
	Fully coupled	Simplified model
4	23.1	4.9
6	22.6	4.9
8	24.8	5.1
10	24.0	5.1
12	22.1	4.9
14	25.6	4.5
16	25.7	4.5
17	22.3	4.6
18	21.8	4.6
20	21.3	4.4
24	21.3	4.6
25	21.9	4.5
Total	276.6	56.4

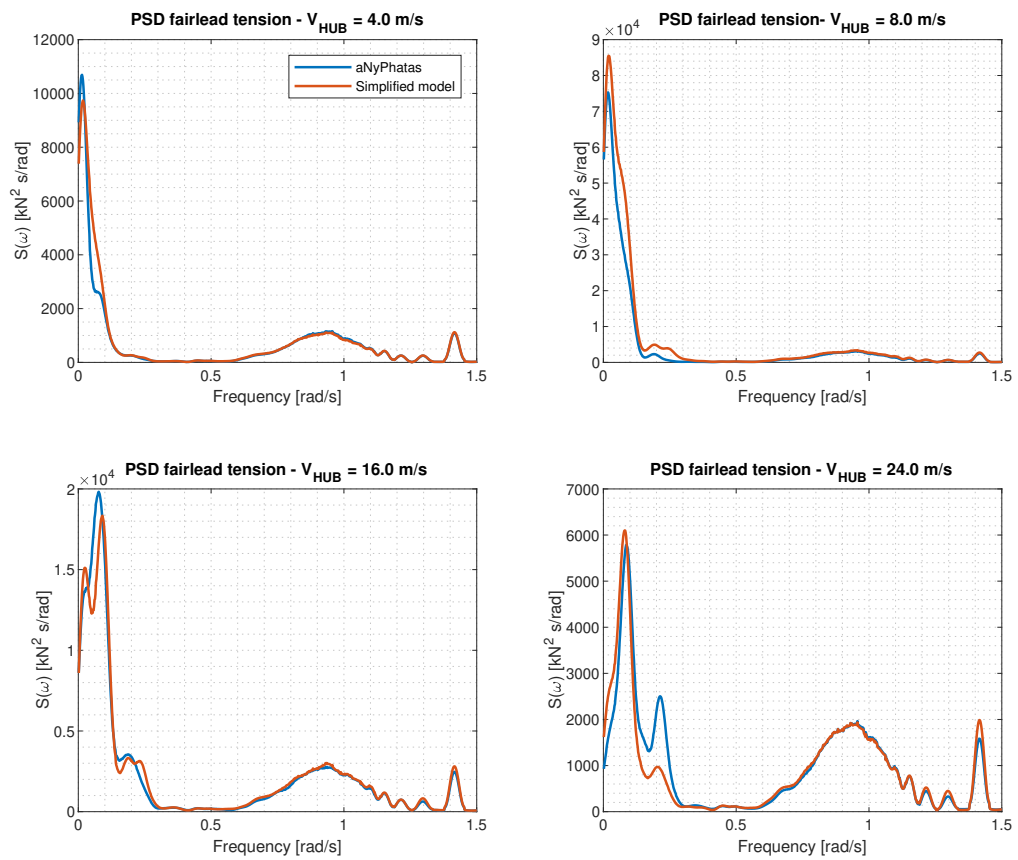


Figure 7.24: PSD of forward fairlead in case the floater is free to move in all its directions.

7.6 Conclusions and recommendations

In this section, the research question formulated in the beginning of the chapter is answered:

To what extend does the simplified model compare to fully coupled aero-hydro-servo-elastic time-domain simulations?

Staircase wind

From the verification, it was shown that the thrust curve is implemented correctly and that the differences with respect to the mean values of the aerodynamic thrust and platform pitch are small.

Constant winds - pitch only

In the constant wind verification, it is shown that the decay simulations matched relatively good, especially in the above rated conditions due to the small aerodynamic thrust variations versus wind speed. After the addition of irregular waves, it is shown that the first order wave forces significantly dominated the aerodynamic loads in the wave frequency range.

Low, natural pitch and high frequency turbulent winds - pitch only

In case the floating platform is subjected to a wind field containing only low-frequency turbulence, the results of the fully coupled and simplified model showed good agreement with respect to the spectra. For a low-frequency turbulent wind field of 12 m/s, it is seen that the fully coupled model does not follow the peak shaved steady state thrust curve. For wind fields containing only turbulence with a frequency equal to the natural platform pitch frequency, it is shown that around rated the thrust sensitivities in the simplified model are not able to capture the response sufficiently.

The platform pitch response under the action of high-frequency turbulent wind speeds showed relatively large differences, especially in the above rated conditions. This is because the simplified model reads the thrust from the thrust curve, while this is not certainly not true for the above rated condition.

Turbulent winds - pitch only

The decay simulations in turbulent wind showed the same trend as the decay simulations in constant wind. Around rated, the wind turbine controller induces non linear aerodynamic response resulting in non linear platform motion. The platform pitch response showed good agreement with respect to the mean values in waves and calm water, both not exceeding 0.32 degrees. It is shown that in the below rated conditions, the effect of the wind speed filter is relatively small. In the above rated condition, the effect of the filter on the thrust is larger, because more energy is present around the natural pitch frequency.

Turbulent winds - all DoF

The ultimate case is tested at last, where the floating platform is free to move in all directions, under the influence of irregular waves and turbulent wind. The mean values of the platform surge and pitch are very satisfactory as the differences do not exceed 5% and 10%, respectively. The maximum absolute differences in the maximum values do not exceed 0.90 meter and 0.52 degrees for platform surge and pitch, respectively. The results of the tension in the forward fairlead of the simplified model are in very good agreement compared to the fully coupled model. The differences in the mean are within 2%, while the differences in the maximum fairlead tensions are within 5%.

With respect to computational time, the simplified simulations are approximately 5 times faster than the fully coupled simulations. Not only a decrease in computational time is achieved by the simplified model, also the complexity compared to the fully coupled model is significantly reduced, i.e. the simplified model is much easier to construct.

7.6.1 Recommendations

Future work must be done to include the wind loads on the floater, tower and nacelle. Also, only one directional (180 degrees) collinear waves and winds were investigated. Therefore, other directions and non-collinear waves and winds are to be investigated.

Chapter 8

Conclusion & Recommendations

This chapter combines the conclusions and recommendations drawn for each chapter and reflects on the main objective. The main objective is formulated as:

Develop a simplified, fast and computational efficient model that predicts the motions and mooring loads of a Floating Offshore Wind Turbine (FOWT) in the concept design phase, based on available wind turbine input data.

8.1 Conclusions

In this thesis, a simplified model is presented in the time domain for the prediction of the motions and mooring loads of a floating wind turbine in the concept design phase. Fully coupled aero-hydro-servo-elastic simulations in aNySIM-Phatas are used, in which the Tri-Floater with a 5 MW NREL reference turbine is modelled. The simplified time domain model is validated with the fully coupled aNySIM-Phatas simulations.

A sensitivity study is performed using fully coupled aero-hydro-servo-elastic simulations. From the sensitivity study, the most influential physics on the platform motions and moorings loads are identified. From the differences in the mean, maximum and Power Spectral Density (PSD) plots of a set of model outputs, the most influential physics are selected that should be included in the simplified model. Simulations are constructed by including and excluding physical phenomena in the fully coupled model. These simulations are compared to a base case simulation, in which all phenomena are enabled. All simulations are performed in a Jonswap wave spectrum with a significant wave height H_s of 4.5 meter and a peak period T_p of 10 seconds. Moreover, collinear wave, current and wind direction are considered of 180 degrees.

The hydrodynamics are not included in the sensitivity analysis, as the focus is on the controller and aero-elastic contributions. From the sensitivity analysis it is concluded that the aerodynamic rotor thrust, calculated from Blade Element Momentum (BEM) theory (without 3D corrections and rootlosses), together with the wind loads on the floater, tower and nacelle are the main contributors to the platform motions and mooring loads. Furthermore, the wind turbine controller developed for a floating platform showed to have a significant effect on the low frequency and platform natural pitch frequency motions. No important contributions to the platform motions and mooring loads are found in case structural physics were considered.

The simplified time domain model is constructed by coupling a Python code to the multi-body time-domain simulation software aNySIM. In the Python code, a thrust is calculated which acts at the center of rotor height. This thrust is calculated by using the steady state thrust curve from a wind turbine. The effect of the floating wind turbine controller is included by aerodynamic damping ratios and filter on the turbulent wind.

In early design stages of a Floating Offshore Wind Turbine (FOWT), the mean and maximum platform

motions and mooring loads are major design requirements. From the comparison of the simplified simulations with the fully coupled simulations, it was shown that the differences in the mean and maximum values of the platform surge are within 5% (0.23 meter) and 10% (0.90 meter), respectively. For platform pitch, the differences in the mean and maximum were found to be less than 10% and 15%, respectively. The forward fairlead tension showed very promising results. The differences in the mean were found to be less than 2%, while the differences in the maximum was found to be less than 5%. Besides the reduction in computational time of the simplified model by a factor 5, the simplified model is significantly simpler to construct and to use.

In conclusion, it is shown that the simplified model accurately predicts the overall response of the floater and the forward fairlead tension, in terms of the mean and maximum values. Especially, the low frequency and wave frequency responses are predicted very well by the simplified. The response around the platform pitch natural frequency, however, was found to be a challenging task due to high non linear thrust excitation. All in all, the presented simplified model is suitable to assess the global motions and mooring loads of a FOWT concept in an early design stage. However, when there is an interest in structural behaviour (fatigue loads), fully coupled aero-hydro-servo-elastic simulations are inevitable.

8.2 Recommendations

At first, to use the simplified model in early concept design phases, the wind loads on the floater, tower and nacelle need to be included.

Secondly, the sensitivity study performed in this thesis was only carried out for one sea state. For more solid results, the same study could be done but then for different directions or sea states. Also, the sensitivity study could be extended with the hydrodynamic contributions, to identify the importance of the different hydrodynamic model inputs and to gain computational speed. Tower bending was not considered in the analysis, as this option was not available at the time this thesis was conducted. It might be of importance, and should be investigated in a later stage.

The thrust sensitivities, which were constructed to include the effect of the controller, were found to have a negligible effect on the damping of the natural platform pitch frequency in fully turbulent winds. For future work, it is recommended to have a closer look in the behaviour of the wind turbine controller contributing to system damping.

In this thesis, only the filtering of the incoming wind speed is studied. It was seen that most of the aerodynamic response was not captured, especially for higher wind speeds. Therefore, for future work it is recommended to have a look to the application of a more state-of-the-art filter on the relative wind speed.

Bibliography

- [1] Y. H. Bae and M. H. Kim. Rotor-floater-tether coupled dynamics including second-order sum-frequency wave loads for a mono-column-TLP-type FOWT (Floating Offshore Wind Turbine). *Ocean Engineering*, 61:109–122, 2013.
- [2] S. Butterfield, W. Musial, J. Jonkman, P. Scavounos, and L. Wayman. Engineering challenges for floating offshore wind turbines. *Journal of applied physics*, 2005.
- [3] C. Casale, E. Lembo, L. Serri, and S. Viani. Preliminary design of a floating wind turbine support structure and relevant system cost assessment. *Wind Engineering*, 34(1):29–50, 2010.
- [4] M.A. Chella, A. Tørum, and D. Myrhaug. An overview of wave impact forces on offshore wind turbine substructures. *Energy Procedia*, 20:217–226, 2012.
- [5] W.E. Cummings. The Impulse Response Function of Ship Motions. *International Symposium on Ship Theory, Hamburg*, (8), 1962.
- [6] DNV-GL. Coupled analysis of floating wind turbines. *Recommended Practice*, May 2019.
- [7] GL Garrad Hassan. *Bladed Theory Manual Version 4.0*, October 2010.
- [8] H. Glauert. *Airplane Propellers. In: Aerodynamic Theory*. Springer, 1935.
- [9] Global Wind Energy Council (GWEC). Global Offshore Wind Report 2020, August 2020.
- [10] S. Gueydon, K. Lindenburg, and F. Savenije. Coupling of two tools for the simulation of floating wind turbine. *32nd International Conference on Ocean, Offshore and Arctic Engineering*, pages 1–12, 2013.
- [11] F. Huijs. The Influence of the Mooring System on the Motions and Stability of a Semi-Submersible Floating Wind Turbine. Volume 9: Ocean Renewable Energy, May 2015.
- [12] F. Huijs, R. De Bruijn, and F. Savenije. Concept design verification of a semi-submersible floating wind turbine using coupled simulations. *Energy Procedia*, 53:2–12, 2014.
- [13] F. Huijs, E. Vlasveld, M. Gormand, F. Savenije, MM Caboni, B. Leblanc, C. Ferreira, K. Lindenburg, S. Gueydon, W. Otto, and B. Paillard. Integrated design of a semi-submersible floating vertical axis wind turbine (vawt) with active blade pitch control. *Journal of Physics: Conference Series*, 1104:012022, 10 2018.
- [14] F.A. Huijs, F. Mikx, J. and Savenije, and E. de Ridder. Integrated design of floater, mooring and control system for a semi-submersible floating wind turbine. *EWAE Offshore Conference. FrankFurt*, 2013.
- [15] J. Jonkman and W. Musial. Offshore code comparison collaboration (oc3) for iea wind task 23 offshore wind technology and deployment. 303, 01 2010.
- [16] J. Jonkman, S. Butterfield, W. Musial, and G. Scott. Definition of a 5-MW reference wind turbine for offshore system development. Technical report, National Renewable Energy Labrotory (NREL), February 2009.

- [17] J. M. Jonkman. Dynamics modeling and loads analysis of an offshore floating wind turbine. *National Renewable Energy Laboratory NREL/TP-500-41958*, 68(November):233, 2007.
- [18] J. M. Jonkman. Influence of Control on the Pitch Damping of a Floating Wind Turbine. *46th AIAA Aerospace Sciences Meeting and Exhibit*, January 2008.
- [19] J.M.J. Journee and W.W. Massie. *Offshore Hydromechanics*. Delft University of Technology, 2008.
- [20] M. Karimirad and T. Moan. A simplified method for coupled analysis of floating offshore wind turbines. *Marine Structures*, 27:45–63, 2012.
- [21] T. J. Larsen and T. D. Hanson. A method to avoid negative damped low frequent tower vibrations for a floating, pitch controlled wind turbine. *Journal of Physics: Conference Series*, 75, 2007.
- [22] F. Lemmer, K. Müller, A. Pegalajar-Jurado, M. Borg, and H. Bredmose. Qualification of innovative floating substructures for 10MW wind turbines and water depths greater than 50m Start. D4.1 Simple numerical models for upscaled design. page 45, 2016.
- [23] K. Lindenburg. *FOCUS6 Wind Turbine Module Modular Phatas versions for floating wind turbines*. WMC Technology Centre, May 2017.
- [24] K. Lindenburg. *Phatas User's Manual*. WMC Technology Centre, May 2019.
- [25] R. C. Lupton. *Frequency-Domain Modelling of Floating Wind Turbines*. PhD thesis, University of Cambridge, December 2014.
- [26] J.F. Manwell, J.G. McGowan, and A.L. Rogers. *Wind Energy Explained. Theory, Design and Application. Second Edition*, chapter 3. John Wiley & Sons Ltd., 2009.
- [27] D. Matha, M. Schlipf, A. Cordle, R. Pereira, and J.M. Jonkman. Challenges in simulation of aerodynamics, hydrodynamics, and mooring-line dynamics of floating offshore wind turbines. *Proceedings of the International Offshore and Polar Engineering Conference*, pages 421–428, October 2011.
- [28] F.G. Nielsen, T. D. Hanson, and B. Skaare. Integrated dynamic analysis of floating offshore wind turbines. *European Wind Energy Conference and Exhibition 2006, EWEC 2007*, 3:1834–1842, January 2007.
- [29] T.A. Nygaard, J. De Vaal, F. Pierella, L. Oggiano, and R. Stenbro. Development, Verification and Validation of 3DFloat; Aero-servo-hydro-elastic Computations of Offshore Structures. *Energy Procedia*, 94(January):425–433, 2016.
- [30] H. Ormberg and E. E. Bachynski. Global analysis of floating wind turbines: Code development, model sensitivity and benchmark study. *Proceedings of the International Offshore and Polar Engineering Conference*, 4:366–373, 2012.
- [31] P. Passon and M. Kühn. State-of-the-art and development needs of simulation codes for offshore wind turbines. January 2005.
- [32] A. Pegalajar-Jurado, H. Bredmose, and M. Borg. Multi-level Hydrodynamic Modelling of a Scaled 10MW TLP Wind Turbine. *Energy Procedia*, 94:124–132, 2016.
- [33] A. Pegalajar-Jurado, M. Borg, and H. Bredmose. An efficient frequency-domain model for quick load analysis of floating offshore wind turbines. *Wind Energy Science*, 3(2):693–712, 2018.
- [34] J.A. Pinkster. *Low Frequency Second Order Wave Exciting Forces on Floating Structures*. PhD thesis, Technische Hogeschool Delft, 1980.
- [35] Principia. DeepLines Wind, Offshore Wind Turbines FEA Software, 2016. Presentation.
- [36] F. Sandner, D. Schlipf, D. Matha, R. Seifried, and P. W. Cheng. Reduced Nonlinear Model of a SPAR-mounted Floating Wind Turbine. *Proc DEWEK 2012*, 2012.

-
- [37] F.J. Savenije. Control development for floating wind: Case study on the GustoMSC Tri-Floater. Technical report, ECN, May 2013.
- [38] S.W. Smith. *The Scientist and Engineer's Guide to Digital Signal Processing*, chapter 16, pages 285–296. California Technical Publisher.
- [39] H. Snel, R. Houwink, and J. Bosschers. Sectional prediction of lift coefficients on rotating wind turbine blades in stall. Technical report, ECN Petten, December 1994.
- [40] S. Thomassen, L. Suja, P.I. Bruheim, and A. Grand. Ashes: A novel tool for FEM analysis of offshore wind turbines with innovative visualization techniques. 2011.
- [41] UN Paris Agreement (adopted 12 Dec. 2015, entered into force 4 Nov. 2016), Accessed: December 2019.

Appendix A

Complete set of PSD plots obtained
from the sensitivity analysis

A.1 Aerodynamics

A.1.1 Platform surge

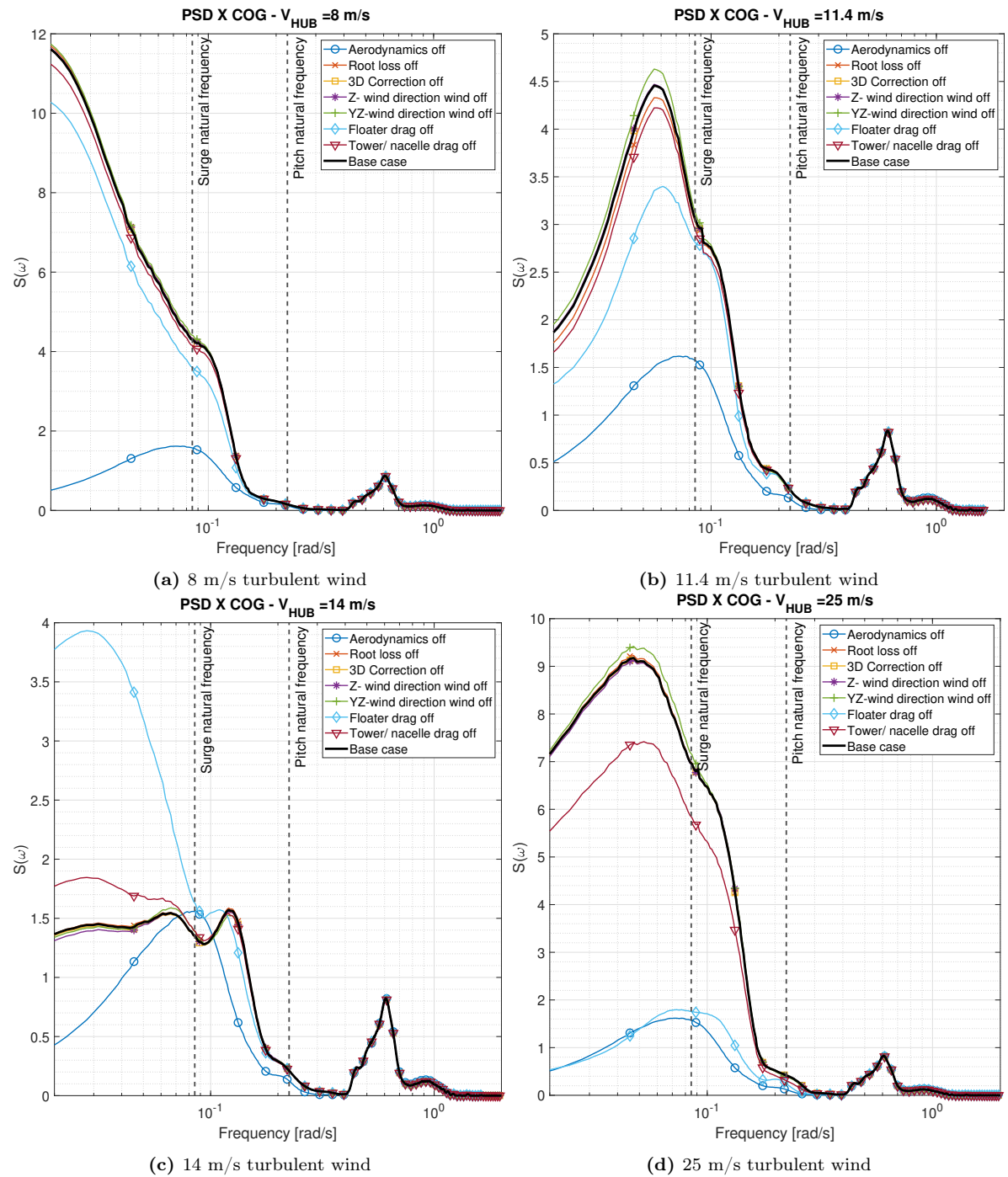


Figure A.1: Comparison of PSD of different aerodynamic model inputs to the base case simulation in turbulent winds for platform surge.

A.1.2 Platform pitch

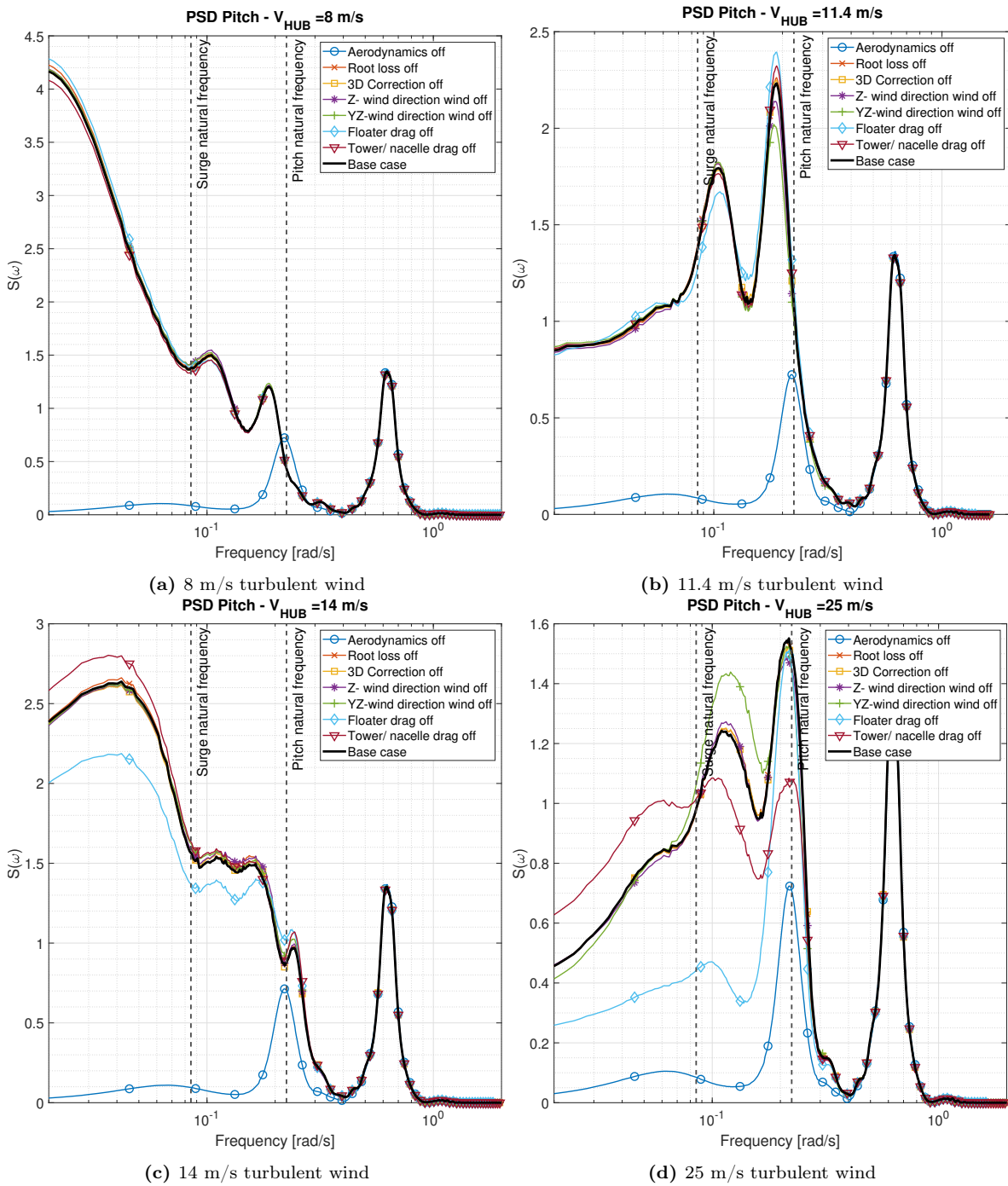


Figure A.2: Comparison of PSD of different aerodynamic model inputs to the base case simulation in turbulent winds for platform pitch.

A.1.3 Fairlead tension

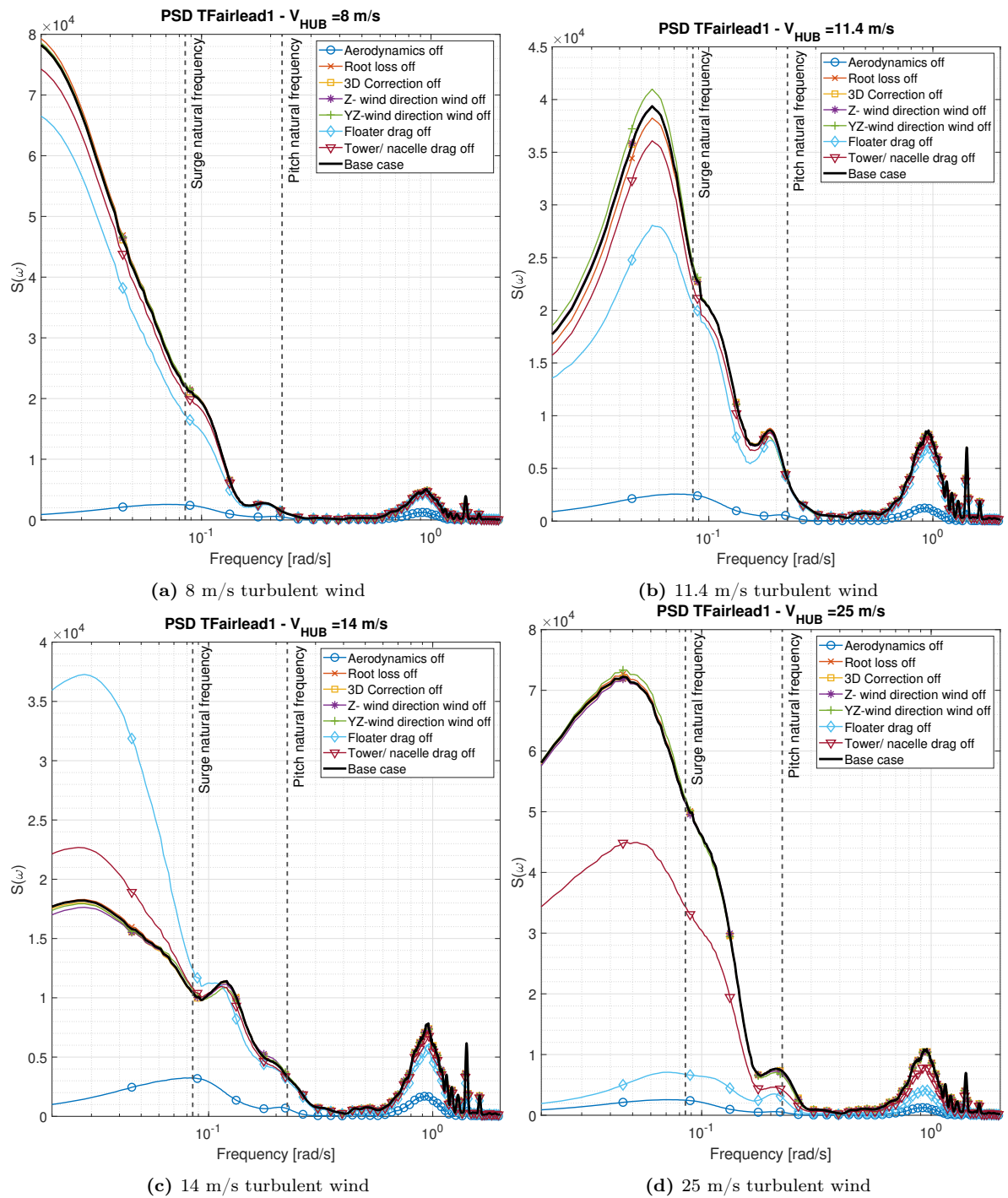


Figure A.3: Comparison of PSD of different aerodynamic model inputs to the base case simulation in turbulent winds for the forward fairlead tension.

A.1.4 Aerodynamic thrust

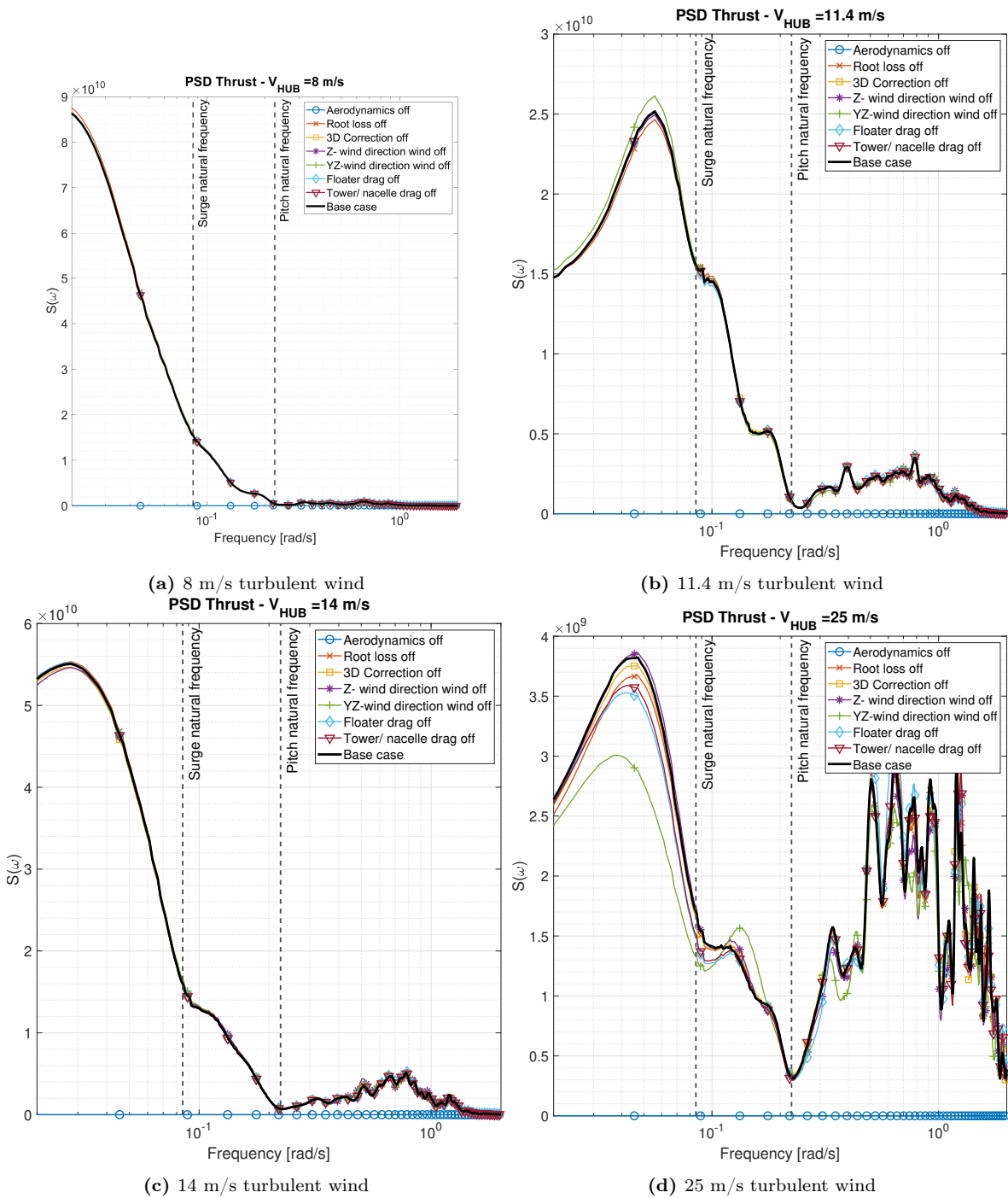


Figure A.4: Comparison of PSD of different aerodynamic model inputs to the base case simulation in turbulent winds for the aerodynamic thrust.

A.1.5 Resultant bending moment in towerbase

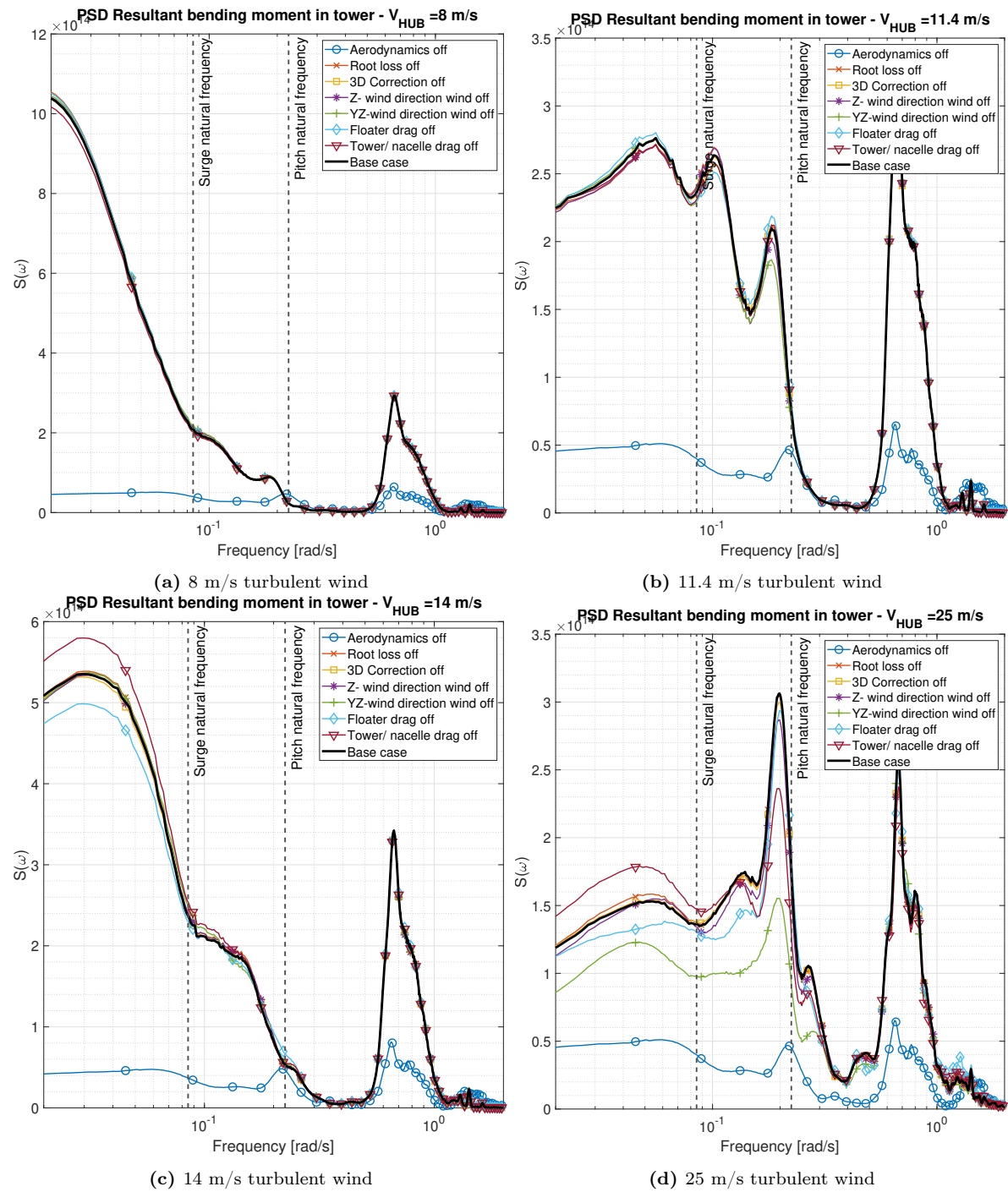


Figure A.5: Comparison of PSD of different aerodynamic model inputs to the base case simulation in turbulent winds for the resultant bending moment in the tower base.

A.2 Controllers

A.2.1 Platform surge

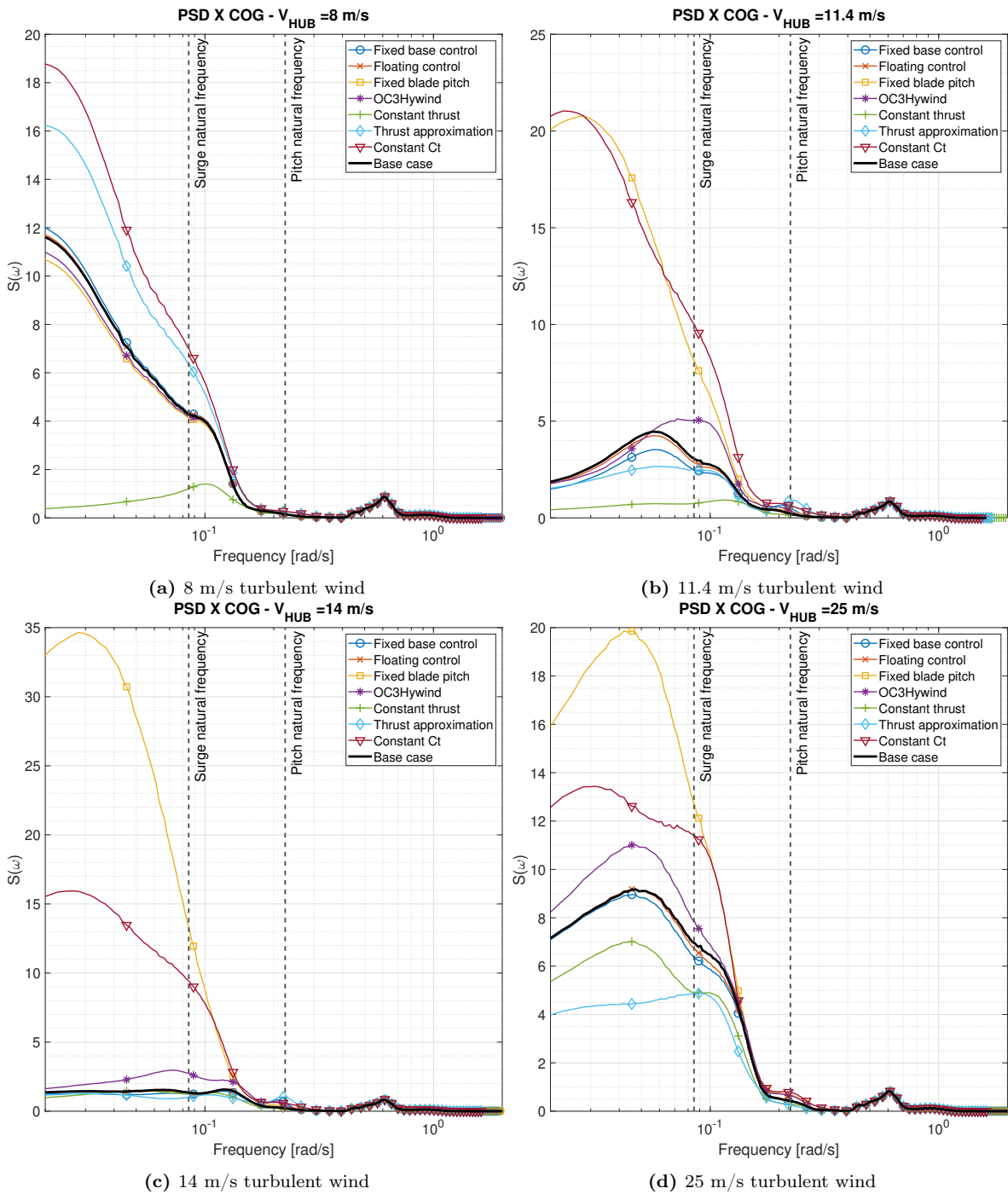


Figure A.6: Comparison of PSD of different control model inputs to the base case simulation in turbulent winds for the platform surge.

A.2.2 Platform pitch

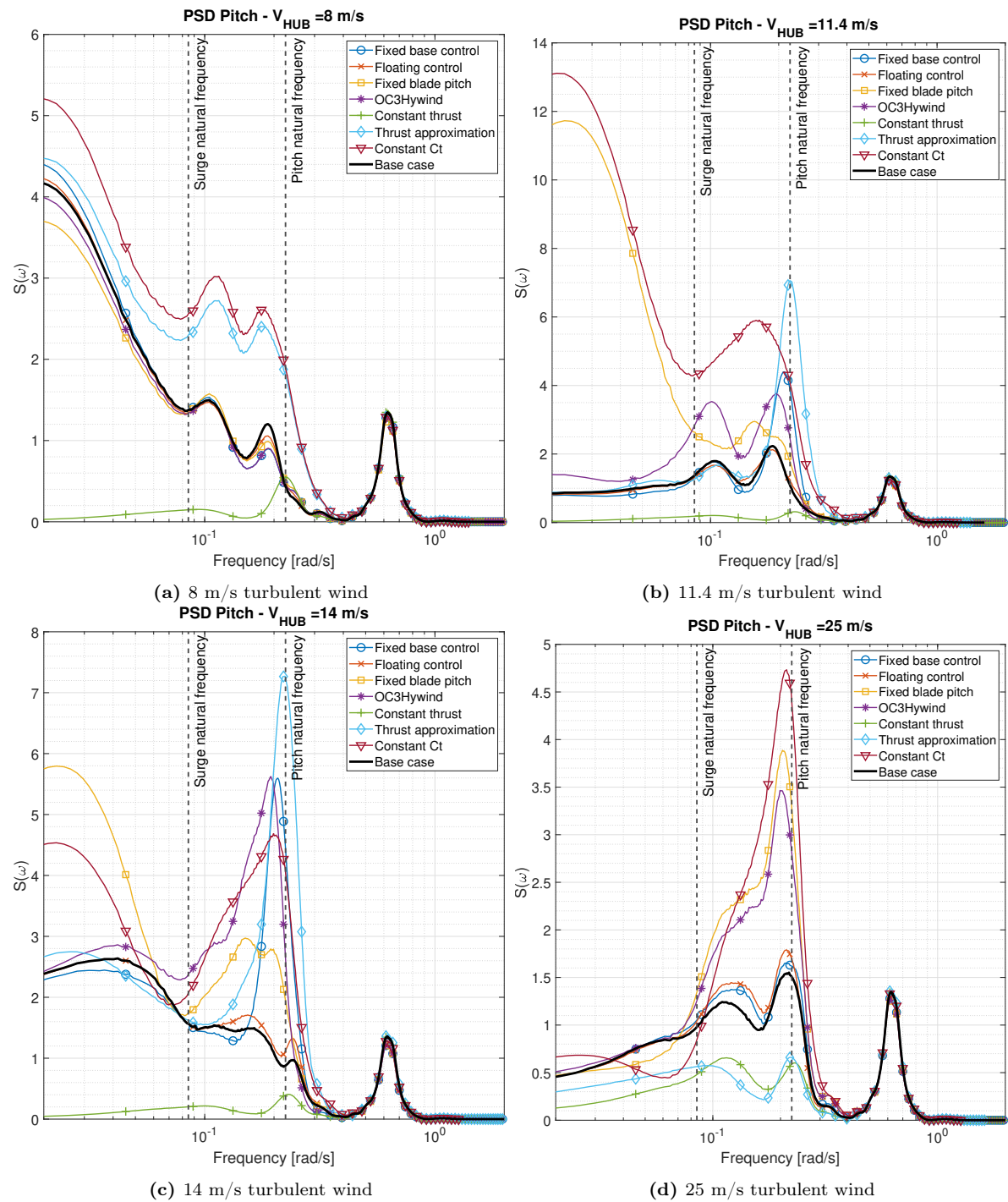


Figure A.7: Comparison of PSD of different control model inputs to the base case simulation in turbulent winds for the platform pitch.

A.2.3 Fairlead tension

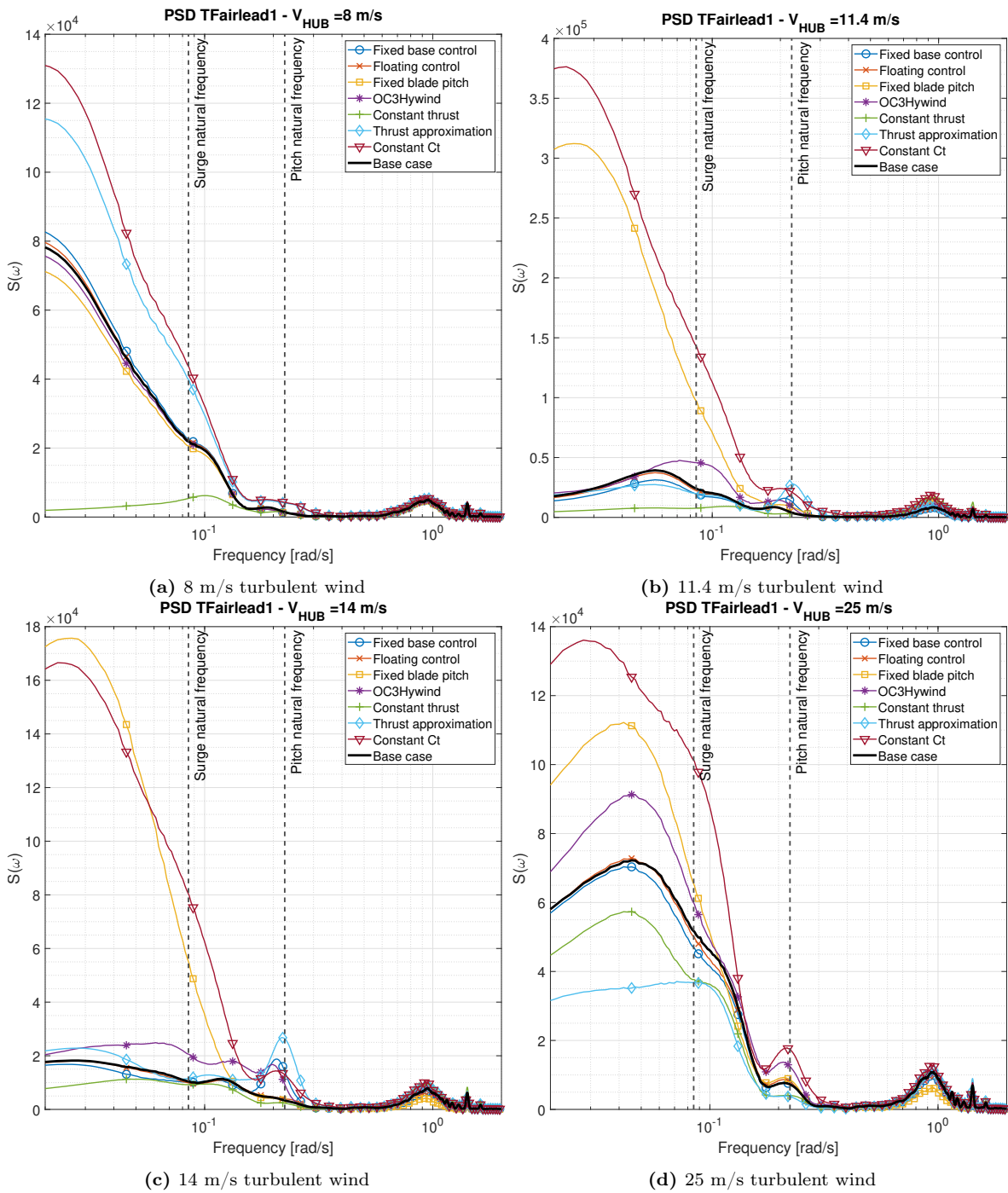


Figure A.8: Comparison of PSD of different control model inputs to the base case simulation in turbulent winds for the forward fairlead tension.

A.2.4 Aerodynamic thrust

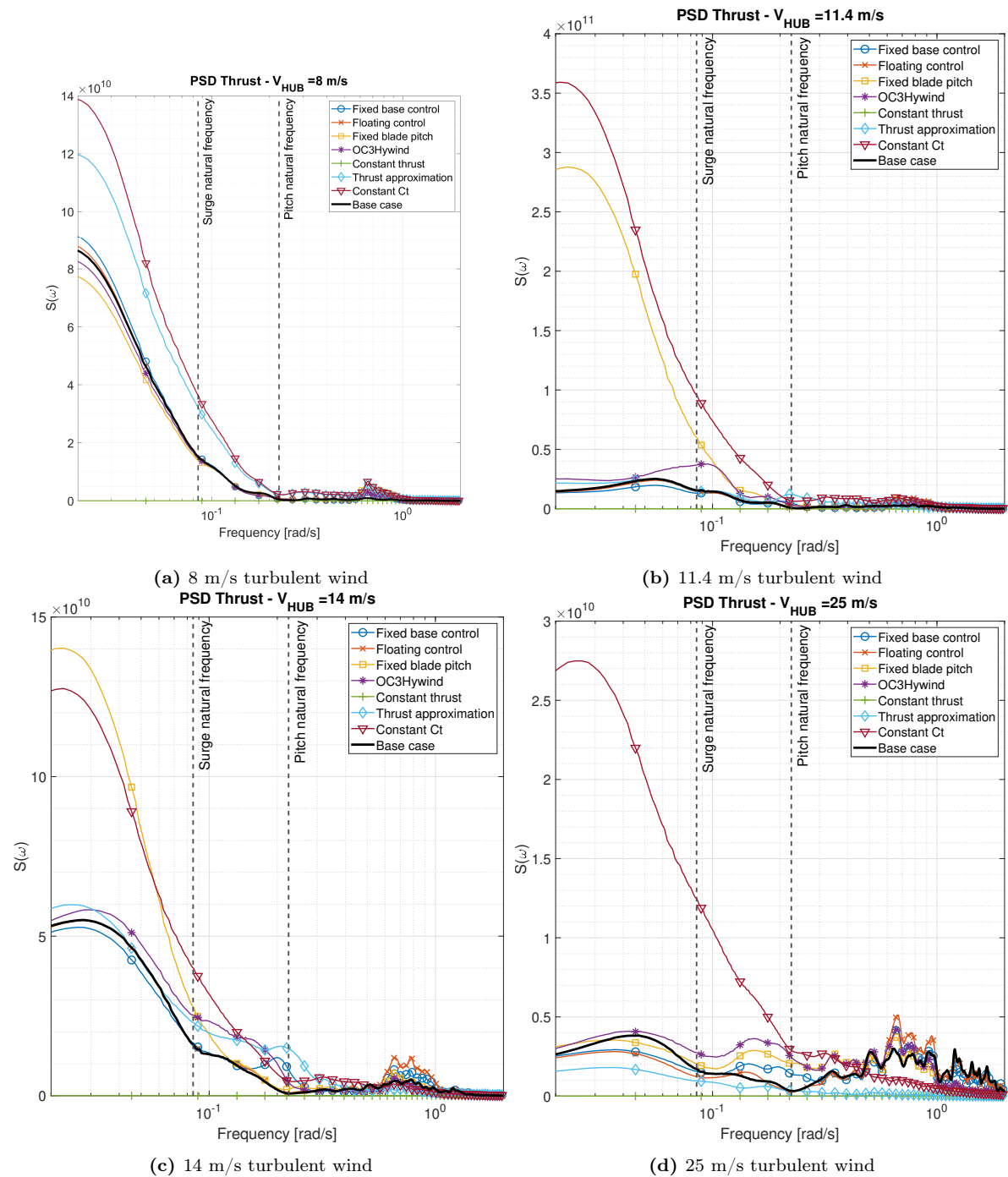


Figure A.9: Comparison of PSD of different control model inputs to the base case simulation in turbulent winds for the aerodynamic thrust.

A.2.5 Resultant bending moment in towerbase

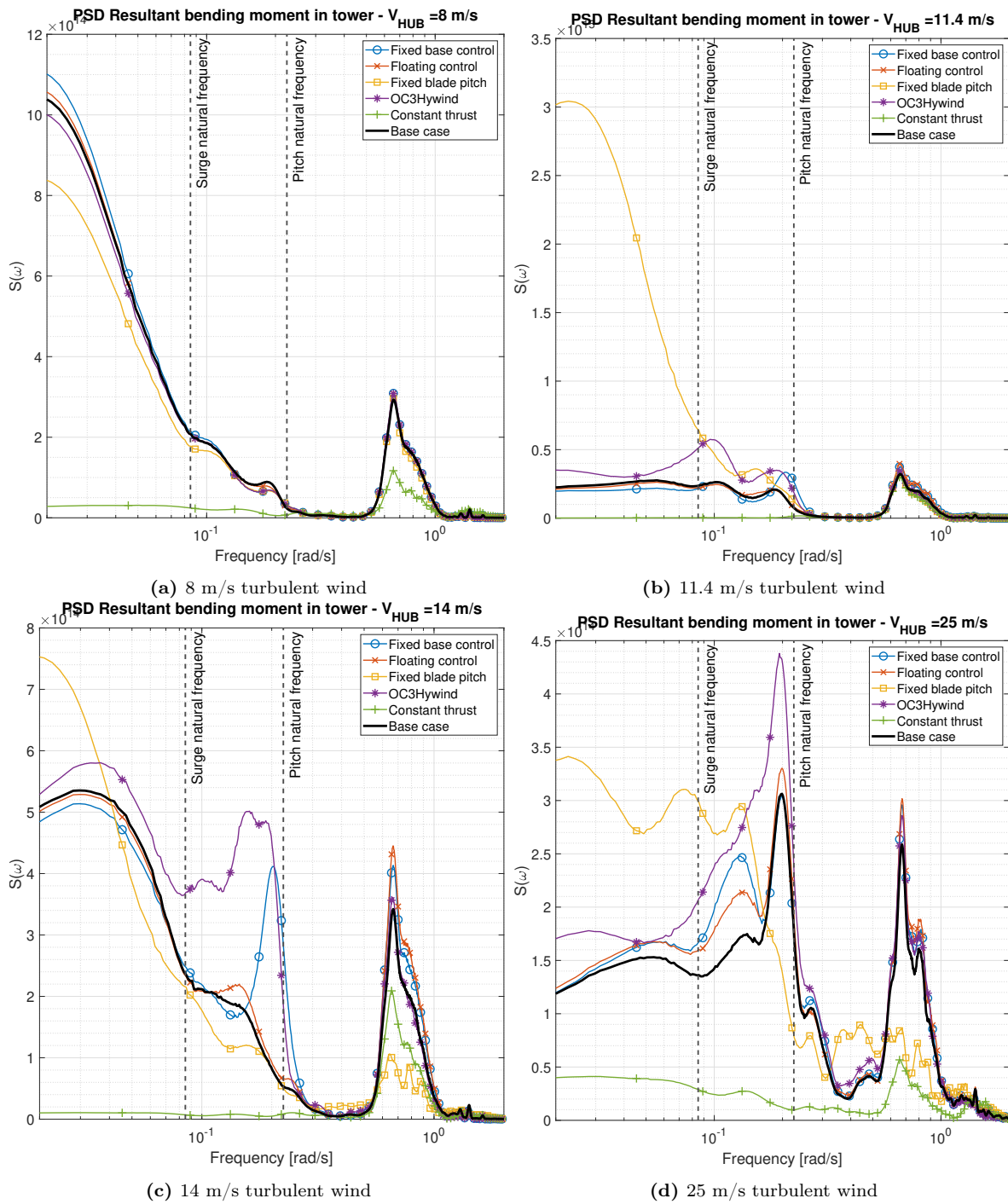


Figure A.10: Comparison of PSD of different control model inputs to the base case simulation in turbulent winds for the resultant bending moment in the towerbase.

A.3 Structures

A.3.1 Platform surge

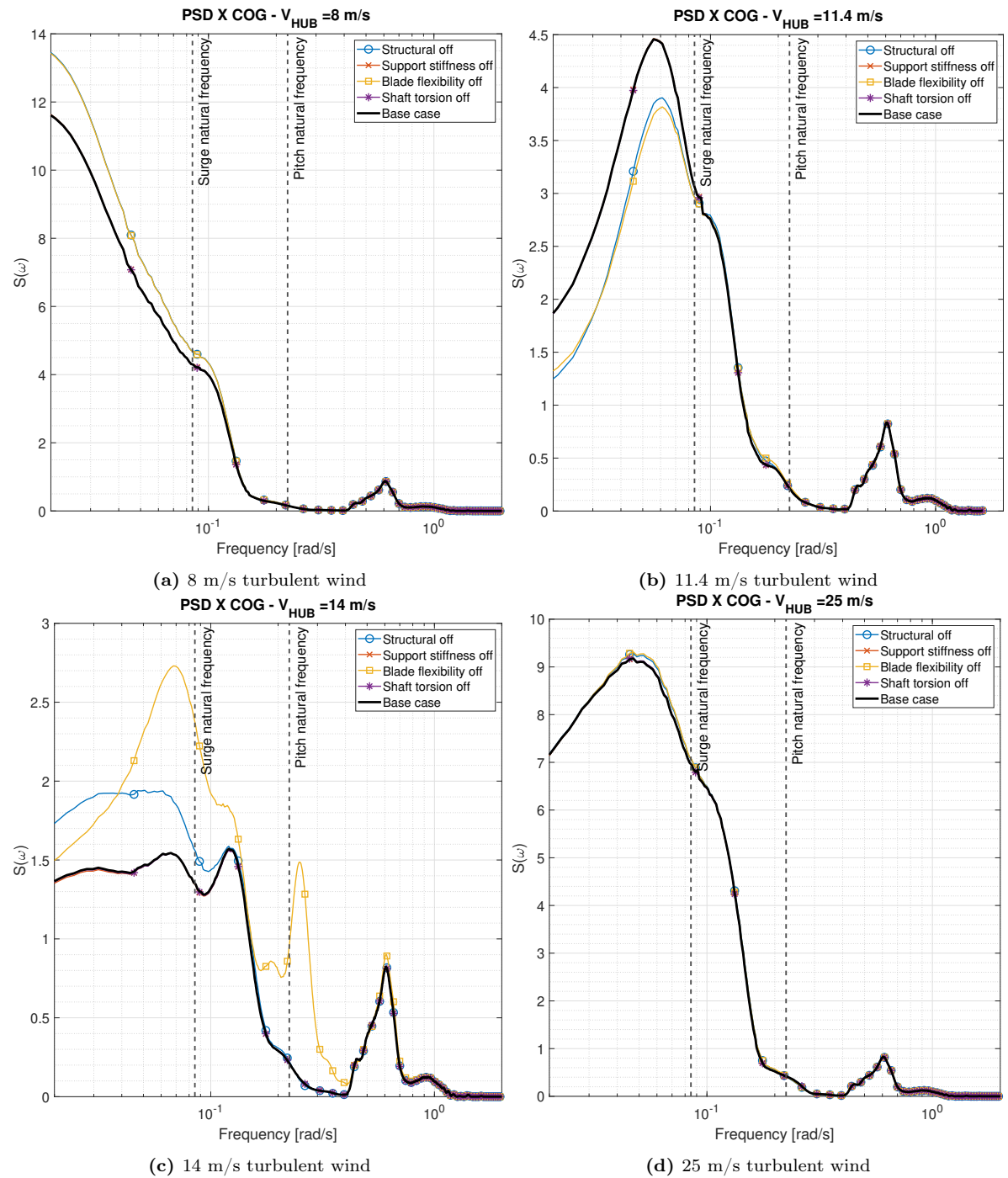


Figure A.11: Comparison of PSD of different structural model inputs to the base case simulation in turbulent winds for the platform surge.

A.3.2 Platform pitch

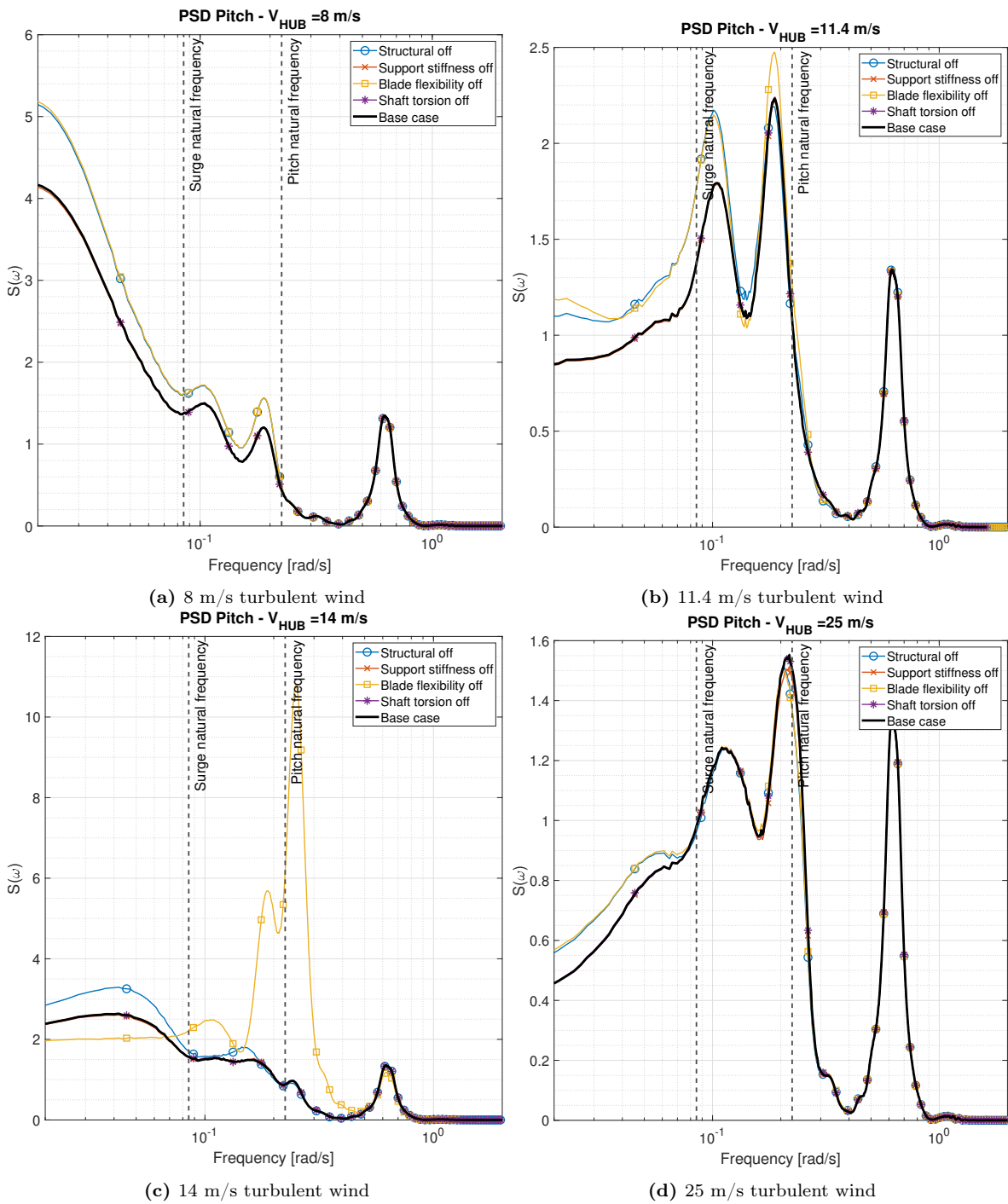


Figure A.12: Comparison of PSD of different structural model inputs to the base case simulation in turbulent winds for the platform pitch.

A.3.3 Fairlead tension

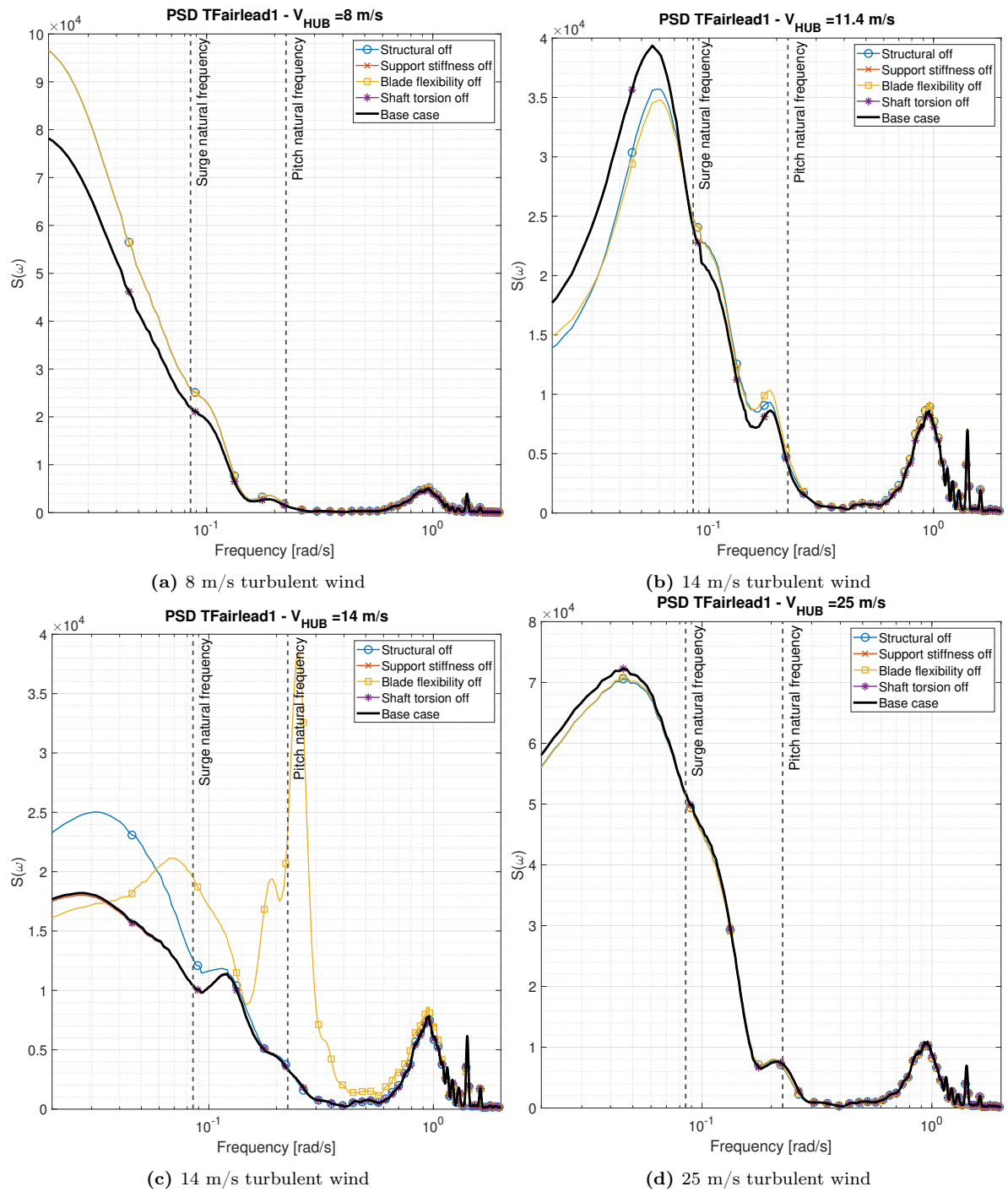


Figure A.13: Comparison of PSD of different structural model inputs to the base case simulation in turbulent winds for the forward fairlead tension.

A.3.4 Aerodynamic thrust

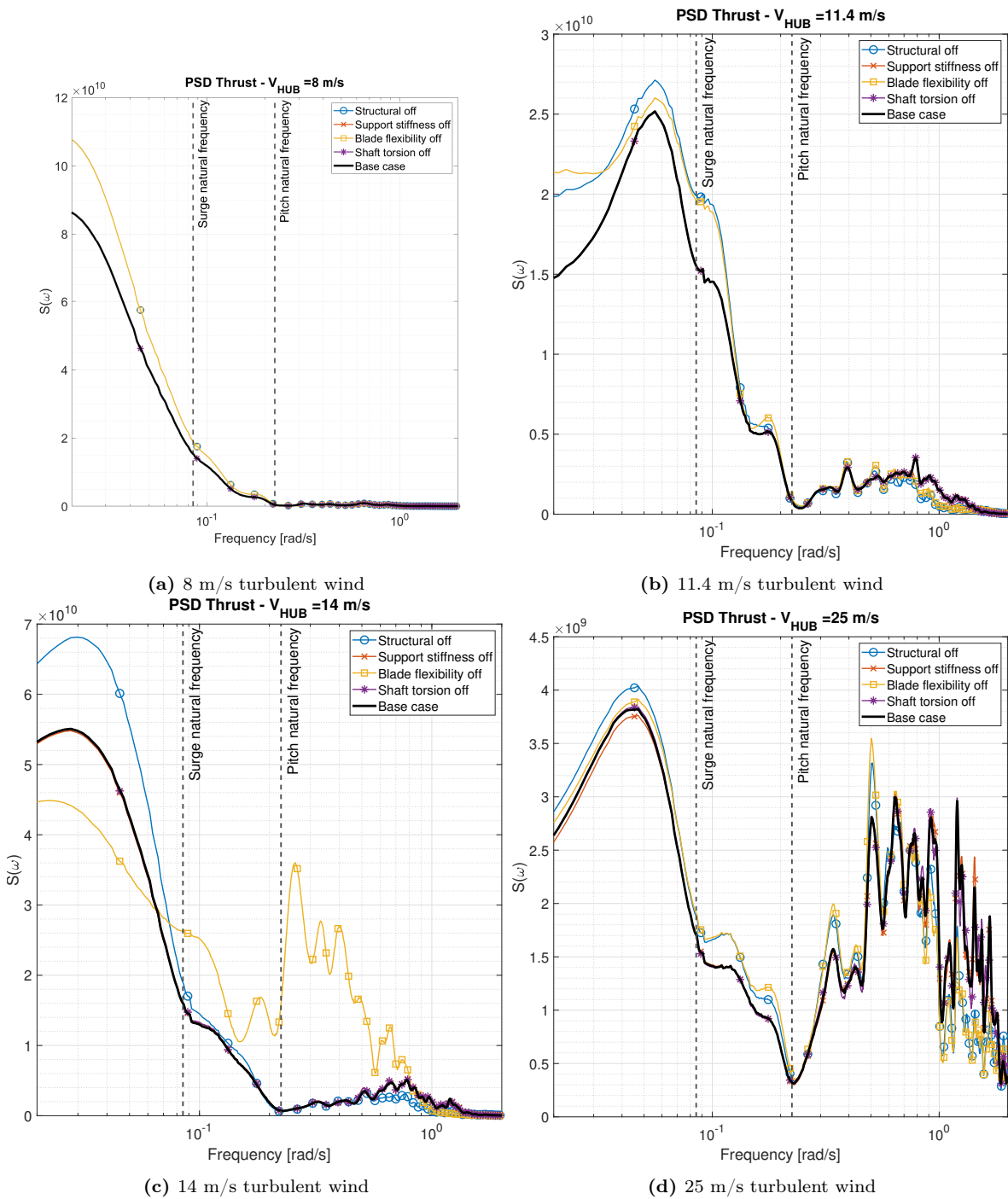


Figure A.14: Comparison of PSD of different structural model inputs to the base case simulation in turbulent winds for the aerodynamic thrust.

A.3.5 Resultant bending moment in towerbase

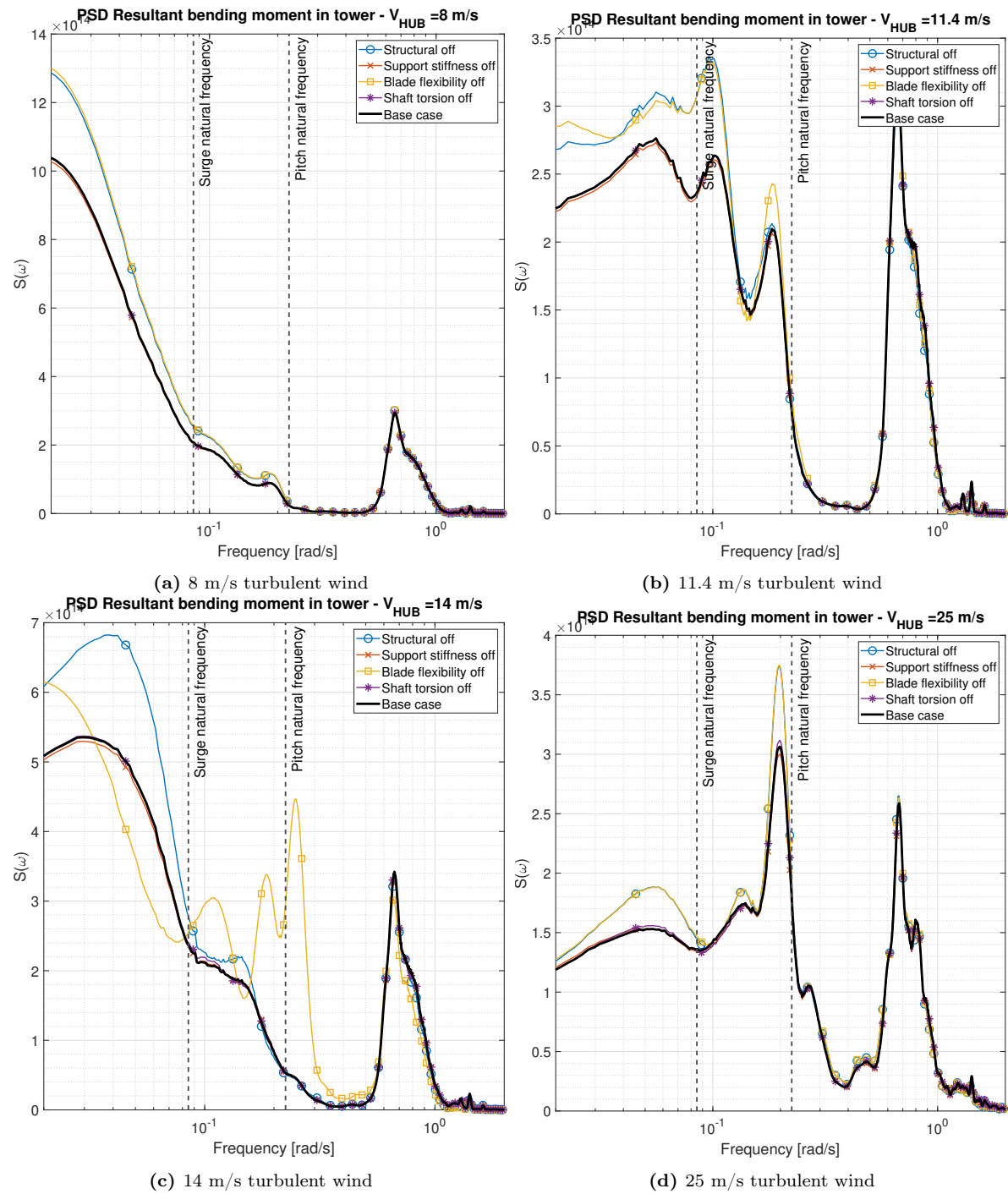


Figure A.15: Comparison of PSD of different structural model inputs to the base case simulation in turbulent winds for the resultant bending moment the towerbase.

Appendix B

Comparison aNySIM-Phatas with simplified model

B.1 Calm water - turbulent wind

Table B.1: Mean, standard deviation and maximum value of platform pitch in turbulent winds in calm water and irregular waves of the fully coupled model (aNySIM-Phatas) and simplified model.

Wind speed [m/s]	Platform pitch [deg] - calm water						Platform pitch [deg] - irregular waves					
	aNySIM-Phatas			Simplified model			aNySIM-Phatas			Simplified model		
	mean	std	max	mean	std	max	mean	std	max	mean	std	max
4	-1.00	0.32	1.74	-1.20	0.38	2.29	-0.96	0.59	2.62	-1.19	0.61	2.98
6	-2.01	0.59	3.80	-2.23	0.78	4.66	-1.97	0.75	4.67	-2.22	0.88	5.07
8	-3.52	0.96	5.89	-3.74	1.25	6.78	-3.46	1.05	6.33	-3.72	1.25	6.79
10	-4.90	0.92	6.95	-4.80	0.92	7.00	-4.85	0.99	7.33	-4.79	0.95	7.33
12	-5.14	0.85	7.14	-4.82	0.85	6.78	-5.12	0.87	7.58	-4.80	0.84	6.92
14	-4.36	0.89	7.05	-4.27	0.96	7.19	-4.35	0.96	7.40	-4.26	0.95	7.13
16	-3.72	0.79	6.24	-3.70	0.81	6.46	-3.71	0.85	6.56	-3.69	0.85	6.85
17	-3.37	0.62	5.13	-3.49	0.72	5.71	-3.36	0.73	5.95	-3.48	0.78	6.01
18	-3.32	0.62	5.46	-3.29	0.64	5.76	-3.31	0.71	5.71	-3.28	0.73	6.08
20	-3.07	0.52	4.99	-3.01	0.46	4.35	-3.06	0.65	5.07	-3.00	0.63	5.11
24	-2.76	0.66	4.35	-2.64	0.36	3.91	-2.74	0.69	4.68	-2.63	0.58	4.33
25	-2.71	0.55	4.12	-2.59	0.33	3.64	-2.70	0.65	4.73	-2.57	0.57	4.35

B.2 Irregular waves in all DoF - turbulent wind

Table B.2: Mean, standard deviation and maximum of platform surge and pitch when all DoF are activated for the fully coupled (aNySIM-Phatas) and simplified model.

Wind speed [m/s]	Platform surge [m]						Platform pitch [deg]					
	aNySIM-Phatas			Simplified model			aNySIM-Phatas			Simplified model		
	mean	std	max	mean	std	max	mean	std	max	mean	std	max
4	-2.38	0.74	4.64	-2.48	0.77	5.11	-0.56	0.55	2.25	-0.81	0.55	2.51
6	-3.96	1.01	7.55	-4.15	1.18	7.93	-1.28	0.65	3.49	-1.52	0.76	4.01
8	-6.02	1.27	10.02	-6.25	1.43	10.09	-2.33	0.86	4.81	-2.56	1.06	5.32
10	-7.59	1.01	10.38	-7.59	0.98	10.24	-3.33	0.86	5.84	-3.30	0.84	5.70
12	-7.82	0.84	10.52	-7.60	0.73	10.19	-3.52	0.79	5.73	-3.30	0.75	5.42
14	-6.93	1.01	10.46	-6.96	0.89	9.57	-3.00	0.87	5.89	-2.93	0.85	5.74
16	-6.13	0.84	9.12	-6.25	0.83	9.89	-2.55	0.82	5.67	-2.53	0.78	5.38
17	-5.91	0.75	8.94	-5.98	0.79	8.89	-2.25	0.71	4.57	-2.38	0.72	4.90
18	-5.60	0.71	8.25	-5.73	0.75	8.59	-2.27	0.70	4.45	-2.25	0.68	4.58
20	-5.23	0.70	7.99	-5.34	0.66	7.91	-2.10	0.65	4.46	-2.06	0.60	4.19
24	-4.70	0.62	7.05	-4.81	0.62	7.40	-1.88	0.68	3.69	-1.80	0.56	3.49
25	-4.65	0.63	7.06	-4.73	0.59	7.15	-1.84	0.66	3.74	-1.76	0.55	3.52

Table B.3: Mean, standard deviation and maximum values of forward fairlead tension of the fully coupled (aNySIM-Phatas) and simplified model.

Wind speed [m/s]	Tension at fairlead [N]					
	aNySIM-Phatas			Simplified model		
	mean	std	max	mean	std	max
4	7.93E+05	3.46E+04	9.18E+05	8.01E+05	3.55E+04	9.22E+05
6	8.75E+05	5.64E+04	1.15E+06	8.89E+05	6.46E+04	1.19E+06
8	1.01E+06	8.56E+04	1.32E+06	1.03E+06	9.74E+04	1.36E+06
10	1.13E+06	8.28E+04	1.37E+06	1.13E+06	7.88E+04	1.37E+06
12	1.15E+06	7.35E+04	1.43E+06	1.13E+06	6.41E+04	1.40E+06
14	1.08E+06	8.04E+04	1.38E+06	1.07E+06	7.07E+04	1.31E+06
16	1.02E+06	6.02E+04	1.28E+06	1.02E+06	6.03E+04	1.31E+06
17	9.95E+05	5.29E+04	1.23E+06	1.00E+06	5.58E+04	1.22E+06
18	9.78E+05	4.75E+04	1.19E+06	9.84E+05	5.15E+04	1.24E+06
20	9.55E+05	4.43E+04	1.14E+06	9.58E+05	4.38E+04	1.15E+06
24	9.23E+05	3.92E+04	1.08E+06	9.24E+05	3.88E+04	1.08E+06
25	9.20E+05	3.82E+04	1.11E+06	9.19E+05	3.66E+04	1.06E+06

Table B.4: Mean, standard deviation and maximum values of aerodynamic rotor thrust of the fully coupled (aNySIM-Phatas) and simplified model.

Wind speed [m/s]	Aerodynamic thrust [N]					
	aNySIM-Phatas			Simplified model		
	mean	std	max	mean	std	max
4	1.14E+05	3.52E+04	2.09E+05	1.22E+05	4.71E+04	2.72E+05
6	2.22E+05	5.76E+04	4.33E+05	2.37E+05	6.91E+04	4.97E+05
8	3.86E+05	8.95E+04	6.52E+05	4.06E+05	1.05E+05	6.05E+05
10	5.33E+05	8.29E+04	7.75E+05	5.25E+05	7.43E+04	5.96E+05
12	5.56E+05	7.89E+04	8.64E+05	5.26E+05	5.46E+04	5.92E+05
14	4.68E+05	9.26E+04	9.01E+05	4.65E+05	6.93E+04	5.91E+05
16	3.92E+05	7.55E+04	8.48E+05	4.01E+05	5.66E+04	5.84E+05
17	3.66E+05	6.84E+04	7.03E+05	3.77E+05	5.30E+04	5.93E+05
18	3.44E+05	6.42E+04	5.90E+05	3.55E+05	4.53E+04	5.84E+05
20	3.12E+05	6.73E+04	5.91E+05	3.24E+05	3.32E+04	5.07E+05
24	2.67E+05	6.66E+04	5.59E+05	2.83E+05	2.45E+04	4.18E+05
25	2.61E+05	6.86E+04	5.76E+05	2.76E+05	2.27E+04	4.02E+05